Fakultät für Medizin

Neurobiologie des Diabetes

Regulation of hypothalamic dopaminergic neurons and systemic energy metabolism by histone deacetylase 5

Raian Eduardo Contreras

Vollständiger Abdruck der von der Fakultät für Medizin der Technischen Universität München zur Erlangung des akademischen Grades eines Doktors der Naturwissenschaften genehmigten Dissertation.

Vorsitzende(r): Prof. Dr. Thomas Misgeld

Prüfer der Dissertation:

1. Prof. Dr. Paul Thomas Pfluger
2. Prof. Dr. Nina H. Uhlenhaut

Die Dissertation wurde am 15.12.2020 bei der Technischen Universität München

eingereicht und durch die Fakultät für Medizin.

am 13.04.2021 angenommen.

Table of contents

Acknowledgement

"It's the questions we can't answer that teach us the most. They teach us how to think. If you give a man an answer, all he gains is a little fact. But give him a question and he'll look for his own answers."

— **Patrick Rothfuss, The Wise Man's Fear**.

- o   To Matthias, thank you for considering and giving me the opportunity to join the institute.

- o   To Paul, so many things happened in such short period of time. There are so many reasons to thank you about but most important to thank you for the support all these years. You trusted me and backed me whenever I needed it. I am very proud of you and I am very thankful for you being my supervisor.

- o   To Jane, thank you for hosting me. It was such a placer for me to be part of your lab. I am thankful for the kindness you always showed to me and the nice conversations we had. You are such a great inspiration.

- o   To NBD, past and former colleagues, I cannot count how many exceptional experiences we had. Sonja, Peter, Luke, Emily, Franziska, Katrin, Ksenja, Louise and Miriam thank you all for sharing happiness, jokes, and smiles.

- o   To my friends, who always supported me, listened to me, laughed with me. Tim, Cristina, Fran, Cassie, Ismael, Franzi, Elena, Gus, Teresa, Tina, Cahue, Alex, David, Laura, Emilja, Simon, Daivirys and Thomas. You will always be part of my life

- o   To the IDO people, it always nice to chat, share meals and jokes, a lot of jokes.

- o   To Alex, I would have to write a new thesis about the ways to thank you. Thank you for standing by side and specially that whole month in Gran Canaria while I was writing my thesis. The sunrise by the sea and your smile every morning was the most vibrant and positive energy I could have never asked for. It was a blessing.

- o   To my family, my mom, my dad, my grandmas, my aunts and cousins, you gave me love and energy everyday throughout the distance. I love you with all my heart

- o   And for you, thank you for taking some of your time to read the thesis.

List of figures

List of tables

Abstract

Obesity is among the most common and costly chronic disorders worldwide. Estimates suggest the prevalence of obesity in adults at 42.4% and almost 30% for the United States and European Union, respectively. Multiple genes were shown to drive the undesired and unhealthy accumulation of fat by creating a positive energy balance. Recently, our group reported such a bias towards high fat diet-induced obesity in global HDAC5-KO mice that was driven by impaired hypothalamic leptin signaling and increased energy intake. Moreover, preliminary data suggested increased fat-mass in HDAC5-KO mice fed chow diet. In my thesis, I aimed to elucidate the role of HDAC5 in energy metabolism and body weight control in a non-obesogenic environment. Metabolic phenotyping of male and female global HDAC5 WT and KO mice fed chow diet unraveled the development of mature-onset obesity and concomitant metabolic syndrome with perturbed energy metabolism in male HDAC5-KO mice. Decreased energy expenditure in the KO mice was associated with reduced BAT-induced thermogenesis, and impaired WAT lipolysis due to diminished adrenergic stimulation by the sympathetic nerve system. Lower cFOS and higher tyroxine hydroxylase (TH) staining in the paraventricular hypothalamus (PVH), a major center controlling SNS activity, suggested attenuated neuronal activity and an elevated dopaminergic (inhibitory) innervation in male HDAC5-KO mice. Chemical analyses confirmed higher hypothalamic dopamine levels in HDAC5-KO mice. Increased hypothalamic gene expression and protein phosphorylation levels of tyrosine hydroxylase, and profoundly diminished circulating prolactin levels, added further proof for an elevated dopaminergic tone in hypothalami of HDAC5 KO. Notably, immunohistochemical stainings for TH revealed a chronic, adult-onset activation of dmARH dopaminergic neurons in male HDAC5 KO mice. Mechanistically, immunoprecipation and Western Blot studies revealed a direct interaction between STAT5b and HDAC5 in the hypothalamus, and a preferential nuclear localization of STAT5b when HDAC5 was absent. These findings point toward an important role of HDAC5 in controlling dmARH dopaminergic neuronal activity via its main transcriptional regulator STAT5b toward PVH-based control of SNS activity. My data further suggests an important role of HDAC5 in regulating adipose tissue thermogenesis and lipolysis under non-obesogenic conditions. Future research is nonetheless

warranted to fully decipher the molecular mechanism underlying the over-activation of dmARH dopaminergic neurons upon HDAC5 deficiency.

Overall, my thesis reveals a pivotal role for HDAC5 in controlling energy metabolism by governing the activation state of dmARH dopaminergic neurons and a PVH-SNS-BAT/eWAT axis that adjusts energy homeostasis to the dietary and thermal environment. In conclusion, my data suggests that hypothalamic HDAC5 may represent a potential therapeutic target to fight obesity by stimulating thermogenesis and WAT lipolysis.

Zusammenfassung

Fettleibigkeit gehört zu den häufigsten und teuersten chronischen Erkrankungen weltweit. Schätzungen zufolge lag die Prävalenz von Fettleibigkeit bei Erwachsenen in den USA bei 42,4% und in der Europäischen Union bei bis zu 30%. Obschon viele Gene an der Entstehung von Fettleibigkeit beteiligt sind, bleiben deren Anteil an der Ausprägung von Fettleibigkeit, und ihre genauen Ursache-Wirkungs-Prinzipien, nur unzureichend verstanden. Vor einigen Jahren konnte mein Labor zeigen, dass Mäuse mit einer Defizienz des Genes Histone Deacetylase 5 (HDAC5) nach Fütterung mit fettreicher Nahrung eine erhöhte Neigung zur Ausbildung von Fettleibigkeit zeigten. Mechanistisch konnte gezeigt werden, dass es bei fehlender HDAC5 zur Bildung einer Leptin-Resistenz und zur erhöhten Zufuhr an Kalorien im Vergleich zum WT kam. In den damaligen Untersuchungen wurde jedoch nicht genau beleuchtet, ob HDAC5 Defizienz auch bei Fütterung mit kalorienarmer Standarddiät eine Wirkung auf den Energiehaushalt ausüben kann. Eine Tendenz zu erhöhter Fettmasse im HDAC5-KO Tier deutete damals allerdings auf eine mögliche Störung des Gewichtsregulation auch bei einer kalorienarmen Ernährung hin.

In meiner Doktorarbeit wollte ich die Rolle von HDAC5 für den Energiestoffwechsel und die Kontrolle des Körpergewichts in einer solchen kalorienarmen Umgebung näher beleuchten. Die metabolische Phänotypisierung und indirekte Kaoriemtrie bestätigte hier für männliche HDAC5-KO Tiere einen erhöhten Grad an Fettleibigkeit der mit einem verminderten Energieverbrauch einherging. Männliche, mit Standarddiät gefütterte HDAC5-KO Mäuse hatten zudem eine verringerte BAT-induzierte Thermogenese und WAT-induzierten Lipolyse, die auf eine verringerte adrenerge Stimulation durch das sympathische Nervensystem zurückgeführt wurde. Entsprechend war die neuronale Aktivität im paraventrikulären Hypothalamus (PVH), einem Hauptzentrum der SNS-Aktivitätskontrolle, verringert, was auf eine zentralnervöse Ursache für den metabolischen Phänotyp hinwies. Im Hypothalamus wurde hierbei ein höherer Dopaminspiegel gefunden, sowie eine erhöhte dopaminerge Innervierung des PVH die dort inhibitorisch wirkt. Die erhöhten Dopaminspiegel im Hypothalamus wurden mittels neu etablierter, auf Fluoreszenz-assistierter Zellsortierung (FACS) auf eine ligandenunabhängige Überaktivierung von dorsomedialen dopaminergen ARH-Neuronen nach HDAC5 Deletion

zurückgeführt. Weiterhin waren die Genexpression und Proteinphosphorylierung der Tyrosinhydroxylase im KO erhöht und der Haupt-Transkriptionsfaktor der dmARH-dopaminergen Neuronen, STAT5b, war bevorzugt im Kern lokalisiert. Ich konnte zudem eine Wechselwirkung zwischen STAT5b und HDAC5 im Hypothalamus nachweisen. Weitere sind hier dennoch erforderlich, um den molekularen Mechanismus, der der Überaktivierung von dmARH-dopaminergen Neuronen bei HDAC5-Mangel zugrunde liegt, vollständig zu entschlüsseln.

Zusammenfassend wurde in meiner Doktorarbeit zum ersten Mal gezeigt, dass HDAC5 eine zentrale Rolle in der Aktivierung dopaminerger dmARH-Neuronen spielt und für eine angemessene Aktivität der PVH-SNS-BAT / eWAT-Achse und damit verbundenen Steuerung der Thermogenese und Lipolyse im Fettgewebe essentiell ist. Hypothalamisches HDAC5 stell somit ein potenzielles therapeutisches Ziel dar, um das Energiegleichgewicht durch Stimulierung des Energieverbrauchs wiederherzustellen.

1. Introduction

1.1. Obesity

Obesity is a complex disease characterized by the undesired increase in fat-mass that represents a risk for health by increasing the likelihood for deadly comorbidities such as type-2 diabetes (T2D), cardiovascular diseases or some forms of cancer (World Health Organization, 2018). In 2017, more than 1.9 billion adults and 340 million children worldwide were classified as overweight or obese, respectively. Aside from being one of the most common diseases, it is also one of the costliest. Only in the United States, the estimated annual medical cost of obesity was $147 billions US dollars in 2018. However, efforts to curb the ever-increasing obesity pandemic have largely failed, creating an enormous demand for weight-loss products and health services.

Body weight maintenance requires a dynamically adjusted homeostasis of energy intake and energy expenditure (Figure 1). Imbalance towards positive or negative homeostasis ultimately affects body weight. Positive balance promotes the accumulation of energy excess in the form of fat whereas negative balance stimulates the utilization of fat stores as fuel for energy demanding situations. Positive balance can occur from increases in energy intake over energy expenditure or decreases in energy expenditure despite normal energy intake. In our Westernized society, a stressful and sedentary lifestyle is combined with an overconsumption of highly palatable and energy-dense food enriched in saturated fats and processed sugars (Melby et al., 2017). Thus, hedonic stimulation overrides metabolic demand and shifts the balance towards fat storage. Hyperphagia was similarly described under non-obesogenic conditions in humans and rodents carrying mutations in defined genes. Leptin, the first cloned gene related to obesity, induced hyperphagia and morbid obesity on chow diet when mutated (Zhang et al., 1994; Friedman, 2016) . Deficiencies in energy expenditure are equally detrimental to energy homeostasis. Insufficient energy to match elevations in food intake influenced gradual body weight gain (Hill et al., 2012). Decreased thermogenic energy expenditure was associated with overweight and obesity compared to normoweight individuals (Thorp and Schlaich, 2015). In UCP1-KO mice kept at thermoneutrality, deficiency a reduction in sympathetic stimulation and decreased

thermogenesis led to the development of obesity when fed high fat diet (Feldmann et al., 2009). In essence, obesity is generally the consequence of small, cumulative shift towards positive energy balance. The causes for this gradual shift are highly heterogenous and involve developmental, environmental, genetic and/or epigenetic factors (Figure 2).

1.2. Physiological adaptations in response to weight loss

Obesity pathogenesis involves mechanisms beyond a passive accumulation of excess calories. Studies on the adaptive response to bodyweight changes in humans and animal models demonstrated the existence of an active energy homeostatic system. Body weight-loss after caloric-restriction is probably one of the most studied and used models in supervised and unsupervised human regimes. To lose weight, obese individuals often undergo severe caloric restriction, i.e. they reduce their overall energy intake to create a negative energy balance (Rosenbaum et al., 2010). In consequence, the body readily adapts by a rapid decrease in the total daily energy expenditure (TDEE) to preserve energy and restore homeostasis (Rosenbaum et al., 2008). This decrease in TDEE can nevertheless be disproportionate to the decrease in energy intake, as evidenced by a report that showed 25% lower TDEE in weight-reduced compared to never-obese individuals (Leibel et al., 1995). By the end of a weight loss period, all three main components of TDEE are reduced, i.e. the thermic effect of food required for the digestion and absorption of ingested calories (Maclean et al., 2011), activity-induced energy expenditure including non-exercise activity thermogenesis (NEAT) and exercise energy expenditure (EEE) (Goldsmith et al., 2010; Hames et al., 2016) and the resting metabolic rate (RMR) (Melby et al., 1990; Astrup et al., 1999; Doucet et al., 2001). The reduction in TDEE after a profound weight loss can last for several years (Camps et al., 2013) and impairs the long-term maintenance of weight loss in both mice and men (Hill et al., 1987; Froidevaux et al., 1993; Maffei et al., 1995; Doucet et al., 2001; MacLean et al., 2004). For instance, participants of the TV show "The Biggest Loser" showed a persistent decrease in their RMR even 6 years after the weight loss intervention, which likely contributed to the regain in body weight in all but one of the 14 subjects (Fothergill et al., 2016). Thus, decreased energy expenditure favors weight (re)gain despite having appropriate food intake for a respective body composition.

On the other side of the balance, our ingestive behavior is built upon parallel and complementary mechanisms that integrate peripheral signals from circulating hormonal factors for hunger or fullness within the homeostatic feeding circuitry in the hypothalamus and brain stem with hedonic processes that are partially beyond our cognitive control (Waterson and Horvath, 2015). Weight loss by calorie restriction is associated with increased hunger and a strongly increased reward value of food (Rosenbaum et al., 2010; Burger and Stice, 2011; Blundell et al., 2012; Caudwell et al., 2013). Notably, the sensation of increased hunger appears to persist beyond the phase of rapid weight loss; previously obese mice that had been subjected to rapid weight loss by calorie restriction showed hyperphagia when re-fed *ad-libitum* chow fed diet*,* leading to accelerated weight re-gain even when compared to never-obese mice subjected to a HFD (Kirchner et al., 2012).
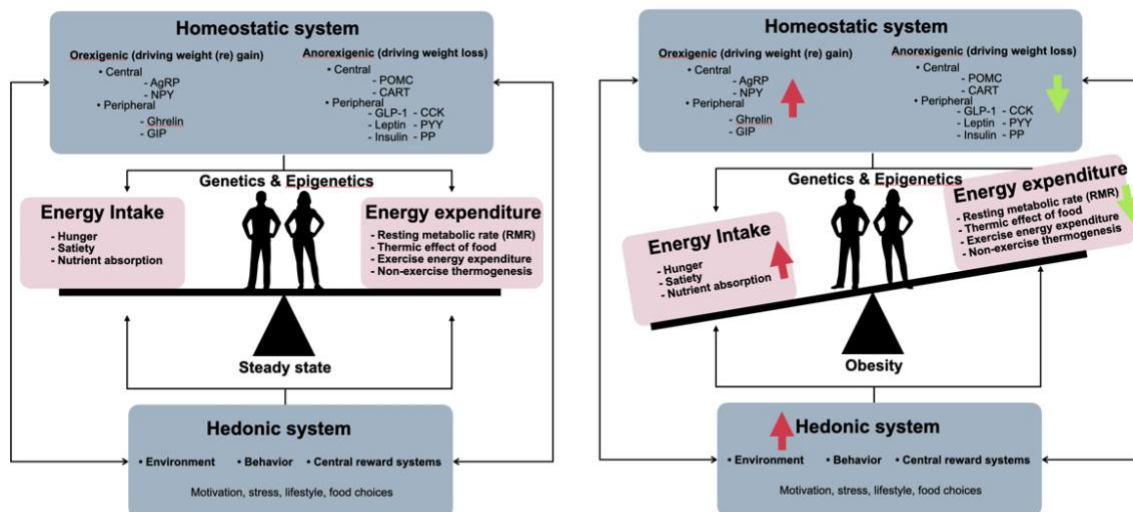
Figure 1: Factors affecting energy balance and ultimately body weight.

In a steady-state where no significant changes in body weight occur, energy intake is balanced to energy expenditure, with homeostatic and hedonic mechanisms being in balance. Instead, positive energy balance leads to energy accumulation in the form of fat and obesity resulting from either or a combination of both increased energy intake and decreased energy expenditure. AgRP, agouti-related peptide; NPY, neuropeptide Y; GIP, gastric inhibitory peptide; POMC, pro-opiomelanocortin; CART, cocaine- and amphetamine-regulated transcript; GLP1, glucagon-like peptide 1; CCK, cholecystokinin; PYY, peptide YY & PP, pancreatic polypeptide. Modified from (Greenway, 2015)

Mechanistically, weight loss was shown to induce a profound deregulation of circulating nutrients such as glucose or free fatty acids which can act as signaling moieties in CNS centers governing energy and glucose homeostasis (Lam et al., 2005; He et al., 2006). Similarly, weight loss and negative energy balance altered the secretion of circulating hormones such as the orexigenic ghrelin or the anorexigenic leptin, insulin, GLP-1, CCK and PYY, Figure 2 (Maffei et al., 1995; Näslund et al., 2000; Crujeiras et al., 2010; Rosenbaum et al., 2010; Maclean et al., 2011; Melby et al., 2017). These endocrine adaptations to chronically negative energy balance are believed to drive hyperphagia and the frequency and/or the size of meals in both humans and rodents (Kirchner et al., 2012; Karatsoreos et al., 2013; Catenacci et al., 2014) . Such altered levels of circulating hormones that facilitate weight regain after diet-induced weight loss appear to persist for at least 1 year (Sumithran et al., 2011; Camps et al., 2013). Accordingly, numerous attempts have tried to utilize hormone replacement interventions to combat weight-loss induced physiological adaptations, i.e. the increase in hunger and decrease in energy expenditure (Kelesidis et al., 2010; Kissileff et al., 2012; Trujillo et al., 2015; Vodnik et al., 2016). For instance, leptin replacement was considered as putative antidote against weight regain based on a clinical study that showed promising benefits of leptin replacement in weight loss patients, i.e. increases in sympathetic nerve system activity and a restoration of skeletal muscle work efficiency (Rosenbaum et al., 2005). Restored hypothalamic leptin sensitivity and the increased expression of the anorexigenic neuropeptide proopiomelanocortin were associated with a normalized energy homeostasis and weight maintenance in mice undergoing leptin replacement therapy (Chhabra et al., 2016). However, chronic leptin infusion studies in mice suggested that the weight maintenance is independent from leptin (Ravussin et al., 2014).

Adaptive physiological processes evolved mainly to defend body weight. In times of plenty, these physiological mechanisms fail to protect us from excessive weight gain. In times of starvation, they protect from life-threatening weight loss by increasing hunger and food reward behavior and decreasing energy expenditure. However, our adaptive physiology appears to mistake the desired weight loss after dieting as a sign of starvation, and is thus inducing the same physiological programs that were evolutionary programmed to defend our body weight. The signals that drive these changes may be hormonal, but their exact nature remains elusive. Nonetheless, the consequence is weight re-gain.

Limiting weight (re)gain by strict adherence to weight loss maintenance strategies appears to be key for 89% of weight losers who successfully maintained the lost weight. These strategies included high levels of physical activity and consuming a low calorie, low fat diet to in order to neutralize the physiological adaptions to weight loss, which center upon decreasing energy usage (adaptive thermogenesis) and increasing energy intake (overfeeding).

1.3. Physiological adaptations in response to overfeeding

Adaptive thermogenesis constitutes the regulated energy expenditure in response to environmental changes in temperature and/or diet, resulting in metabolic (in)efficiency. Adaptive thermogenesis protecting against weight gain after overfeeding is been known for years but much less studied than adaptive thermogenesis favoring weight regain after weight-loss. A study by Leibel and collaborators evidenced adaptive thermogenesis playing a role in both directions. In healthy and obese individuals under isocaloric conditions after overfeeding (10% weight gain) and underfeeding (10% weight loss), energy expenditure was increased and decreased respectively to maintain body weight (Leibel et al., 1995). A recent single-blinded randomized controlled trial in weight stable female and male subjects confirmed the increment on resting energy expenditure after 8-weeks overfed normal-protein or high-protein diets (Bray et al., 2012). Intriguingly, adaptive thermogenesis apparently compensated relative short to mid-term overfeeding. Healthy men overfed for 100 days experienced elevations in fat storage but concomitant increase in energy expenditure in proportion to their body weight, thus restoring the pre-overfeeding body weight when returning to normal daily-life habits after four months (Tremblay et al., 1992). Likewise,1.5 to 2 years after an initial 4-to-6-months overfeeding weight gain program the increases in weight in overfed individuals returned to the initial values without any further weight loss stimuli (Pasquet and Apfelbaum, 1994). Moreover, the degree of adaptive thermogenesis influenced variations in body weight. Energy expenditure measurements in healthy volunteers after 8 weeks in an overfeeding program showed considerable interindividual changes in correlation with the magnitude of body weight gain despite the same caloric ingestion and physical activity (Levine et al., 1999). Findings that similar caloric intake and physical activity drives different weight gain in a population, clearly pleaded for differences in dissipated energy as heat in those to resist weight gain.

It has been recognized for decades that energy expenditure is partially regulated by the SNS. Epinephrine or propranolol (ß-adrenergic antagonist) infusions in healthy individuals boosted or inhibited energy expenditure, respectively (Acheson et al., 1983). In this regard, hypoglycemia-induced elevations of norepinephrine and the hemodynamic-induced response were blunted in adrenalectomized patients compared to healthy participants (DeRosa and Cryer, 2004). In accordance, an overfeeding study in 12 pairs of identical twins identified a strong association between ß2-adrenergic receptor polymorphisms and the gain in subcutaneous fat and body weight (O et al., 2003; Ukkola and Bouchard, 2004). In support, ß-adrenergic triple-KO mice developed normophagic obesity and cold intolerance whilst ß3-adrenergic receptor-KO mice exhibited susceptibility to diet-induced obesity but normal cold-induced thermogenesis (Jimenez et al., 2002; Preite et al., 2016). ß-adrenergic receptors are tightly involved in the dissipation of energy as heat by uncoupling proteins in brown adipose tissue. Another factor counteracting overfeeding is satiety; increased satiety after overfeeding is well documented in humans and rodents. Normoweight subjects sensed positive energy intake when contrasted to reduced-obese individuals (Cornier et al., 2004). Individuals exhibiting weak satiety in response to food who consumed significantly more energy in *ad libitum* meals, displayed traits for increased overeating and future weight gain (Figure 2; (Drapeau et al., 2007; Dalton et al., 2015). Furthermore, homeostatic satiation was quickly overridden by hedonic reward instigating uncontrolled overfeeding (Mirch et al., 2006). A hyposensitive striatal reward system was likely to elevate the risk for overfeeding and weight gain. In this regard, genetic differences in the regulation of opioid and dopaminergic receptors were associated with the potential over-consumption of highly rewarding sweet-fat food and an elevated susceptibility for obesity (Stice et al., 2010; Davis et al., 2011).

Based on the evidence of physiological adaptations to control weight, the question arises about how long and far these mechanisms can buffer, or defend, a defined variation in body weight. It takes a considerable amount of time under constant positive-energy balance pressure to develop adiposity. This length in time also allows an individual´s biology to adapt to the new state of obesity (Corbett et al., 1986). This adaptive process defines a state in which energy expenditure and high energy intake are balanced to defend the newly gained weight and adiposity.

1.4. The set-point theory

Many hypotheses have been postulated regarding 'body weight points' and acting compensatory mechanisms. One of the most debated ones, the set-point or lipostatic theory, was first introduced by Kennedy in the early 50s (Kennedy, 1953). A fat derived signal, conveying the status of fat-depots, is sensed by the brain where it is compared to a target level, in order to trigger compensatory mechanisms upon any disturbance. This negative feedback loop was strongly supported by the discovery of leptin (Zhang et al., 1994), genetic mutations in leptin and the MC4R family (Farooqi et al., 1999; Farooqi and O'Rahilly, 2008) and the description of leptin resistance in diet-induced obese mice and obese humans (Maffei et al., 1995; Schwartz et al., 1996; Halaas et al., 1997; Friedman, 2016). However, in this past decade several studies questioned the existence of leptin resistance (Ottaway et al., 2015; Harrison et al., 2018; Pan and Myers Jr, 2018). Moreover, leptin infusion studies in mice revealed that hyperleptinemia is unlikely to define an obese body weight set point (Ravussin et al., 2014).

The set-point theory remains to be controversially discussed, with both reports corroborating a set point in human and animal studies, and multiple reports that find no experimental evidence for a set point (Halaas et al., 1997; Carhuatanta et al., 2011; Ravussin et al., 2014; Chhabra et al., 2016; Jansson et al., 2018). Yet, models describing single factors fail to fully explain the observed obesity epidemic. As an alternative concept, the dual intervention point theory uses two independent upper and lower weight levels as boundaries for active regulation. A lower weight boundary is indispensable to avoid starvation in times of low energy availability, and compensatory mechanisms that counteract starvation and weight loss are evolutionary conserved and privileged. An upper weight level was delimited by the risk of predation that required a certain leanness and fitness. However, around 2 Mio years ago early humans evolved enough to partially release the risk for predation (Speakman, 2018), which liberated the upper weight level and mechanisms that prevented from excessive weight and fat accumulation. The phenomenon, also described as genetic drift, has been suggested as a major driver for the obesity epidemic (Speakman, 2007). De Castro and Plunkett in 2002 (de Castro and Plunkett, 2002) proposed the multifactorial 'general model of intake regulation', which is based on uncompensated (environmental) and compensated (physiological) factors that affect food intake. Food intake only affects the compensated factors, mainly through negative feedback-loops. The responsiveness to each

factor is represented by weighing factors. The model does not use defined set points but malleable levels that provide stability under persistent perturbations to one or more factors. Hence, when transiting to a new stable level, a defensive behavior similar to a set point is observed (de Castro and Plunkett, 2002). Under environmental turmoil, i.e. under constant obesogenic pressure due to reduced activity and energy expenditure, the model accurately predicts a new higher level of body weight (de Castro and Plunkett, 2002).

1.5. Cellular heterogeneity in CNS control centers for body weight homeostasis

It is widely accepted that the central nervous system (CNS) regulates energy homeostasis and body weight via hedonic and homeostatic neuronal circuits that integrate higher brain functions with sensory information and peripheral cues such as hormones and nutrients. The hypothalamus positioned around a small ventral portion of the third ventricle serves as master regulator sensing soluble factors transported from the portal system through the median eminence and central signals coming from the hindbrain and the corticolimbic system (Waterson and Horvath, 2015). The hypothalamus consists of several distinct nuclei, including the arcuate nucleus (ARH), paraventricular nucleus of the hypothalamus (PVH), supraoptic nucleus (SON), suprachiasmatic nucleus (SCN), dorsomedial nucleus of the hypothalamus (DMH), ventromedial nucleus of the hypothalamus (VMH), and lateral hypothalamus area. Early studies found that lesions in the ventromedial hypothalamus (VMH) of the rat significantly increased feeding whereas those in the lateral hypothalamus (LH) led to the contrary effect and malnutrition (Anand and Brobeck, 1951; Anand et al., 1955). Such studies prompted the analysis for all other nuclei.
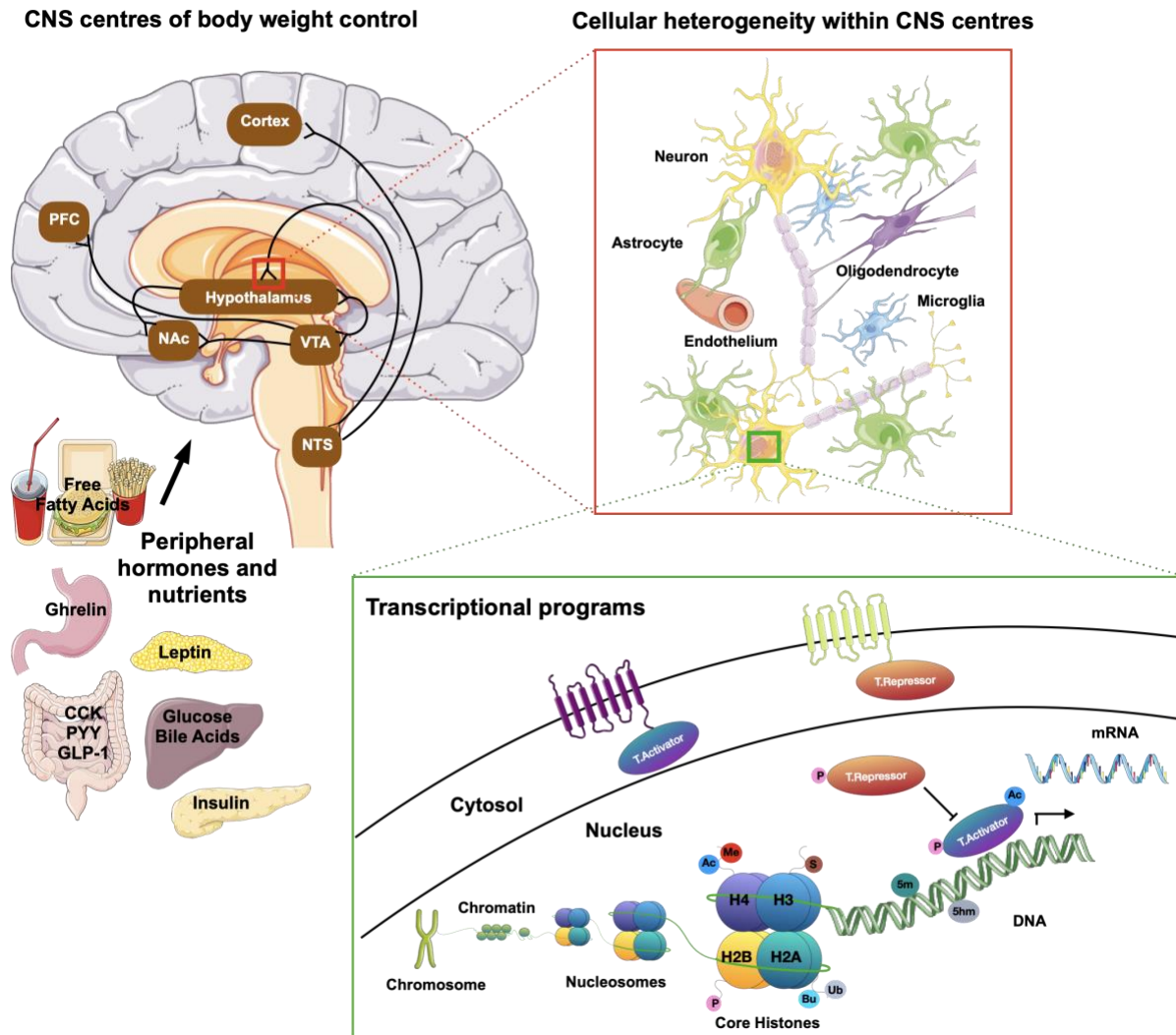
Figure 2. Anatomical, cellular and molecular heterogeneity in the CNS control of food intake and energy homeostasis.

Hormonal and nutrient cues from peripheral tissues signal the state of our dietary and energetic requirements to brain regions that govern our homeostatic and hedonic control of food intake and body weight. These neuronal circuits are deeply interconnected, and embedded within a network of vascular cells and highly diverse glial cell populations ranging from astrocytes to microglia and oligodendrocytes. The lineages and identities of these highly diverse neuronal and glial subpopulations are in part driven by variations in their transcriptional programs. Transcriptional programs are dictated by differences in the activation of transcriptional factor and epigenetic modifications such as DNA methylation and histone post-translation modifications. Ac, acetylation; Me, methylation-Ub, ubiquitination; P, propionylation; Bu, butyrylation and S, sumoylation; PFC, pre-frontal cortex; NAc, nucleus accumbens;

VTA, ventral tegmental area; NTS, nucleus of the solitary tract; CCK, cholecystokinin; PYY, peptide YY; GLP-1, glucagon-like peptide 1. Modified from (Contreras et al., 2019).

Deciphering the cell (sub)population that contribute to physiological adaptations is of utmost interest in such heterogenous tissue like the CNS. Numerous neuronal subpopulations are part of a complex and incompletely understood network that orchestrates our metabolic homeostasis. Next to neurons, there is a multitude of glial cell types, ranging from oligodendrocyte species to astrocyte and microglial subpopulations. These are embedded within a dense network of blood vessels with endothelial cells and pericytes, and form a functional blood brain barrier interface that plays a vital role in nutrient (e.g. glucose) and endocrine (e.g. insulin and leptin) sensing and the CNS control of feeding behavior and energy homeostasis as well as brain glucose uptake, Figure 3, (Kim et al., 2014; García-Cáceres et al., 2016).

All these cell types contain the same copy of the genome, but they greatly differ in the spatial and temporal expression of defined portions of the genome that define and drive the lineage of the respective cellular sub-population. Isolating RNA or DNA from a specific CNS cell type nonetheless remains a major experimental challenge due to the fragility and high interconnection. Accordingly, most of the research on adult CNS has been limited to the analysis of molecular mechanisms in bulk brain tissue. Pooling multiple cell types together likely masks cell type-specific variations and requires complex bioinformatical deconvolution algorithms. Gene co-expression modules, i.e. co-expressed genes of a cell type that are highly correlated to the proportion of the cell type in a sample and deduced from a large number of independent datasets, permit to determine core transcriptional features of specific cell-types (Kelley et al., 2018). However, whether they are universally applicable to specific brain-region and cell-type analyses remains underexplored.

1.6. Novel tools to disentangle the brain mosaic

In the past decades, several approaches were introduced to dissociate and isolate specific CNS populations for downstream molecular analyses. Fluorescence activated cell sorting (FACS) and magnetic activated cell sorting (MACS) in combination with specific antibody panels are now used since

more than 30 years to isolate the three main brain cell types, i.e. neurons, astrocytes and microglia (Paden et al., 1986; Martin et al., 2017; Contreras et al., 2019). However, working with fresh tissue requires enzymatic dissociation and a time-consuming sorting, which can result in low cell recovery and artefactual stress responses as well as gene expression patterns. Embryonal and neo-natal brains appear to be more suitable for FACS/MACS of whole cells, but the approach has also been used in adult rodents (García-Cáceres et al., 2016; Paeger et al., 2017). For instance, in post-natal forebrains, transcriptome profiling of FACS-sorted neurons, astrocytes and oligodendrocytes revealed common metabolic pathways, but also a high variety and several highly dissimilar sub-clusters within the glial cell class (Cahoy et al., 2008). Differences in transcriptome profiles are likely reflected by differences in gene regulation, as highlighted by specific cell-type DNA methylation profiling in hypothalamic post-natal neurons versus glia (Li et al., 2014).

The dissociation and isolation of nuclei from frozen or fixed tissue has shown the potential to overcome the challenges associated with isolating intact cells from fresh tissue (Jiang et al., 2008; Krishnaswami et al., 2016a). Depending on the cellular subtype, nuclei may express specific membrane-bound antigens such as NeuN (*Rbfox3*) or OLIG2 which mark them as neuronal or oligodendrocyte nuclei, respectively (Xu et al., 2018). By applying specific antibodies and FACS or MACS, these nuclear subpopulations can be sorted and characterized from adult brain tissues. Next to recent advances in methods and genetic tools to isolate CNS sub-populations, downstream next generation sequencing (NGS) applications have undergone major technological improvements to also allow molecular profiling of low input material. Regular high-throughput NGS protocols continue to require millions of cells, which goes beyond the typical yield achieved when working with small brain regions and rare cellular CNS sub-populations. However, in the last years single cell RNAseq (scRNA) became a new standard in the field and is now widely used to interrogate cellular identities and lineages of whole organisms (Plass et al., 2018), whole peripheral organs (Tritschler et al., 2017; Angelidis et al., 2019) or small brain regions (Zeisel et al., 2015; Lam et al., 2017; Moffitt et al., 2018). Recent findings using scRNA identified up 62 neuronal and 11 non-neuronal subclasses with distinct transcriptional signatures in the adult mouse hypothalamus and 24 distinct neuronal types in the ARH-ME (Campbell et al., 2017; Chen et al., 2017; Romanov et al., 2017). Therefore, developing new strategies for the analysis of specific cell

subpopulations in the brain is of greatest importance for detailed description of pathological mechanisms and the discovery of novel treatments for neurological disorders.

1.7. Histone deacetylases

In the last two decades, histone deacetylases were linked to the development or treatment of several metabolic and neurological diseases. Histone deacetylases (HDACs) are enzymes catalyzing the removal of acetyl functional groups from lysine residues in histones and non-histone proteins. In histones, acetylation occurs at the ε-amino group of lysine residues in the N-terminus of protruding tails, thereby neutralizing a positive charge. Chromatin thus changes its conformational state and the DNA becomes accessible for transcription factors to target genes. Transcription factors, heat-shock proteins and structural proteins were reported to undergo similar lysine deacetylation to alter diverse biological functions including DNA recognition, protein-protein interaction and protein stability (Seto and Yoshida, 2014). Overall, the acetylation state profoundly influences the biological function of a modified protein and has been proposed as a rival for phosphorylation based on its importance (Kouzarides, 2000).
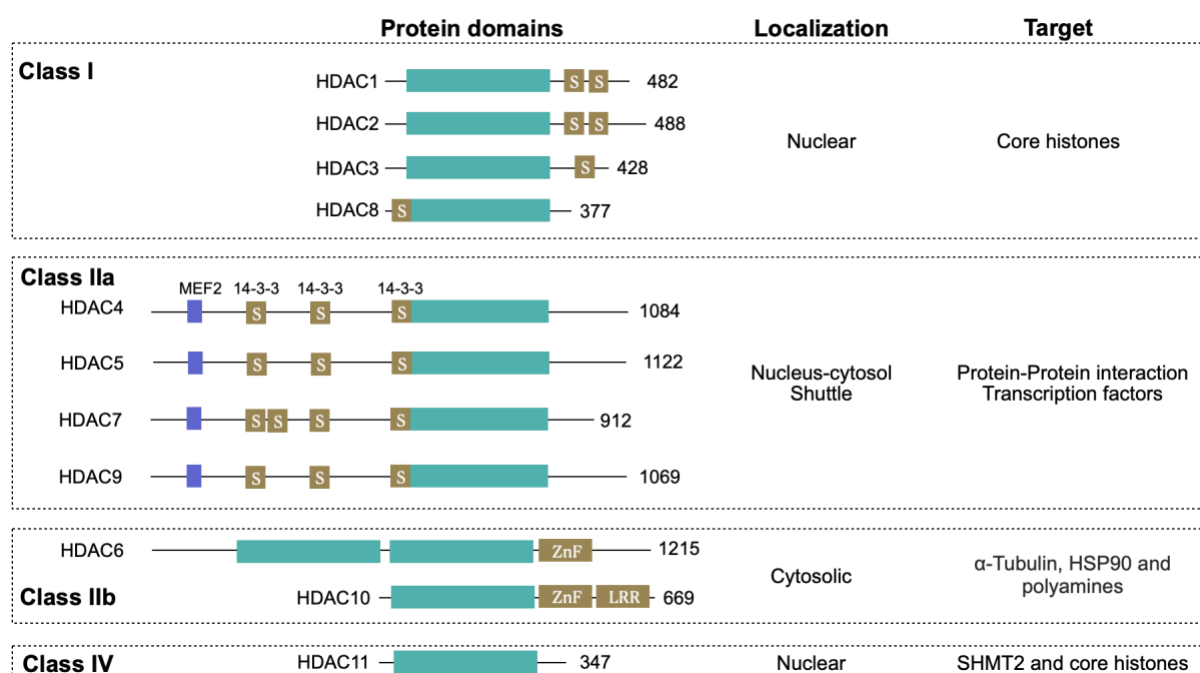
Figure 3. Protein domains, subcellular localization and described targets for the classical histone deacetylases (HDAC) classes.

Aquamarine rectangles depict the conserved HDAC domain, purple rectangles represent Myocyte enhancer factor 2 (MEF2)-binding domains and binding sites for 14-3-3 chaperon protein are depicted by brown rectangles. The length of the amino acid chain is shown at the end of each HDAC. Further depicted are the site of localization of the HDAC members, and their main targets. S, serine phosphorylation sites; ZnF, zinc finger; LRR, leucine rich domain; HSP90, heat-shock protein 90; SMHT2, serine hydroxymethyltransferase-2. Modified from (Haberland et al., 2009).

1.7.1. Histone deacetylase 5

HDACs are a superfamily divided into 4 classes and two families which possess a conserved deacetylase domain but differ in their global protein structure, enzymatic activity, subcellular localization and expression pattern (Figure 4). Classical HDACs comprise class I, IIa, IIb and IV and non-classical HDACs or class III comprise the sirtuins (Gallinari et al., 2007). All HDAC family members possess a catalytic conserved Tyr residue in the deacetylase domain except for vertebrate class IIa where the residue is replaced by His. The His residue is less effective in stabilizing a transition-state during the deacetylation reaction, reducing the catalytic efficiency 1000-fold when measured *in vitro* (Lahm et al., 2007). Subcellular localization is also particular depending on the class. Class I HDACs are devoted to

a nuclear localization forming part of corepressor complexes which reaffirms their high deacetylase activity toward core histones. Class IIb HDACs have a preferential cytosolic localization in accordance to their function on deacetylating α-tubulin, Hsp90 and polyamines (Hubbert et al., 2002; Kovacs et al., 2005; Hai et al., 2017). In contrast, class IIa HDACs shuttle between nucleus and cytosol serving as co-regulators at the occurrence of activating stimulus. Stimulus induced-shuttling is attributed to extra conserved motives in the N-terminus of this class. A binding motive for 14-3-3 enables the interaction with respective chaperones to facilitate nuclear export and a biding motive for MEF2, probably the most studied so far, converts MEF2 into a transcriptional repressor upon protein-protein interaction (Grozinger and Schreiber, 2000). Finally, class IV HDAC11 acts similar to class I HDACs, i.e. it has a nuclear localization with deacetylation and defatty-acylation enzymatic activity regulating immune activation and tumorigenesis (Villagra et al., 2009; Cao et al., 2019) (Figure 4).

Histone deacetylase 5 (HDAC5), a member of the class IIa family, is highly expressed in heart, muscle, bone marrow and lymphoid tissue and brain. HDAC5 contains 17 phospho-acceptor residues, suggesting a plethora of phosphorylation-dependent mechanisms that may affect the nuclear-cytosol shuttle function. Phosphorylation-dependent HDAC5-nuclear exporting has been implicated in the development of cardiac hypertrophy, in striatal reward mechanisms induced by cocaine, optic nerve regeneration after axon injury and glucose sensing and differentiation in skeletal muscle (Vega et al., 2004; Taniguchi et al., 2012; Meng et al., 2017; Pita-Thomas et al., 2019; He et al., 2020). HDAC5-nuclear export was associated with a de-repressive effect on transcription when HDAC5 was dissociated from MEF2 (Cho et al., 2013, 5; He et al., 2020, 2). Phosphorylated-HDAC5 separates from MEF2, which allows its subsequent interaction with the histone acetyl transferase (HAT) p300 to induce a switch from a transcriptional repressor to an activator of tissue specific transcriptional programs (McKinsey et al., 2000; Tian et al., 2020). The phosphorylation-dependent nuclear export of HDAC5, or HDAC5-ablation, further correlated with increased Histone 3 acetylation (H3-ac). Specifically, dephosphorylated nuclear HDAC5 associated with an activity-sensitive enhancer in *Npas4* to reduce H3-ac and negatively impact gene expression in the nucleus accumbens, which had an impact on cocaine conditioned place preference *in vivo* in HDAC5 KO mice (Taniguchi et al., 2017)*.* In myotubes with a viral knockdown of HDAC5-KD, lysine 9 of histone 3 was hyperacetylated (H3k9-ac) in the promoter regions of *Il-6* and *Slc2a4, which* augmented gene expression in response to electric pulse

stimulation (Klymenko et al., 2020). Increases in H3-ac are mediated by the interaction of HDAC5 with the corepressor complex NcoR-HDAC3, and requires phosphorylation at Ser269 in the nuclear localization signal (NLS) of HDAC5 (Greco et al., 2011; Kim et al., 2015). Our group reported STAT3 hyperacetylation at Lys685 and nuclear accumulation of HDAC5 in hypothalamic neuronal cells, which inhibited STAT3-phosphorylation, the transcriptional activation of *Pomc*, and hypothalamic leptin sensitivity (Kabra et al., 2016a). In summary, HDAC5 is known to repress tissue-specific transcriptional programs in response to physiological and environmental stimuli by versatile-mechanisms that involve the interaction with transcription factor and multiprotein repressor complexes.

2. Aims of the project

Histone deacetylase 5 (HDAC5) has been revealed as an important player in regulating skeletal muscle glucose utilization, addiction behavior and cancer cell proliferation (Cho et al., 2013, 5; He et al., 2020, 5). In 2016, my laboratory furthermore unraveled an important role of HDAC5 in controlling body weight and food intake in mice exposed to an obesogenic environment (Kabra et al., 2016a). However, whether HDAC5 is critical for perpetuating energy homeostasis in mice exposed to a non-obesogenic dietary environment remained unexplored. In this project, I thus aimed to explore the physiological role of HDAC5 in the regulation of energy homeostasis in male and female global HDAC5 WT and KO mice exposed to standard chow diet. Specifically, I aimed to delineate how HDAC5 deficiency affects central and peripheral mechanisms associated with the accurate maintenance of thermogenic energy expenditure, food consumption and body weight.

My thesis was built on the hypothesis that HDAC5 deficiency creates a positive energy balance even under non-obesogenic conditions. To interrogate the physiological mechanisms that drive a positive energy balance, I employed a range of state-of-the-art metabolic phenotyping techniques such as combined indirect calorimetry, infrared thermography, *ex vivo* assays, HPLC-ECD and immunodetections. Furthermore, I established and utilized two novel FACS techniques for the analysis of specific brain subpopulations. My major focus in elucidating the mechanistic underpinnings of energy control by HDAC5, also building on our earlier work on the topic (Kabra et al., 2016a), was directed toward the hypothalamus as master center for the homeostatic control of energy homeostasis. To decipher the mechanistic consequences of HDAC5 deletion on specific cell subpopulations in this brain region, I aimed to establish new techniques for the isolation and sorting of specific cell populations from adult murine brain samples that can be readily adapted also to other ongoing projects within my, or surrounding, laboratories.

3. Materials

3.1 Reagents

- µMACS G-protein MicroBeads, 130 071 101, Miltenyi Biotec.
- AccuGene 0.5 EDTA, 51201, SZABO SCANDI.
- AMPure XP beads, A63882, Beckman Coulter.
- Bovine Serum Albumin (BSA), 422361V, VWR.
- Clarity™ ECL substrate, 1705060, Bio-Rad
- Criterion™ TGX™ Precast Gels, 5671093, Bio-Rad.
- DABCO, 0718m Carl ROTH.
- Dithriothreitol (DTT), R0861, Thermo Fischer.
- D(+)-Saccharose, 4621.2, Carl ROTH.
- Dulbecco's Modified Eagle's Medium DMEM, 11880-028, Sigma-Aldrich
- Gelatin, Carl ROTH.
- Glycine, G7126-100G, Sigma-Aldrich.
- HALT™ (100X), phosphatase and protease inhibitor, 78429, Thermo Fischer.
- IGEPAL® CA-630, 18896-50ML, Sigma-Aldrich.
- Isoproterenol hydrochloride, 16504-100MG, Sigma-Aldrich.
- KCL (2M), AM9640G, Thermo Fisher.
- Methanol ≥99.9%, EMSURE® ACS, 1.06009.2500, VWR
- $MgCl_2$ (1M), AM9530G, Thermo Fisher.
- Mowiol 4-88, 0713, Carl ROTH.
- NaCl, 9265.1, Carl ROTH.
- NuPAGE™ LDS sample buffer, NP0008, Thermo Fischer.
- O.C.T, 4583, Tissue-TeK, Alphen aan den Rijn.
- PBS pH 7.4, 10010, Thermo Fischer.
- Penicillin-Streptomycin (PenStrep), 15140-122, Gibco / ThermoFischer.
- Phenyl-methane-sulfonylfluorid (PMSF), Carl ROTH.
- Restore™ Plus stripping buffer, 46430, Thermo Fischer.
- RNasin® Plus, N2111, Promega.
- Spermidine trihydrochloride, 85580-5G, Sigma-Aldrich.
- Spermine, S3256-1G, Sigma-Aldrich.
- SUPERase In™ (20U/µL), AM2694, Thermo Fischer.
- Trans-Blot Turbo 0.2µm PVDF Transfer Packs, 170-4157, Bio-Rad.
- Trans-Blot Turbo 0.2µm Nitrocellulose Transfer Packs, 170-4159, Bio-Rad.

- Triton X-100, T8532, Sigma-Aldrich.
- Tris (1M) pH 8, AM9855G, Thermo Fisher.
- Tris PUFFERAN® ≥99,9% p.a., 4855.2, Carl ROTH.
- Tween 20, P1379-500ML, Sigma-Aldrich.

3.2. Materials

- Large clearance Pestle A, 885301-0007, Kimble Chase.
- Large clearance Pestle B, 885302-0007, Kimble Chase.
- Low Protein binding collection tubes 1.5mL, 90410, Thermo Fischer.
- PluriStrainer mini 10µm, 43-10010-40, PluriSelect.
- SDS pellets, CN30.2, Carl ROTH.
- Tissue grinder (douncer) 7mL, 885303-0007, Kimble Chase.

3.3. Commercial kits

- Agilent RNA 6000 Pico kit, 5067-1513, Agilent.
- Free glycerol colorimetric assay kit, K630-100, Quimigen.
- Rat/Mouse growth hormone ELISA kit, EZRMGH-45K, Merk.
- Ultra-sensitive mouse insulin ELISA kit, 90082, Crystal Chem.
- Rat/Mouse leptin quantikine ELISA kit, MOB00, R&D Systems.
- LabAssay™ Cholesterol, Wako, FUJIFILM.
- LabAssay™ Tricylglyceride, Wako, FUJIFILM.
- Non-esterified fatty acids, NEFA-HR(2) Assay, Wako, FUJIFILM.
- Pierce™ BCA Protein Assay Kit, 23225, Thermo Fischer.
- Prolactin mouse ELISA, EMPRL, Life Technologies
- QuantiTect® Reverse Transcription Kit, 205311, QIAGEN.
- RNeasy Micro Kit, 74004, QIAGEN.
- SMART-Seq® v4 Ultra® Low Input RNA kit, 634888, Takara Bio USA, Inc.
- Tshb mouse ELISA, USC-CEA463MU-96, Biozol diagnostica.

3.4. Antibodies

- α-Tubulin, T5168-100UL, Sigma-Aldrich.
- β-Actin (C4), sc-47778, Santa Cruz Biotechnology.
- cFOS, 226-003, Synaptic Systems.
- Donkey anti-rabbit IgG-Alexa Fluor 568, A10042, Thermo Fischer.
- Donkey anti-mouse IgG-Alexa Fluor 488, A21202, Thermo Fischer.
- Donkey anti-goat IgG-Alexa Fluor 647, A21447, Thermo Fischer

- Donkey-anti-goat IgG-HRP, sc-2020, Santa Cruz Biotechnology.
- GAPDH (D6), sc-166545, Santa Cruz Biotechnology.
- Goat anti-rabbit IgG-HRP, A16096, Life Technologies.
- Goat-anti-mouse IgG-HRP, sc2005, Santa Cruz Biotechnology.
- HDAC5 (B-11), sc133106, Santa Cruz Biotechnology.
- Histone 3 (H3), ab1791, Abcam.
- HSL, 4107S, Cell Signaling.
- Mouse (G3A1) IgG1-isotype control, 5415S, Cell Signaling.
- NeuN-conjugated Alexa fluor® 488, MAB377X, Sigma-Aldrich.
- UCP1, ab10983, Abcam.
- p44/42 MAPK (Erk1/2), 9102S, Cell Signaling.
- Phospho-p44/42 MAPK (Erk1/2) (Thr202/Tyr204), 9101S, Cell Signaling.
- Phospho-HSL (Ser660), 4126S, Cell Signaling.
- Phospho-STAT5 (Tyr694), 9351S, Cell Signaling
- Phospho-TH (Ser40), 36 8600, Thermo Fischer.
- STAT5, 9363S, Cell Signaling.
- STAT5b, 13-5300, Thermo Fischer.
- Tyrosine hydroxylase, AB1542, Sigma-Aldrich.

3.5. Instruments

- ChemiDoc™ Imager, Bio-Rad.
- EcoMRI, E26-217M, EchoMRI.
- FACS-Aria III, BD Biosciences.
- FreeStyle™ Blood Glucometer, Abbot.
- FreeStyle™ Lite Blood Glucose Test strips, 70814-70, Abbot.
- Infrared camera PI450i, Optris Infrared measurements.
- Leica CM3050 Cryostat, Leica Biosystems.
- Leica TCS SP5, Leica Biosystems.
- NanoDrop 2000 Spectophotometer, Thermo Fischer.
- Perfusion pump, P720/66, Instech Laboratories.
- Tissue Lyser II, QIAGEN.
- Trans-Blot® Turbo™ Transfer system, Bio-Rad.
- Ultrasonic homogenizer, model 150V/T, Biologics Inc.
- Viia7 cycler, Applied Biosystems, Thermo Fischer.

3.6. Taqman assays

Table 1. Taqman assays for selected genes.

Gene name	Taqman assay
Adr2b	Mm02524224_s1
Adr3b	Mm02601819_g1
Adra2a	Mm07295458_s1
Agrp	Mm00475829_g1
Drd2	Mm00438545_m1
Fasn	Mm00662318_g1
Gh	Mm00433590_g1
Ghsr	Mm00616415_m1
Gfap	Mm01253033_m1
Hdac5	Mm01246076_m1
Hprt	Mm01545399_m1
Iba1	Mm00479862_g1
Lpl	Mm00434764_m1
Malat1	Mm01227912_s1
Pomc	Mm00435874_m1
Ppargc1a	Mm01208835_m1
Prdm16	Mm00712556_m1
Rbfox3	Mm01248771_m1
Slc6a3	Mm00438388_m1
Th	Mm00447557_m1
Ucp1	Mm01244861_m1

3.7. SYBR-green primers

Table 2. SYBR-green primer pairs for selected genes.

Gene name	Primer	5'-Primer Sequences-3'
Acc	Forward	CTAGTAGCTCTTACTTCCGGGAC
Acc	Reverse	GAAACTGGTCTCCCATGTTCAT
Atgl	Forward	CACAGCGCTGGTCACTGGGG
Atgl	Reverse	CCGGGCCTCCTTGGACACCT
Fasn	Forward	AGAGATCCCGAGACGCTTCT
Fasn	Reverse	GCTTGGTCCTTTGAAGTCGAAGA

Gad1	Forward	CACAGGTCACCCTCGATTTTT
	Reverse	ACCATCCAACGATCTCTCATC
Gad2	Forward	TCCGGCTTTTGGTCCTTCG
	Reverse	ATGCCGCCCGTGAACTTTT
Hsl	Forward	CCGTTCCTGCAGACTCTCTC
	Reverse	CCACGCAACTCTGGGTCTAT
Nr4a3	Forward	TGGACAAGAGACGCCGAAAC
	Reverse	TGGTTTGGAAGGCAGACGAC
Oxtr	Forward	GATCACGCTCGCCGTCTAC
	Reverse	CCGTCTTGAGTCGCAGATTC
Ppara	Forward	TACTGCCGTTTTCACAAGTGC
	Reverse	AGGTCGTGTTCACAGGTAAGA
Pparg	Forward	CCAGAGCATGGTGCCTTCGCT
	Reverse	CAGCAACCATTGGGTCAG
Prl	Forward	CAGGGGTCAGCCCAGAAAG
	Reverse	TCACCAGCGGAACAGATTGG
Prlr	Forward	CCACATTCCTGTGCTCATCCT
	Reverse	AGTCTGACTTACATGGTGTCCA
Tshb	Forward	TGGATAGGAGAGAGTGTGCC
	Reverse	GTGTCATACAATACCCAGCACAG

3.8. Genotyping primers

Table 3. Primers for the genotyping of AgRP-Cre, global HDAC5-KO and Sun1-sfGFP-myc mice.

Primers ID	5'-Primer sequences-3'
Cre	
1084	GCGGTCTGGCAGTAAAAACTATC
1085	GTGAAACAGCATTGCTGTCACTT
42	CTA GGCCACAGAATTGAAAGATCT
43	GTAGGTGGAAATTCTAGCATCATCC
HDAC5-KO	
LacZ 3'2:	GCCAGTTTGAGGGGACGACGACAGTATCG
HD5 gt 5':	CAAGGCCTTGTGCATGCTGGGCTGG
HD5 gt low 3'1:	CTGCTCCCGTAGCGCAGGGTCCATG
Sun1-sfGFP-Myc	
15020	CTGAACTTGTGGCCGTTTAC
24500	CAGGACAACGCCCACACA

36178	ACACTTGCCTCTACCGGTTC
oIMR9020	AAGGGAGCTGCAGTGGAGTA

4. Methods

4.1. Fluorescence-Activated Cell Sorting for brain samples

4.1.1. Fluorescence-Activated Cell Sorting for hypothalamic nuclei

Hypothalami were individually processed as previously described by (Krishnaswami et al., 2016b) with some modifications to the protocols. Briefly, frozen hypothalamic/MBH were transferred to a Dounce homogenizer containing 1mL of freshly prepared ice-cold nuclei isolation buffer (0.25M sucrose, 25mM KCl, 5mM MgCl2, 20mM Tris pH 8.0, 0.4% IGEPAL 630, 1mM DTT, 0.15mM spermine, 0.5mM spermidine, 1x phosphatase & protease inhibitors, 0.4 units RNasin Plus RNase Inhibitor, 0.2 units SuperAsin RNase inhibitor). Homogenization was achieved by carefully douncing 10 strokes with the loose pestle, incubating on ice for 5 min and further doucing 15 more strokes with the tight pestle. The homogenate was filtered through a 20µm cell strainer, centrifuged at 1000 x g for 10min at 4°C, the nuclei pellet resuspended in 450µl of staining buffer (PBS, 0.15mM spermine, 0.5mM spermidine, 0.4 units RNasin Plus RNase Inhibitor, 0.4% IGEPAL-630, 0.5% BSA) and incubated for 15min on ice to allow blocking of unspecific binding. Staining was achieved by adding 50µl of Anti-NeuN AlexaFlour-488 or IgG-isotype control (1:100 in staining buffer) and incubating for 30min in dark at 4°C. Unbound antibody was washed with one volume of staining buffer and centrifuged at 1000 x g for 5min at 4°C. Nuclei pellet was resuspended in 1mL of fresh staining buffer supplemented with DAPI 1µg/µL. Nuclei integrity was assessed in the DAPI channel under a Zeiss microscope (Axio Scope, Zeiss, Germany). We employed FACS with a 70µm nozzle for nuclei sorting. Doublet discrimination and DAPI staining were used for appropriate gating of single nuclei and the signal on the green (FITC) channel on the IgG-isotype control determined the adequate gating of NeuN⁻ and NeuN⁺ nuclei. Positive and negative fractions were sorted into cold RLT buffer supplemented with DTT, immediately frozen and stored at -80°C until RNA extraction.

4.1.2. Fluorescence-Activated Cell Sorting for Sun1-sfGFP-Myc-tagged nuclei

For the establishment of FACS for Sun1-sfGFP-Myc tagged nuclei, Sun1-sfGFP-Myc$^+$ mice (INTACT mice) were crossed with AgRP-Cre$^+$ mice to generate heterozygous mice (*Agrp-Cre::R26-CAG-LSL-Sun1-sfGFP-Myc*) in which Cre-recombination occurred only in AgRP expressing neurons (Tong et al., 2008; Deal and Henikoff, 2011). Medial basal hypothalamus samples were individually transferred to a dounce homogenizer containing 1mL of freshly prepared ice-cold nuclei isolation buffer. Homogenization was achieved by carefully douncing 10 strokes with the loose pestle, incubating on ice for 5 min and further doucing 15 more strokes with the tight pestle. The homogenate was filtered through a 20µm cell strainer, centrifuged at 1000 x g for 10min at 4°C, and the nuclei pellet was resuspended in 500µl of staining buffer supplemented with DAPI 1µg/µL. Sorting was performed as previously described for whole hypothalamus samples but the signal on the green (FITC) channel was determined by using a AgRP-Cre$^-$ sample as a negative control.

4.1.3. Fluorescence-Activated Cell Sorting and Magnetic-Activated Cell Sorting for astrocytes

In order to validate the efficient deletion of exon 2 in *HIF-1α$^{loxP/loxP}$* mice, dual fluorescent reporter mice (*HIF-1α$^{loxP/loxP}$::hGFAP.CreER^{T2}::ROSA26$^{mT/mG}$*) were generated. Cre-mediated recombination was induced by tamoxifen injection at the age of 6 weeks (10 mg/5 d). At 12 weeks of age, mice were sacrificed, their brains were rapidly removed and one hemisphere, respectively, subjected to magnetic-bead assisted cell sorting (MACS) enrichment using the astrocyte-specific surface marker ACSA-2. ACSA-2$^+$ astrocytes were enriched according to a commercially available standard protocol (Isolation and Cultivation of Astrocytes from Adult Mouse Brain; Miltenyi Biotec) using LS columns and an elution volume of 1 mL PBS. Single cell suspensions were then rapidly subjected to FACS. Accurate sorting for tdTomato$^-$ EGFP$^+$ ACSA-2$^+$ cells was achieved by gating EGFP$^+$ and EGFP$^-$ on a non-tamoxifen injected littermate reporter mouse (tdTomato$^+$ EGFP$^-$ ACSA-2$^+$) and a non-fluorescent C57BL6J wildtype mouse (tdTomato$^-$ EGFP$^-$ ACSA-2$^+$). Sorting was performed using FACS with the 85 µm nozzle. For optimal visualization of all ACSA-2+ astrocytes, logarithmic scales and low acquisition voltages (75 and 190) were implemented for forward scatter (FSC) and side scatter (SSC) plots,

respectively. Sorted cells were collected in cold PBS, pelleted by centrifugation for 5 min at 600 x g and 4°C, resuspended in RLT buffer supplemented with 0.4 mM DTT and stored at -80°C until RNA extraction.

4.2. Animal experiments

4.2.1. HDAC5-KO animal model and body composition

Global HDAC5 KO mice with excision of coding exons 3 to 7 for a lacZ-neomycin resistance cassette were derived from breeding of HDAC5 heterozygous mice with pure C57BL/6J background as described previously (Kabra et al., 2016). All experiments were conducted in 4 months aged-matched WT and HDAC5-KO mice. All mice were group-housed on a 12:12-h light-dark cycle at 23 °C and *ad libitum* fed on standard chow diet, unless differently indicated. Fat mass and lean mass were measured via whole body Nuclear Magnetic Resonance (NMR) technology (EchoMRI, Houston, TX, USA). All procedures involving animal handling were approved by the committee for Care and Use of Laboratory Animals of the Government of Upper Bavaria, Germany.

4.2.2. Genotyping of mouse lines

Eartags were notched from mice at weaning (21 days old) and DNA was isolated by boiling the eartags for 60 min in 100 µl 50 mM NaOH at 95 °C (ThermoMixer C, Eppendorf). 10µl 1 M Tris was added to neutralize the reaction. 2µl of isolated genomic DNA was used for the genotyping PCR (Promega) using respective protocols in the following tables. A list of primers is given in table 3. Tables 4 to 9 depict the Master Mixes and PCR conditions for the three mouse lines.

Table 4. Master mix for Cre-PCR.

Master Mix	Concentration	Volumen (µL)
MilliQ H_2O		4,00
Rx buffer	5X	3,00
MgCl2	25mM	1,28
dNTP	10mM	0,32
Cre primer 1084	20µM	0,32

Cre primer 1085	20µM	0,32
Cre primer 42	20µM	0,32
Cre primer 43	20µM	0,32
Betaine (sigma)	5M	3,00
Promega Go-Taq flexi	5U/µl	0,13
cDNA		2

Table 5. PCR protocol for Cre-PCR.

Step	Temperature [°C]	Time	N° cycles
Initial denaturation	94	3 min	1
Denaturation	94	45 s	
Annealing	60	45 s	36
Elongation	72	1 min	
Final elongation	72	2 min	1
Hold	4	∞	

Table 6. Master mix for Sun1-sf-GFP-Myc PCR.

Master Mix	Concentration	Volumen (µL)
MilliQ H_2O		3,60
Rx buffer	5X	3,90
MgCl2	25mM	1,55
dNTP	10mM	0,39
15020	20µM	0,38
24500	20µM	0,38
36178	20µM	0,38
olMR9020	20µM	0,38
Glycerol	50%	1,95
Promega Go-Taq flexi	5U/µl	0,09
cDNA		2

Table 7. PCR protocol for Sun1-sfGFP-Myc mice.

Step	Temperature [°C]	Time	N° cycles
Initial denaturation	94	3 min	1
Denaturation	94	45 s	
Annealing	60	45 s	36
Elongation	72	1 min	
Final elongation	72	2 min	1
Hold	4	∞	

Table 8. Master Mix for HDAC5-KO mouse genotyping.

Master Mix	Concentration	Volumen (µL)
MilliQ H$_2$0		7,18
Rx buffer	5X	3,00
MgCl2	25mM	1,20
dNTP	10mM	0,30
HD5 gt 5' primer	20µM	0,60
HD5 gt low 3'-1	20µM	0,30
LacZ 3'-2	20µM	0,30
Promega Go-Taq flexi	5U/µl	0,12
cDNA		2

Table 9. PCR protocol for HDAC5-KO mice.

Step	Temperature [°C]	Time	N° cycles
Initial denaturation	95	4 min	1
Denaturation	95	30 s	
Annealing	62	30 s	35
Elongation	72	45 min	
Final elongation	72	5 min	1
Hold	4	∞	

4.2.3. Metabolic cages and cold exposure (TSE)

Mice were single housed inside the metabolic cages in the TSE. An acclimation period of 48h was required for mice to adapt to the new environment. The system was calibrated for a gas reference of 20.9% O_2, 0.05% CO_2 and 79.05% N_2 previous to start measurements. Subsequently, measurements for O_2 and CO_2 along with heat, locomotor activity and food and drink intake were recorded every 10 min for 72 h at 24°C.

For cold exposure, the system was similarly calibrated but the metabolic cages were acclimatized to 4°C and the mice were individually place per cage for 5h with measurements of 10 min per unit of time.

4.2.4. Infrared measurement of brown adipose tissue temperature

Mice were individually placed inside a cage under the infrared camera which was fixed to a tripod. One video per animal was recorded, always taking care to have good visibility of the BAT in the extended position when mice were on moving. Subsequently on the software Optris PI connect™, we set the measurement for mean value and emissivity = 1.0. The region of interest (ROI) for BAT was defined in the intrascapular region of each mouse.

4.3. Post-mortem analyses

4.3.1 Tissue collection

Prior to sacrifice, mice were fasted for 6h and glycemia was measured by sampling blood from the tail vein with a handheld glucometer. Rapidly after cervical dislocation, blood was taken in EDTA-coated syringes, and centrifuged at 2,000 x g for 10 min at 4°C to separate the plasma. Rapidly, the skull bone was cut open and the brain lifted. The exposed pituitary gland was extracted from the *sella turcica* and the hypothalamus was dissected from the base of brain. The pre-frontal cortex (PFC), striatum and ventral tegmental area (VTA) were thoroughly punched from coronal slices using anatomical references for guidance. Brown adipose tissue was dissected from the intrascapular region following the characteristic butterfly-shape and cleaning surrounding WAT. Subcutaneous adipose tissue was

dissected by carefully peeling back the skin from the peritoneal cavity and the leg to find it associated with the skin. Finally, eWAT was dissected from the testis and carefully cleaned from seminal ducts. All samples were snap frozen in liquid nitrogen and stored at -80°C.

4.3.2. Blood chemistry

4.3.2.1. Enzymatic assays

Plasma triglycerides, cholesterol and non-esterified fatty acids were measured by commercial enzymatic colorimetric assay kits (Wako Chemicals, Neuss, Germany). Insulin, leptin, prolactin, GH and TSHb were measured using murine sandwich (capture) ELISA kits. All assays were performed according to the manufacturer's instructions. Homeostatic model assessment for insulin resistance (HOMA-IR) was calculated using the formula: HOMA-IR = [fasting serum glucose × fasting serum insulin/22.5] (Turner et al., 1979).

4.3.2.2. tT4 and tT3 measurement by LC-MS/MS (collaboration)

Thyroid hormones in mouse plasma were analyzed and detected with an UPLC system coupled with a triple quadrupole (QQQ) mass detector. The conditions employed for the elution and quantification were already described for the detection of thyroid hormones in breast milk (Li et al., 2020). The sample clean-up was performed according to the following protocol: 40-50 µL of mouse plasma was mixed with 60 µL of internal standard (10 pg/µL) and an antioxidant solution (0.15 mL; 25 mg ascorbic acid + 25 mg citric acid + 25 mg dithiothreitol in 1 mL H_2O). The mixture was vortexed for 10 sec and equilibrated for 1h at 0° C. Subsequently, 25 µL of $ZnCl_2$ (2M in H_2O) and 200 µL of CH_3OH were added and additionally incubated for 30 min at 0° C for. Then, the sample was centrifuged at 7000 g for 10 min and supernatant collected. The solid residue was further resuspended in a solution of $CH_3OH:H_2O$ ((1:1), 0.2 mL), centrifuged, and then extracted as described before. Chloroform (0.6 mL) was added to the combined extracts and the mixture was centrifuged again (7000 x g, 10 min). The upper level was decanted while the lower phase was re-extracted ($CH_3OH:H_2O$ 1:1, 0.2 mL). The pooled upper phases were diluted with 1.5 mL pure water. Phosphoric acid was added to reach a final concentration of 2%, followed by the addition of the antioxidant solution (0.2 mL). After vortexing, the mixture was loaded

onto a Bond Elut Plexa PCX cartridge, which was preconditioned sequentially with 1.5 mL of pure MeOH and 1.5 mL of water. The cartridge was first washed with 2 mL of 2% formic acid in water and then with 2 mL of MeOH: acetonitrile (1:1, v/v). Analytes were eluted into a vial with 1 mL of 5% ammonium hydroxide in MeOH: acetonitrile (1:1, v/v). The solvent was evaporated and the compounds re-dissolved in 60 µL of a mixture of 20% acetonitrile in water containing 0.1% formic acid for instrumental analysis.

4.3.2.3. *Ex vivo* lipolysis assay in white adipose tissue

Mice were euthanized by cervical dislocation and eWAT was dissected and cut into small pieces. On a precision balance, eWAT pieces ranging 3-5mg were selected, transferred one per well into a 96-well plate containing 250µl of pre-warmed (37ºC) assay medium (DMEM supplemented with 2%BSA and 1% Pen/Strep). The plate was incubated for 30 min at 37ºC to allow equilibration of the tissue. Then, eWAT pieces were transferred into another 96-well plate containing 250µl of pre-warmed (37ºC) stimulation medium (assay medium supplemented with 1µM isoproterenol or DMSO) and incubated for 3 hours at 37ºC in 5% CO_2. Following the stimulation, each piece was moved to a fresh tube for delipidation containing 1mL of chloroform methanol (2:1) and incubated for 1 hour at 37ºC in a thermomixer at 300rpm. The plate containing the stimulation medium was covered, sealed and stored at -20ºC for later measurements. Delipidated samples were passed on to a fresh tube filled with 700µl of 0.3n NaOH and 0.1% SDS and incubated overnight at 40ºC in a thermomixer at 600rpm. The following day, protein concentration was measured from each sample using BCA protein assay. Finally, lipolysis was calculated by measuring free glycerol from the stimulation medium with a free glycerol determination kit and normalizing these values to the respective protein concentrations.

4.3.3. Monoamine measurement by HPLC-ECD (collaboration)
4.3.3.1. Adipose tissue monoamines

Adipose tissue monoamines were analyzed and detected with a HPLC system coupled with electrochemical detection (ECD) as described previously (Nagler et al., 2018). Briefly, adipose tissue (eWAT, 100–120 mg or BAT 50-70 mg) was homogenized in 200 µL of 0.3 M $HclO_4$ and 4 µL of DHBA (IS) by ultrasonication on ice for 30s. Homogenates were centrifuged at 8000 x g for 10 min. The

solution was collected with a 1 mL syringe and a cannula without disrupting the top fat layer. To remove traces of fat, samples were filtered through a 0.2 µm filter (Whatman, P/N 6784-0402). The filtrate was collected in a sample vial and injected into the system.

4.3.3.2. Brain monoamines

Brain monoamines were similarly analyzed and detected with a HPLC-ECD as described previously (Nagler et al., 2018). Sample clean-up was performed according to the protocol for extraction of monoamines from mouse hypothalamus. Briefly, samples (10-15mg) were individually homogenized in 200 µl of 0.3 M $HClO_4$ and 4 µL of DHBA 1 ng/µL (internal standard) via ultrasonication (Bandelin Electronics, UW-70) on ice for 30s. Homogenate was centrifuged at 7000 x g for 10 min at 4°C and then 20 µL of the supernatant was directly injected into a HPLC-ECD system.

4.4. Immunofluorescence in brain slices

4.4.1. Brain collection and sectioning

For preparing immunostaining on brain slices, mice were euthanized with CO_2 and perfused through the heart using a peristaltic pump. After a washing step with ice cold PBS, animals were perfused with 4 % paraformaldehyde (PFA). Brains were post-fixed overnight in 4% PFA at 4°C, followed by equilibration with 30% sucrose in Tris-buffered saline (TBS, pH 7.2) for 48 h before sectioning into 30 µm coronal slices using a cryostat (CM3050S; Leica, Germany). Per mouse, three to four brain sections containing the middle portion of the MBH were selected and subjected to immunostaining.

4.4.2. Immunostaining for brain slices

Brains sections were first washed with TBS, incubated in 0.1M glycine for 30 min with agitation at room temperature and then washed three times with TBS. Subsequently, slices were incubated overnight at 4°C with primary antibodies (anti-TH, anti-cFOS and anti-NeuN diluted 1:1000) in a solution containing 0.25% porcine gelatine and 0.5% Triton X-100 in TBS, pH 7.2. The following day, sections were rinsed three times in TBS, pH 7.2, and incubated with respective secondary antibodies (anti-goat AlexaFluor-647, anti-rabbit AlexaFluor-568 and anti-mouse AlexaFluor-488, diluted 1:5000) diluted in TBS, pH 7.2

containing 0.25% porcine gelatine and 0.5% Triton X-100 for 2h. Sections were serially washed three times in TBS with the last washing additionally containing DAPI (2 µg/ml in TBS, pH 7.2). Sections were covered in Elvanol mounting medium (150mM Tris, 12% Mowiol 4-88, 2% DABCO) and sealed under a coverslip. Acquisition was performed on a Leica SP5.

4.5. Gene and protein expression analyses

4.5.1. Low-input RNA isolation and gene expression analysis

RNA from all sorted samples was isolated using the RNeasy Micro Kit and measured with the Agilent RNA 6000 Pico Kit following manufacturer's indications. RNA concentrations were adjusted and 1- 3ng was used as input for cDNA synthesis employing the SMART-Seq V4 Ultra® Low Input RNA kit. Gene expression was quantified using validated SYBR-green primers or TaqMan probes **(tables 4 to 9)** in a ViiATM7 Real Time PCR System. Differential gene expression was calculated using the 2-ΔΔCt method normalized to the housekeeping gene *Malat1* or *Hprt* for sorted nuclei or astrocytes respectively.

4.5.2. General RNA isolation and qRT-PCR

Each pituitary was homogenized in RA1 buffer supplemented with DTT with a sonicator in on ice in sonicator in two pulses of 40% potency for 30 sec at low power and RNA was isolated using the NucleoSpin RNA isolation kit following manufacturer's instructions. For eWAT, tissue was pulverized, 50mg was weighed, and further homogenized in 500µl of Qiazol lysis reagent in a Tissue Lyser II for 3 min at 30/sec. After a 5 min incubation at RT, 100µl chloroform was added to each sample, vigorously mixed and incubated for another 3 min at RT. Centrifugation at 12000 x g for 15 min at 4ºC resolved the different phases and supernatant was used for RNA isolation using the NucleoSpin RNA isolation kit. Subsequently, RNA concentrations were measured on a Nanodrop and 1µg of RNA per sample was reverse-transcribed into cDNA using QuantiTect® Reverse Transcription Kit. Gene expression was quantified using validated SYBR-green primers or TaqMan probes, **Tables 1 & 2,** in a ViiATM7 Real Time PCR System. Differential gene expression was calculated using the 2-ΔΔCt method normalized to the housekeeping gene *Hprt*.

4.5.3. Protein extraction from adipose tissue

On a mortar filled with liquid nitrogen, adipose tissue (BAT or eWAT) was carefully pulverized. Then 30-40mg of tissue-powder was weighed and lysed in 400µl RIPA buffer supplemented with 1% phosphatase and protease Inhibitor Cocktail and 1 mM phenyl-methane-sulfonylfluorid (PMSF) in a Tissue Lyser II for 3 min at 30/sec in pre-cooled racks. Lysates were then cleared by centrifugation at 12,000 x g for 10 min at 4ºC and supernatants were collected and stored at -80ºC until further processing.

4.5.4. Protein extraction from ARH micro-punches

Arcuate nucleus was micro-punched from 1mm fresh brain slices and flash-frozen in liquid nitrogen. ARH micro-punches were lysed in 50µl of RIPA buffer supplemented with 1% phosphatase and protease Inhibitor Cocktail and 1 mM phenyl-methane-sulfonylfluorid (PMSF) on ice in sonicator in two pulses of 40% potency for 30 sec at low power. Lysates were stored at -80ºC until further processing.

4.5.6. SDS-PAGE and western blot

Protein concentrations were measured using BCA protein assay. Concentrations were adjusted in order to load 10 µg per well, complemented with Laemmli loading buffer plus 5% DTT (sampling buffer), denatured by heating at 95°C for 5 min and separated on 4-20 % gradient CriterionTM TGXTM Precast Gels. Proteins were transferred to nitrocellulose membranes using a Trans-Blot® Turbo™ (BioRad) set to the mix molecular weight program. Transferred-membranes were blocked with 5% BSA diluted in TBS with 0.1% Tween20 (TBS-T) for one hour with agitation at RT and incubated with the desired primary antibodies overnight at 4°C with agitation. The following day, membranes were washed 5 times in TBS-T for 5 min at RT and incubated with the respective HRP-coupled secondary antibodies for one hour at room temperature with agitation. Washing step was repeated 5 times prior to protein detection with ECL clarity for HRP-induced chemiluminescence inside a ChemiDoc. When necessary, membranes were stripped with pre-warmed (37ºC) Restore PLUS Western Blot Stripping Buffer for 15 min, re-blocked for 1 h, and blotted with the desired antibodies. Densitometric analyses of the bands were performed with NIH FIJI software, and arbitrary units were normalized to appropriate controls.

4.5.7. Co-immunoprecipitation assay

Individual hypothalami were transferred to a dounce homogenizer containing 1mL of freshly prepared ice-cold immunoprecipitation (IP) buffer (50mM Tris pH 8.0, 1% IGEPAL-630, 150mM NaCl, 1mM PMSF, 1mM sodium butyrate, 1x phosphatase & protease inhibitors). Homogenization was achieved by carefully douncing 30 strokes with the loose pestle, incubating on ice for 10 min and further doucing 30 more strokes with the tight pestle. The homogenate was filtered through a 20µm cell strainer and incubated for 30 min with agitation at 4ºC. Protein concentration was measured by BCA protein assay and adjusted to 0.7 µg/µl. Per sample, 1 mL of protein lysate was incubated with 1.0µg of antibody (anti-STAT5b, anti-HDAC5, or IgG-isotype control) in Lo binding tubes for 4 hours at 4°C while rotating. Then, 50µl of µMACS protein-G µBeads were added per sample and incubated for another 30 min at 4 °C with rotation. All further steps were performed at 4°C and the IP was performed according to the manufacturer's protocol. Proteins were eluted in 40 µl of preheated (95 °C) sampling buffer, separated by SDS-PAGE and transferred to a PVDF membrane for western blotting as previously described in section 4.5.6. After blocking, membranes were first incubated with the respective Co-IP protein (anti-STAT5b or anti-HDAC5, diluted 1:1000 in blocking buffer) over-night at 4ºC with agitation. The following steps were performed as previously described. After detection of Co-IP proteins, membranes were stripped and blotted for the respective IP proteins (anti-STAT5b or anti-HDAC5, diluted 1:5000 in blocking buffer) following the same previous protocol.

4.5.7. Sub-cellular fractioning

Individual hypothalami were homogenized as previously described for nuclei isolation in section 4.1.1. with the only difference of reducing the homogenization buffer volume to 400µl. The homogenate was filtered through a 20µm cell strainer and centrifuged at 1000 x g for 10min at 4°C. Supernatant was collected on a new tube and nuclei pellet resuspended in 300µl of nuclear lysis buffer (50mM Tris pH 8.0, 1% IGEPAL-630, 0.5mM sodium deoxycholate, 1mM PMSF, 1mM sodium butyrate, 1x phosphatase and protease inhibitors). The first representing the cytosolic fraction and the later the nuclear fraction. Protein concentration measurement and subsequent steps were performed as previously described for SDS-PAGE and western blotting. Histone 3 (H3) was used as loading control for nuclear fractions and GAPDH served the same role for cytosolic fractions.

4.8. Statistical analysis

All statistical analyses were performed using GraphPad Prism. Two-tailed unpaired Student's t-test was applied for comparisons between two groups while one- or two-way analysis of variances (ANOVA) corrected by Bonferroni *post-hoc* tests were performed for multiple comparisons when appropriate. Statistically significant outliers in datasets were detected using the Grubb's test. Statistically significant differences were considered by $p \leq 0.05$. All data is presented as mean ± standard error of the mean (SEM).

5. Results

5.1. Fluorescence-activated sorting of cellular sub-populations from brain tissue

Isolation of specific (sub) populations from heterogenous tissues is of critical importance to correctly assign cellular and molecular mechanisms to relevant *in vivo* physiological pathways. Here, we established three different approaches for the study of specific (sub) population from mouse brain tissue. First, we transferred a nuclei isolation technique reported for frozen normal human cortical brain tissue to frozen mouse hypothalamus (Krishnaswami et al., 2016). To limited mRNA degradation and further damage of nuclei after freeze-thawing, the iodixanol centrifugation-based purification was omitted and thorough but delicate resuspension was assured. Their NeuN staining protocol required two consecutive staining steps including primary staining with anti-NeuN antibody followed by secondary staining with secondary-labeled antibody. In order to reduce incubation times and further damage, we thus separately tested two customized anti-NeuN antibodies coupled to Alexa Fluor®-488 or Alexa Fluor®-647 from Abcam. The best separation between NeuN$^+$ and NeuN$^-$ populations was achieved with anti-NeuN-Alexa Fluor®488 (Figure 5, A). Using anti-NeuN-Alexa Fluor®647 did not yield a clear separation between NeuN$^+$ and NeuN$^-$ populations (data not shown). Validation for the sorted samples was carried out by isolation and reverse-transcription of mRNA into cDNA using the SMART-seq® V4 Ultra ® Low input RNA kit and ultimately qPCR gene enrichment analysis. Supporting the accurate gating for FACS, NeuN$^+$ fractions were significantly enriched in *Rbfox3* (NeuN), *Agrp* and *Pomc*, the two latter genes being neuronal hypothalamic specific markers and NeuN$^-$ fractions were enriched in *Gfap* -an astrocyitic marker; *Aif1* – a microglial marker was not enriched in any fraction, (Figure 5, A) (Deng et al., 2020). Second, we scaled-down the INTACT protocol using a pool of two neocortices to the aforementioned FACS pipeline using one single hypothalamus (Mo et al., 2015). For this purpose we produced a *Agrp-Cre::R26-CAG-LSL-Sun1-sfGFP-Myc* and instead of staining against NeuN, we stained for Myc with anti-Myc coupled Alexa Fluor®-647 and took advantage of the enhanced brightness in the superfolder GFP (sfGFP) within the *R26-CAG-LSL-Sun1-sfGFP-Myc* cassette

(Pédelacq et al., 2006; Mo et al., 2015)**.** Successfully, the number of recorded events was similar between sfGFP[+] and Myc[+] nuclei, and the separation of respective negative populations was comparable between both markers (Figure 6, B). Sorting validation was conducted similarly to the FACS pipeline for NeuN, showing enrichment only of *Agrp* in the sfGFP[+] fraction. Third, to tagged specific astrocyte subpopulations, we used a previously described mouse line carrying the dual reporter cassette *mT/mG (loxP-mT-pA-LoxP-mG-pA*) (Muzumdar et al., 2007)*.* In the absence of Cre, all cells in this mouse line express a cytoplasmic membrane tagged version of tdTomato (mT) but when crossing it with a Cre[+] line, Cre^{+} cells express a cytoplasmic membrane tagged version of EGFP (mG) instead. We used ACSA-2^{+} MACS pre-enriched astrocytes from the mouse line *HIF-1α^{loxP/loxP}::hGFAP.CreER^{T2}::ROSA26^{mT/mG}* for FACS. The 85μm nozzle and the logarithmic scale the FSC-A and SSC-A channels allowed the clear identification of astrocytes based on their size and complexity and gating for GFP[+] and GFP[-] was achieved by analysis of a non-recombined sample. Gene expression analysis revealed the rightful deletion of exon 2 of *HIF-1α* in Cre-recombined GFP[+] astrocytes compared to non-recombined GFP[-] astrocytes (Figure 5, C)
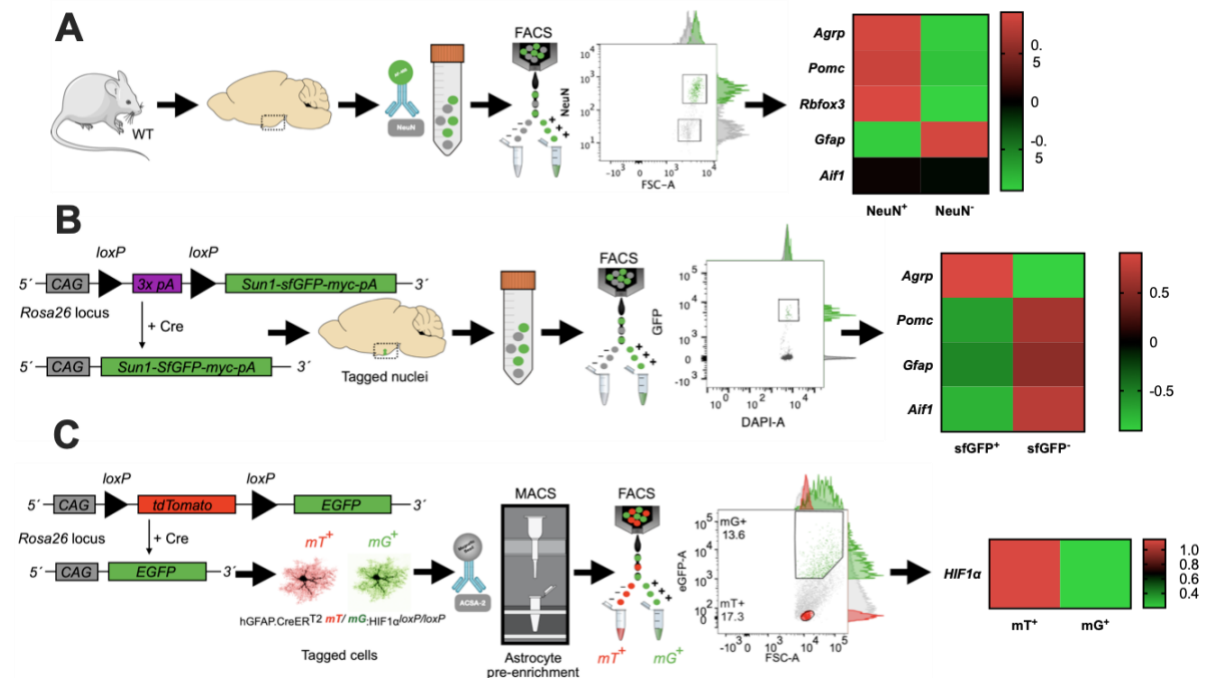
Figure 4. Sorting pipelines for specific subpopulations from brain tissue.

A, sorting pipeline for neuronal nuclei employing NeuN-staining and heat-map evidencing the enrichment of hypothalamic neuronal markers. B, sorting pipeline using the INTACT protocol with an

Agrp-Cre mouse line. Heat-map showing the enrichment of *Agrp* transcript. C, sorting pipeline for astrocytes using the *mTmG* dual reporter and validation of the deletion of exon 2 of *HIF-1α* in GFAP[+] astrocytes.

5.2. HDAC5-KO male mice develop metabolic dysfunction under non-obesogenic conditions

Previously our group revealed that under obesogenic conditions, HDAC5 is necessary for appropriate hypothalamic leptin signaling and energy homeostasis (Kabra et al., 2016). Herein, we aimed to decipher the role of HDAC5 in the control of energy homeostasis under non-obesogenic conditions which remained unexplored to date. We therefore monitored body weight and body composition using magnetic resonance (ecoMRI) in global HDAC5-KO and WT male and female mice over a period of 17 months and 11 months respectively. The first lead for deregulated energy homeostasis under non-obesogenic conditions appeared in 5-months-old male mice, in which fat mass was significantly higher in HDAC5-KO as compared to WT male mice (Figure 6,B). The increment in fat mass was aggravated with age, reaching up to 188% increment in fat mass compared to WT mice aged of 17 months. Despite the increased fat mass at 5 months, a significant elevation in body weight was only observed at 6 months old and reached a similar 13,5% increase in body weight as compared to WT mice (Figure 6,A). Concomitant to obesity, irregularities in circulating metabolic parameters were detected among individuals of different genotypes at the age of 6 months. *Ad libitum* fed and fasted HDAC5-KO mice showed elevated post-prandial blood glucose and HOMA-IR when compared to WT mice (Figure 6, C & D), respectively. Similarly, obese mice had increased plasma leptin concentrations and alterations in the lipid profiles with elevated values of cholesterol and non-esterified free fatty acids (NEFA), whereas triacylglycerides levels remained unchanged (Figure 6, E-H). The marked obesity, with the associated insulin resistance and dyslipidemia in male HDAC5 null male mice, clearly manifested the importance of this enzyme in the regulation of energy homeostasis under non-obesogenic conditions.
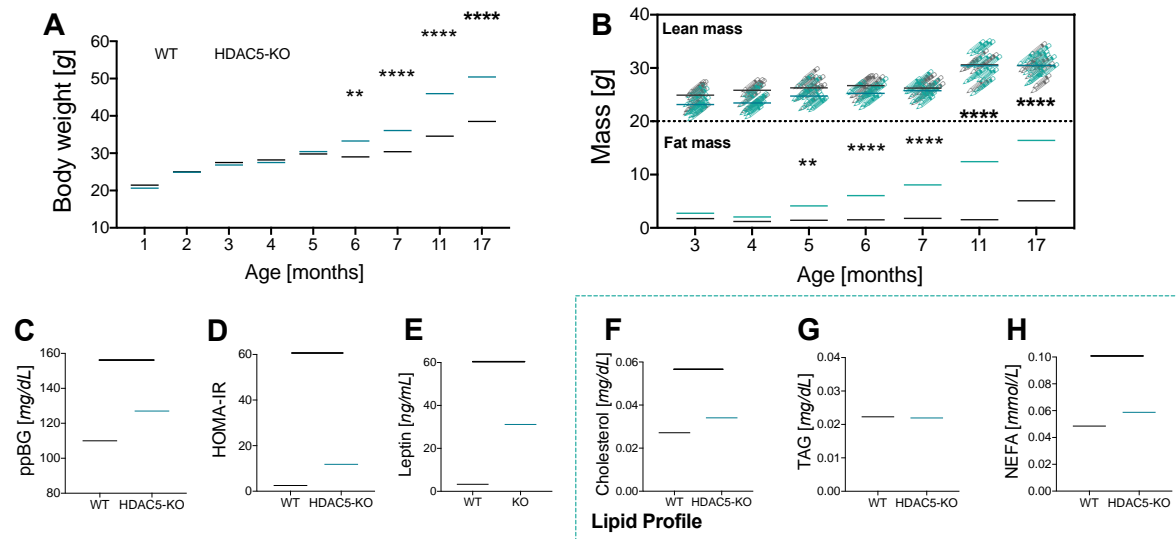
Figure 5. Time course analysis of body composition and metabolic parameters of HDAC5-KO male mice.

HDAC5-KO and WT male mice ($n=$ 24, 12 KO & 12 WT) were evaluated for A. body weight and B. body composition over a period of 17 months. Plasma analysis for C. post-prandial blood glucose (ppBG), D. homeostatic metabolic assessment for insulin-resistance (HOMA-IR), E. leptin, F. cholesterol, G. triglycerides (TAG) and H. non-esterified free fatty-acids (NEFA) at the age of 6 months. Values represent means ± S.E.M. Statistical analysis were done by either two-way ANOVA with Bonferroni *post-hoc* test (A,B) or two-tailed unpaired Students' t-test (C-H). * $p \leq 0.05$, ** $p \leq 0.01$, *** $p \leq 0.001$ and **** $p \leq 0.0001$.

5.3. Decreased energy metabolism in male HDAC5-KO mice

In order to identify the underlying mechanism of the increased body weight in HDAC5-KO males under non-obesogenic conditions, their energy homeostasis was measured in the TSE, an indirect calorimetry system. Energy expenditure was calculated based on changes in O_2 consumption and CO_2 production within an open flow system, physical activity was monitored by infrared beam breaks or electromagnetic sensors and energy intake (food and drink) was quantified by sensitive mass balances (Even and Nadkarni, 2012). Due to the controversy about the influence of body mass on energy expenditure when

measuring indirect calorimetry (Corrigan et al.; Tschöp et al., 2012) and to avoid concerns about normalization of energy expenditure to total or lean mass, energy homeostasis was measured prior to the onset of obesity at 3 months of age. The indirect calorimetry analyses revealed total energy expenditure to be significantly reduced in pre-obese mice with global HDAC5 deletion when contrasted with WT mice (Figure 7A & B). When analyzed on 12h-cycles for light and dark phases, the reduction in EE was attributed to the dark phase (Figure 7,B). Dark phase corresponds to the active phase for nocturnal species like mice, yet no significant difference was detected between genotypes although a tendency toward lower locomotion was observed in HDAC5-KO mice (Figure 7 C & D). Conversely, food intake and respiratory exchange ratio (RER), representing substrate oxidation, were largely reduced in both the light and dark phases in the knock-out model. (Figure 7 E-H). Based on the TSE results, pre-obese HDAC5 null mice showed an overall reduction in energy metabolism: energy expenditure, energy intake (food intake), RER, and locomotion, suggesting a sluggish metabolism.
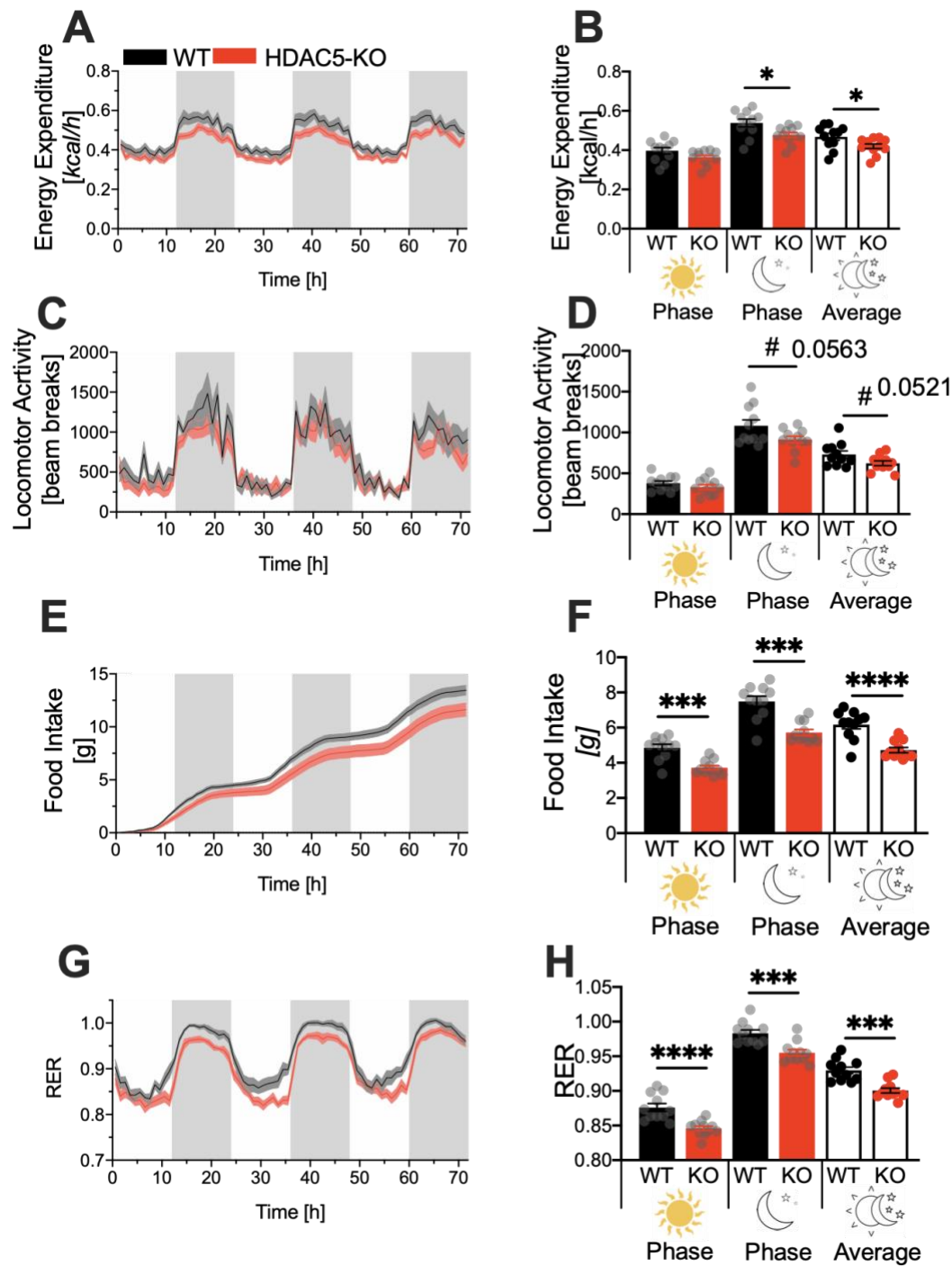
Figure 6. Metabolic and behavioral parameters modulating energy homeostasis in HDAC5-KO male mice.

Pre-obese HDAC5-KO and WT mice (n= 24, 12 KO & 12 WT) at the age of 3 months were studied in a TSE system for 72 h. A, Energy Expenditure (EE) and B, light, dark or total phase average EE. C, locomotor activity and D, light, dark or total phase average locomotor activity. E, Food intake and F, light, dark or total phase average food intake. G, respiratory exchange ratio (RER) and H, light, dark or

total phase average RER. Values represent means ± S.E.M. Statistical analysis were done by either two-tailed unpaired Students' t-tests or ANCOVA (D). * $p \leq 0.05$, ** $p \leq 0.01$, *** $p \leq 0.001$ and **** $p \leq 0.0001$.

5.4. The Hypothalamus-Pituitary-Thyroid axis and adrenomedullary functions were not affected by HDAC5-ablation

Slow metabolism can result from a shift in endocrine activity. It is well known that thyroid hormones stimulate basal metabolism, thermogenesis, lipid and glucose metabolism, fat oxidation, and food intake (Longhi and Radetti, 2013). In accordance, hypothyroidism causes weight gain with decreased thermogenesis and basal metabolism, and around 20% of severely obese people have subclinical hypothyroidism (Michalaki et al., 2006; Rotondi et al., 2009; Xu et al., 2019). Significant lower levels of circulating levels of epinephrine were also detected in overweight and obese subjects when compared to normoweight and a similar profile was detected in MSG-induced obese mice, pointing to adrenal medullary dysfunction in obesity (Martins et al., 2004; Reimann et al., 2017). Using HPLC-ECD, we quantified the free forms of thyroid hormones T3 and T4 and the catecholamines epinephrine and norepinephrine in plasma from WT and obese HDAC5 male mice. We did not detect any significant alterations in plasma thyroid hormone and catecholamine levels in obese HDAC5-KO mice at the age of xx months compared to WT controls (Figure 8). However, plasma epinephrine levels were greatly reduced in HDAC5 KO males, but the difference to WT mice did not reach statistical significance (Figure 8B). Additionally, to the T3 and T4 levels measured with HPLC-ECD, the measurement of plasma TSHb levels by ELISA did not present any altered profile between genotypes (Figure 8C). These results point towards an intact hypothalamus-pituitary-thyroid (HPT) axis and unaltered adrenomedullary secretion in obese HDAC5 mice.
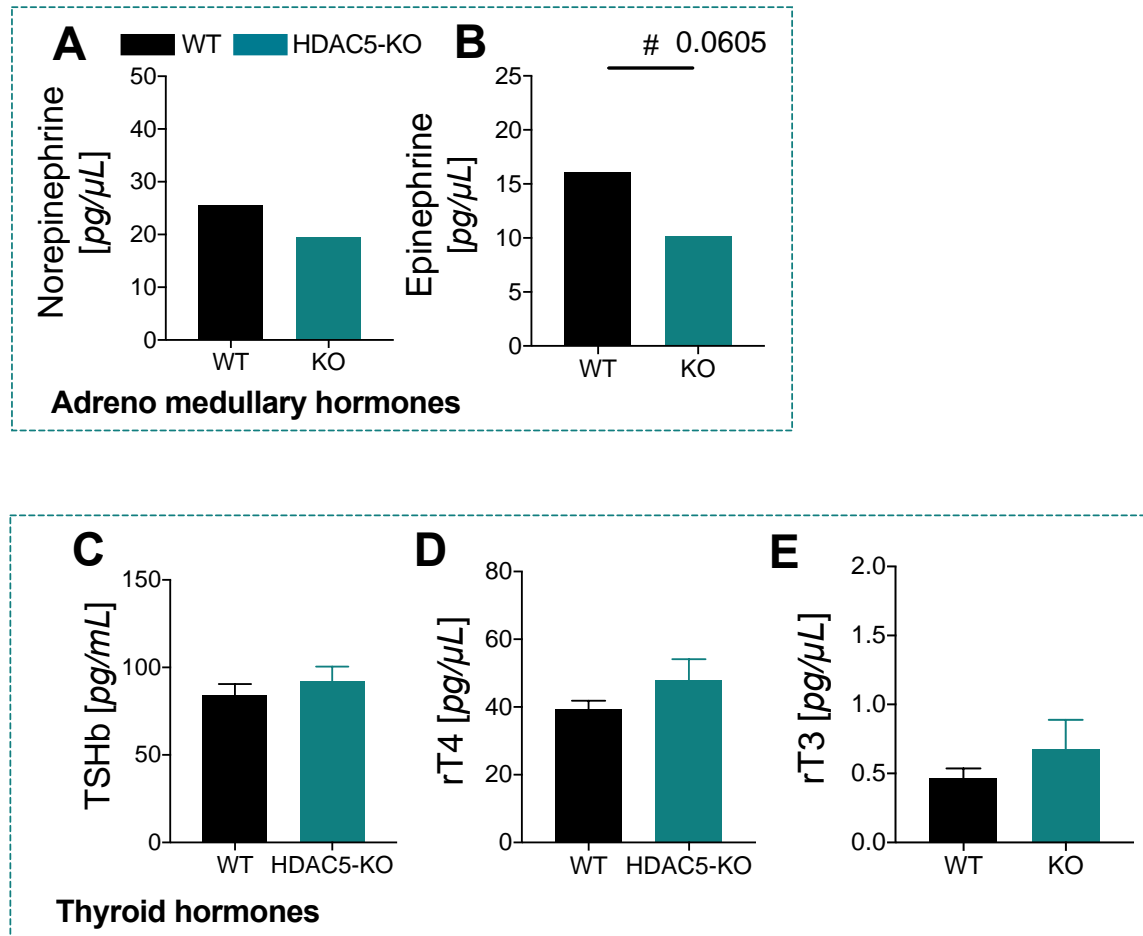
Figure 7. Plasma analysis for adreno catecholamines and pituitary-thyroid axis in HDAC5-KO mice.

Plasma from 6 months old HDAC5-KO and WT mice (n= 24, 12 KO & 12 WT) was used for quantifying A, norepinephrine; B, epinephrine; C, Tshb; D, free thyroxine (tT4) and E, free triiodothyronine (tT3). Values represent means ± S.E.M. Statistical analysis were done by two-tailed unpaired Students' t-test. * $p ≤ 0.05$, ** $p ≤ 0.01$, *** $p ≤ 0.001$ and **** $p ≤ 0.0001$.

5.5. HDAC5-KO mice display impaired SNS-driven adipose tissue metabolism

5.5.1. HDAC5-KO mice show reduced BAT-induced thermogenesis

Despite no alterations in adrenomedullary hormone secretion, the tendency of decreased epinephrine intrigued us regarding the status of the sympathetic nervous system (SNS) in an obese HDAC5 deleted phenotype since catecholamine release is mediated by the SNS. Low SNS activity has been long suggested as a risk factor predisposing one for weight gain and the development of obesity (Bray, 1991; Ravussin and Tataranni, 1996). Aside from being the main system in charge of stimulating the fight or flight response, basal activation of the SNS maintains energy homeostasis by innervating almost every organ within an individual. Particularly SNS postganglionic nerves activate brown adipose tissue (BAT), known as the thermogenic organ responsible for non-shivering thermogenesis. Activated SNS terminals release NE to stimulate ß-adrenergic receptors (ß2 and ß3) and thus raising intracellular cycling-AMP (cAMP) in BAT. cAMP in turn activates protein kinase A (PKA) leading to phosphorylation and translocation of cAMP-response-element binding protein (CREB) for transcriptional activation of target genes including uncoupling protein 1 (*Ucp1*). UCP1 uncouples mitochondrial oxidation of substrates by dissipating the proton gradient back to the mitochondrion, short-circuiting ATP synthesis to generate heat (Cannon and Nedergaard, 2004; González-García et al., 2020). Savoring the hypothesis of decreased energy expenditure due to decreased SNS activity in BAT, we first measured heat production in BAT under isothermal conditions (24-25ºC) by means of an infrared sensing camera (Optris PI 450i). We recorded significant lower temperature in the BAT of HDAC5-KO mice compared to WT (Figure 9, A & B). In accordance with reduced heat production, BAT UCP1 protein expression in HDAC5-KO was reduced 37% in respect to male WT controls (Figure 9, C & D). By further assessing SNS basal stimulation by HPLC-ECD monoaminergic quantification in BAT explants, we revealed 52% reduction in NE and 69,7% in E concentrations in HDAC5-KO in contrast to WT (Fig. 5, E & F). Exposure to cold further activates the SNS activity and NE release from efferent terminals to burst BAT

thermogenesis in a urge maintain thermal and energy homeostasis (Kozyreva et al., 2015). For *in vivo*

functional probe of concept, exposed WT and pre-obese HDAC5-KO mice to cold (4ºC) in a TSE system

corroborated significant failure of KO mice to increase energy expenditure to the same extent WT mice

did (Figure 9, G). Together, *in vivo* and *ex vivo* observations exposed an impaired connection between

SNS and BAT under basal and cold exposure conditions leading to decreased BAT thermogenesis in

the absence of HDAC5.
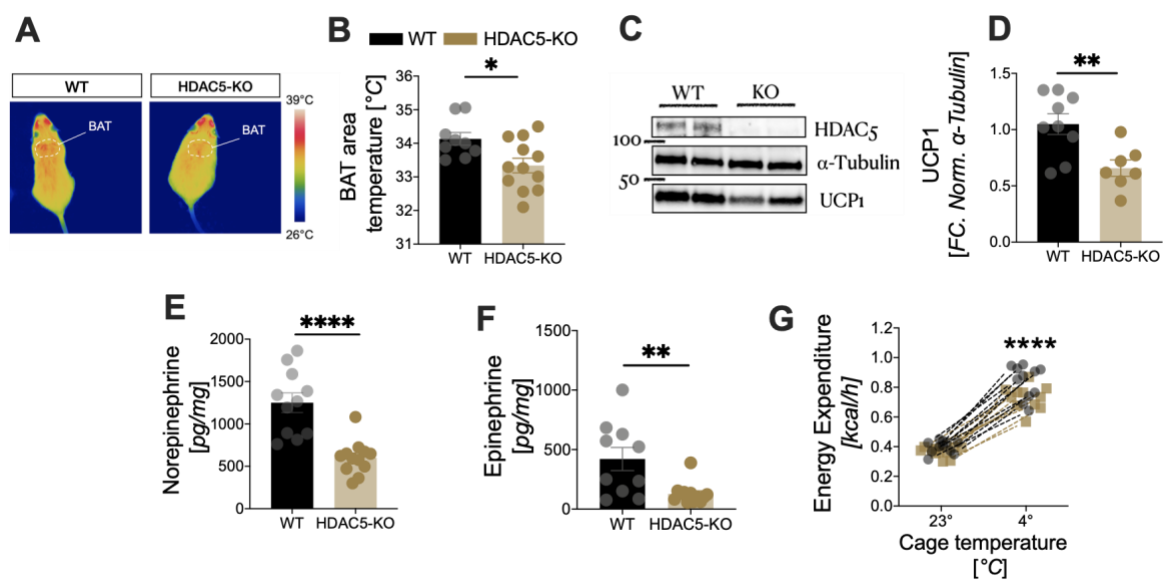
Figure 8. Assessment of the functionality of brow adipose tissue in HDAC5-KO mice.

BAT function was assessed by different parameters in HDAC5-KO and WT mice at the age of 6 months

(*n*= 24, 12 KO & 12 WT). A, infrared image depicting heat production; B, quantification of BAT-

temperature; C-D western blot and densitometry for UCP1 protein levels. HPLC-measurement for E,

norepinephrine and F, epinephrine. G, Energy expenditure evoked at standard room temperature

(23°C) and cold exposure (4°C) for 5 h in mice at the age of 3 months. Values represent means ±

S.E.M. Statistical analysis were done by two-tailed unpaired Students' t-test (A-F) or either two-way

ANOVA with Bonferroni *post-hoc* test (G). * $p \leq 0.05$, ** $p \leq 0.01$, *** $p \leq 0.001$ and **** $p \leq 0.0001$.

5.5.2. HDAC5-KO mice have decreased white adipose tissue lipolysis

BAT-induced thermogenesis requires a sufficient supply of fuel sources derived from dietary nutrients or energy deposits. Glucose and FFA serve as fuel in the fed state whilst FFA derived from lipolysis are the primary fuel during nutritionally demanding situations like fasting or cold exposure (Shin et al., 2017). Lipolysis proceeds in regulated and sequential enzymatic reactions which first hydrolyze TAG into diacylglycerol (DAG), then monoacylglycerol (MAG), and ultimately releasing the glycerol backbone and a (F) fatty acid (FA) per enzymatic reaction. Although lipolysis is co-stimulated upon NE binding to ß3-adrenergic receptor, BAT primordially relays on lipolytic products mobilized from energy stores in visceral or epidydimal white adipose tissue (eWAT) (Shin et al., 2017). Rapid mobilization of energy stores through lipolysis is mainly initiated by the SNS (Bartness et al., 2014). SNS-released NE mediates ß-adrenergic receptor stimulation, leading to PKA activation, and ultimately phosphorylation and activation of the hormone-sensitive lipase (HSL) and perilipin (Duncan et al., 2007). HSL is the major lipase for catecholamine-stimulated lipolysis whereas other lipases counting the desnutrin or adipocyte triacylglyceride lipase (ATGL), carboxylesterase 3, and adiponutrin mediate triacylglycerides hydrolysis during basal lipolysis (Strålfors et al., 1984; Baulande et al., 2001; Holm, 2003; Soni et al., 2004; Villena et al., 2004).

Our findings of reduced SNS-stimulated thermogenesis in BAT, prompted us to suspect a similar effect on SNS-stimulated lipolysis in WAT. Despite unaltered gene expression of the ß-adrenergic receptors *Adrab3* and *Adra2a,* significantly lower gene expression was quantified in *Adrab2,* the critical lipolytic enzymes *Hsl* and *Atgl,* and SNS-sensitive transcription factor *Nr4a3* (NOR1) in eWAT from HDAC5-KO in reference to WT mice (Figure 10, A). Conversely, HSL protein expression did not vary between groups but phosphorylation at Ser660 was completely abolished in eWAT from HDAC5-KO mice (Figure 10, B & C). Next, we employed HPLC-ECD to assess the state of SNS activity, and found 61% lower NE levels in eWAT of HDAC5-KO collated to WTs (Figure 10, D). *Ex vivo* eWAT explants from pre-obese mice stimulated with isoproterenol, a ß1 and ß2 adrenergic agonist, further ratified a decrease in the maximal catecholamine-stimulated lipolysis upon HDAC5-ablation to almost half (48%)

of the stimulated lipolysis in WT explants (Figure 10, E). Gene expression of key lipogenic and adipogenic targets in eWAT (Figure 10, F), and genes involved in browning of subcutaneous WAT (scWAT) (Figure 10, G) remained unchanged between genotypes. Altogether, these results evidenced decreased SNS stimulation in eWAT leading to reduced HSL gene expression and activation, and further catecholamine-induced lipolysis in eWAT of HDAC5-KO mice.
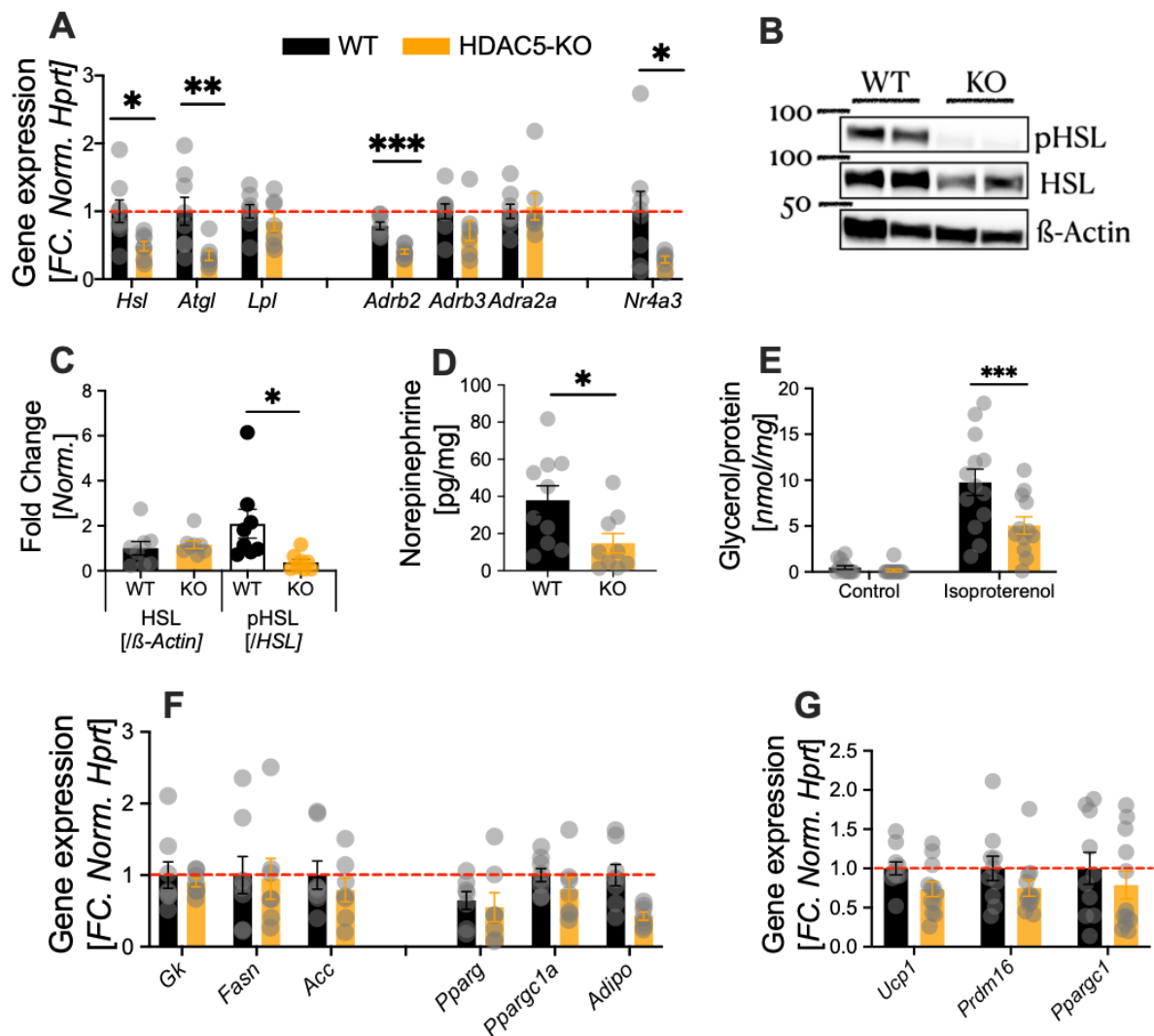
Figure 9. Impaired functionality of white adipose tissue in HDAC5-KO mice.

WAT of HDAC5-KO and WT mice ($n = 24$, 12 KO & 12 WT) was subjected to the assessment of A, gene expression of critical genes involved in hormonal-induced lipolysis in eWAT; B, western blotting and C densitometry for total HSL (normalized to ß-actin) and pHSL (normalized to total HSL); D, HPLC-

quantification of norepinephrine; E, *ex vivo* lipolytic assay with isoproterenol in eWAT explants; F, gene expression for critical lipogenic and adipogenic markers in eWAT; G, gene expression of browning markers in scWAT. Values represent means ± S.E.M. Statistical analysis were done by two-tailed unpaired Students' t-test or either two-way ANOVA with Bonferroni *post-hoc* test. * $p \leq 0.05$, ** $p \leq 0.01$, *** $p \leq 0.001$ and **** $p \leq 0.0001$.

5.6. HDAC5-KO mice display elevated hypothalamic dopamine but lower PVH neuronal activity

My data revealed that HDAC5 is required for adequate SNS stimulation of BAT and WAT, respectively. The reduced sympathetic tone in the periphery hinted toward an inactivation of SNS-regulatory centers in the CNS and specifically the hypothalamus, which is located in the ventral forebrain and composed of several small essential nuclei such as the supraoptic nucleus (SON), suprachiasmatic nucleus (SCN), lateral hypothalamic area (LH), arcuate nucleus (ARH), dorsomedial nucleus (DMH), ventromedial nucleus (VMH), and, paraventricular nucleus of the hypothalamus (PVH). The PVH in the ventral diencephalon adjacent to the third ventricle, is of particular importance for the regulation of energy homeostasis and SNS activity. Postnatal ablation of Single-minded 1 (*Sim1)*, one of the few genes implicated in monogenic obesity that encodes for a transcription factor dictating the development of several PVH neuronal populations, induced obesity with transient hyperphagia, but marked reduction in energy expenditure and BAT thermogenesis (Xi et al., 2012). *Bdnf* deletion in Sim1^{+} neurons and OXT deletion in the PVH (OXT^{-/-}) caused lower sympathetic tone, BAT thermogenesis, and obesity, with variable effects on food intake. Given the similarities in the metabolic dysregulation between PVH inactivation and HDAC5-KO mice, I thus aimed to interrogate the activation of PVH neurons relying on the expression of cFOS, an early marker for neuronal activation. Immunoreactivity for cFOS was significantly lower in the PVH from HDAC5-KO compared to WT mice (Figure 11, A). Co-staining for OXT but did not yield co-localization between the two markers. The dorsal medial-posterior distribution of cFOS activated neurons from WT mice advocated for a similar anatomical distribution to the previously described BDNF^{+} neurons in the PVH (An et al., 2015). In spite the authors describing BDNF^{+} neurons as a unique population of neurons that co-localized up to 13% with tyrosine hydroxylase, a

marker for dopaminergic neurons. Recently, recording of postsynaptic inhibitory currents (IPSCs) in brain slices evidenced hyperpolarization and reduced spike frequency in the PVH after dopamine treatment (Zhang and van den Pol, 2016). Herein, we observed much broader TH-stained axonal innervation in the PVH from HDAC5-KO compared to WT mice, suggesting a more active dopaminergic neurotransmission in the nucleus, although this did not reach statistical significance (Figure 11, B). We further detected few TH$^+$ cell bodies in the periventricular area but no differences were detected when comparing genotypes. Significantly reduced cFOS activity levels, the lack of co-localization of OXT and the increase in inhibitory TH innervation in the PVH of HDAC5 null mice suggest a mode whereby the impairments of thermogenesis and lipolysis the HDAC5-KO mice are causally linked to an increased dopaminergic inhibition in the PVH

In the late 60s, the theory about the effect of hypothalamic monoamines on thermoregulation was postulated by several groups (Feldberg and Myers, 1963; Cooper et al., 1976; Cox and Lee, 1980). Initially based on epinephrine, norepinephrine, and serotonin intraventricular injections in anesthetized cats, Feldberg and Myers postulated that normal body temperature is delicately balanced by the release of these monoamines in the hypothalamus (Feldberg and Myers, 1963). Norepinephrine, dopamine, and acetylcholine evoked hypothermic effects when intrahypothalamically infused (Myers and Yaksh, 1969; Cox and Lee, 1978, 1980; Schelkunov et al., 1981) Dopamine-induced hypothermia is a highly conserved physiological mechanism found in goldfishes, pigeons, cats, monkeys, rats, mice and humans (Boyd et al., 1974; Hissa and Rautenberg, 1974; Saxena et al., 1977; Cox and Lee, 1980; Gisolfi et al., 1980; Pyörnilä, 1980; Lee et al., 1985; Wollmuth et al., 1989). Due to the higher TH innervation and reduced cFOS staining in the PVH, I interrogated whether monoamine profiles were altered among genotypes. Employing HPCL-ECD, I measured the monoaminergic neurotransmitters dopamine, norepinephrine, epinephrine, and serotonin and their metabolites in hypothalamic samples from both genotypes. In HDAC5-KO hypothalamic samples, I quantified a significant 2.4-fold increase of dopamine and 1.2-fold in norepinephrine when compared to WT samples. Epinephrine concentration was slightly but not significant elevated in HDAC5-KO samples whilst HVA remained unaltered between genotypes (Figure 11, C-H). I next assessed whether monoaminergic neurotransmitters are also increased in the striatum and PFC of the mesocorticolimbic system, but all neurotransmitters or their

metabolites were unchanged between between genotypes (Figure 11, C-H). Overall, my data suggests a specific increase of dopamine and norepinephrine within the hypothalamus of global HDAC5-KO mice
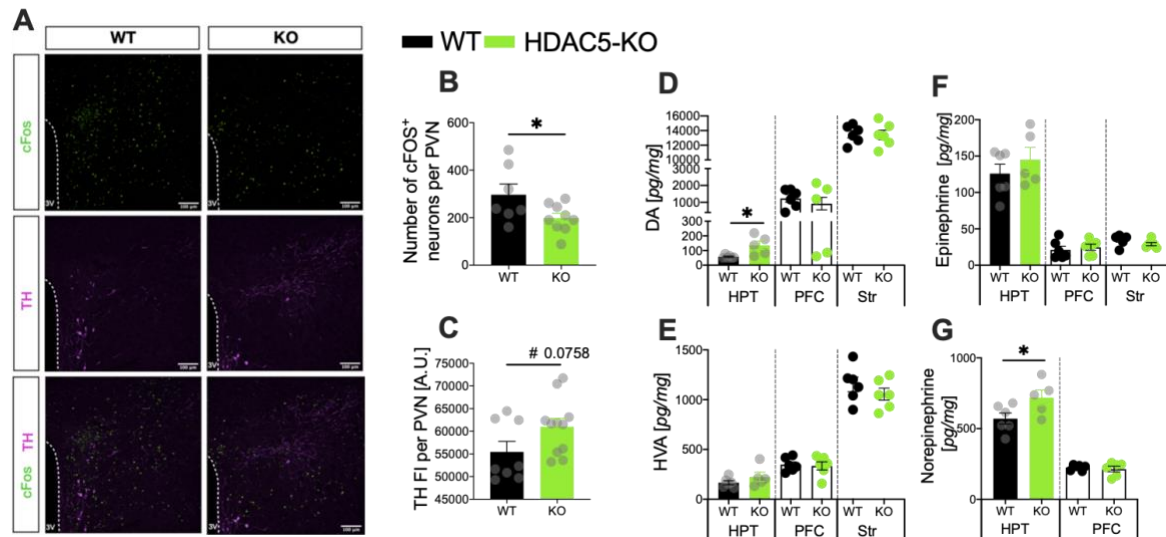
Figure 10. Paraventricular hypothalamic nucleus and hypothalamic monoaminergic concentrations in HDAC5-KO mice.

A, Co-immunostaining for cFOS and TH in the PVH from HDAC5-KO and WT mice (n= 12, 6 KO & 6 WT); B, number of cFOS^{+} neurons and C, TH fluorescence intensity (FI) in the PVH; HPCL-quantification of D, dopamine (DA); E, homovanillic acid (HVA); F, epinephrine and G, norepinephrine in the hypothalamus. Values represent means ± S.E.M. Statistical analysis were done by two-tailed unpaired Students' t-test or either two-way ANOVA with Bonferroni *post-hoc* test. * $p \le 0.05$, ** $p \le 0.01$, *** $p \le 0.001$ and **** $p \le 0.0001$.

5.7. Persistent activation of dopaminergic neurons in the dorsomedial ARH of HDAC5 KO mice

In the hypothalamus, dopaminergic neurons in the dorsomedial ARH (dmARH) constitute a fundamental source of dopamine for the control of our endocrine system as well as energy homeostasis. Historically, dmARH dopaminergic neurons were considered a homogenous population denoted tuberoinfundibular dopaminergic (TIDA) neurons based on their anatomical projections of their axons through the

infundibulum towards the median eminence (ME). In the ME, dopamine is released from the pre-synaptic terminals and transported by the portal system to the pituitary in order to inhibit prolactin secretion (Lechan and Toni, 2000; Le Tissier et al., 2017). Recently, dmARH proved to be a heterogeneous population, not only projecting to the ME, but locally in the ARH to melanocortin neurons and to unidentified neurons in the PVH (Zhang and van den Pol, 2015, 2016). To unravel the plausible contribution of dmARH TH neurons to elevated hypothalamic dopamine concentrations and PVH inhibition in HDAC5 deleted conditions, we co-stained for TH and cFOS in coronal sections containing the ARH and observed a 1.6-fold increase in the number of dmARH TH$^+$ neurons and 5.4-fold increase in co-localized TH$^+$cFOS$^+$ neurons in HDAC5-KO compared to WT mice. (Figure 12, A & C). Interestingly, general activation in the ARH was detected with a 2.2-fold elevation in the number of cFOS$^+$ neurons in HDAC5-KO in reference to WT mice. (Figure 12, B). This over-activation was not evidenced in the other hypothalamic nuclei including the VMH, DMH or LH, although a 2-way ANOVA highlighted a significant genotype effect in cFOS expression ($p<0.0001$, $F(2, 92) = 27.08$) (Figure 12, D). As previously mentioned dmARH neurons project to the PVH and/or the ME; quantification of TH immunoreactivity in the ME unearthed higher values in HDAC5-KO compared to WT (Figure 12, E). Consistent with the increased activation of dmARH TH neurons and TH protections to the ME, *Prl* gene expression in the pituitary was reduced and its secretion from lactotrophs was fully abolished respectively in HDAC5-KO compared to WT counterparts (Figure 12, F & G). Conversely, neither plasma levels of TSHb and GH, nor their respective gene expression in the pituitary, which are partially regulated by dopamine, were altered between genotypes (Figure 8,D. 8, F & H) (Flurkey et al., 2002). In view of this, over-activation of dmARH dopaminergic neurons led to the abolishment of Prl release from lactotrophs and plausibly to elevated hypothalamic dopamine concentrations in HDAC5-KO mice.
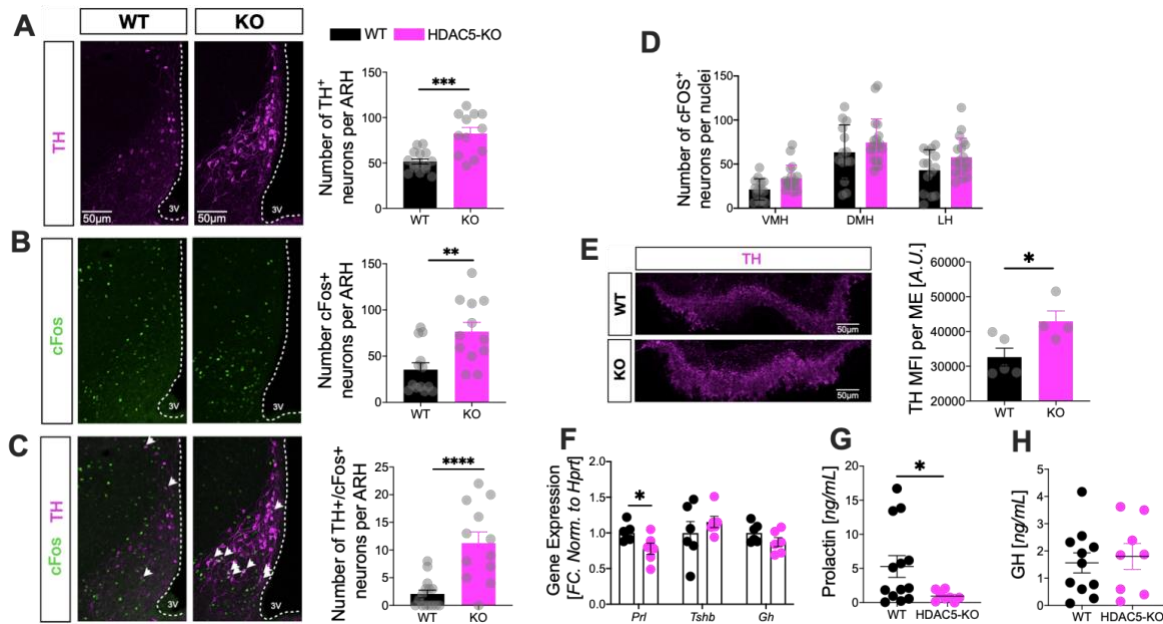
Figure 11. Arcuate dopaminergic neuros and the negative feedback loop regulating prolactin in HDAC5-KO mice.

Confocal overview scans in the ARH and quantification for A, TH+ neurons; B, cFOS+ neurons and C, respective colocalization. D, quantification of cFOS+ neurons in the VMH, DMH and LH. E, confocal overview scans and fluorescence intensity for TH in the median eminence (ME); F, gene expression for hormonal genes *Prl, Tshb* and *Gh* in the pituitary. Plasma concentrations of G, prolactin and H, growth hormone. Values represent means ± S.E.M. Statistical analysis were done by either two-tailed unpaired Students' t-test or two-way ANOVA with Bonferroni *post-hoc* test. * $p \leq 0.05$, ** $p \leq 0.01$, *** $p \leq 0.001$ and **** $p \leq 0.0001$.

dmARH dopaminergic neurons in neonates, undergo further differentiation and preservation of phenotype depending of endogenous PRL (Phelps et al., 1994, 2003). Ames dwarf mice carrying the recessive *Prop1* mutation in homozygosis have undetectable pituitary prolactin (PRL) levels accompanied by reduction in TIDA neurons and hypothalamic dopamine production after 21 days of age (after weaning) (Phelps et al., 1993). Thenceforth, I next questioned whether the increased number and over-activation of dmARH TH+ neurons observed in HDAC5-KO mice was already present in neonates or develop in late postnatal stages. Time course analysis for the number of TH+ neurons in neonates (7 days old), young (45 days old), and adult (180 days old) mice showed no differences in neonates, but significantly larger numbers of TH+ neurons in young mice that persisted throughout

adulthood (Figure 12, A). From this young age onwards, a higher number of TH+ neurons correlated with increased neuronal activation as evidenced by TH+cFOS+ co-localization and moreover a widely spread activation in the ARH in HDAC5 null mice (Figure 13, B & C). Finally, TH intensity only differed in adult mice between genotypes (Figure 13, D). Overall, my results point to an increased and PRL-independent differentiation and activation of dmARH TH+ neurons in young HDAC5-KO mice that persists through adulthood.
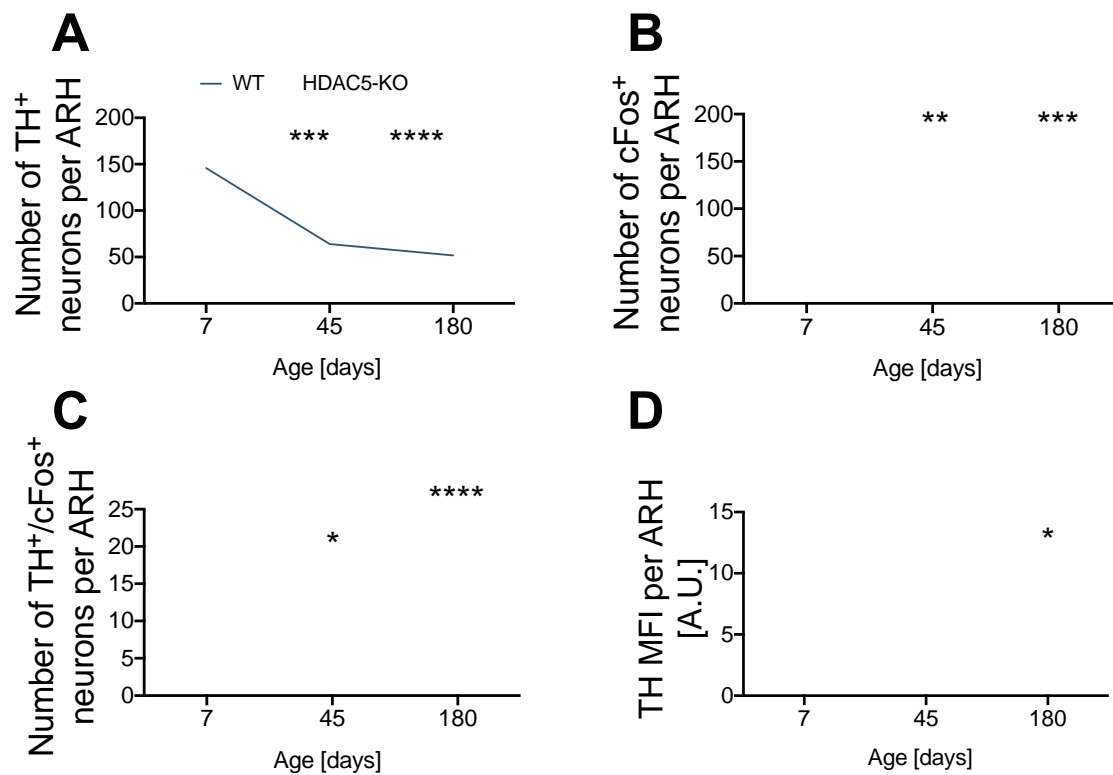
Figure 12. Development and activation of arcuate dopaminergic neuros in neonates, young and adult HDAC5-KO mice.

Quantification of A, TH+ neurons; B, cFOS+ neurons: C, respective colocalization and TH fluorescence intensity from ARH confocal scans at different maturation ages in HDAC5-KO and WT mice (*n*=12, KO = 6 and WT = 6). Values represent means ± S.E.M. Statistical analysis were done by two-way ANOVA with Bonferroni *post-hoc* test. * $p \leq 0.05$, ** $p \leq 0.01$, *** $p \leq 0.001$ and **** $p \leq 0.0001$.

In the dmARH, tyrosine hydroxylase gene expression and subsequently enzymatic activation has been shown to be stimulated by ligand binding to prolactin receptor (PrlR). In vitro studies in primary ARH

neurons revealed a dose response to Prl in the expression of *Th*, phosphorylation of TH protein and dopamine synthesis (Ma et al., 2005). Once we observed the increased hypothalamic levels of dopamine in HDAC5-KO male mice, I interrogated the regulation of TH at the gene and protein level. . Using the FACS pipeline that I had standardized for neuronal nuclei (NeuN$^+$), I aimed to enrich dmARH TH$^+$ neurons by separating the NeuN$^+$ and NeuN$^-$ fractions. My approach was based on the lack of co-localization between NeuN$^+$ and TH$^+$ neurons in the dmARH, as evidenced by immunofluorescence co-staining (Figure 14, A). Accordingly, by employing my FACS pipeline and collecting the NeuN$^-$ fraction, I could profoundly enrich dmARH TH nuclei. In the gene expression analysis, I found significant up-regulation of *Th, Drd2,* and *Prlr* expression in HDAC5-KO NeuN$^-$ nuclei compared to WT NeuN$^-$ nuclei, but unchanged levels of *Slc6a3* mRNA (Figure 14, B). None of these changes were observed in the NeuN$^+$ fraction (Figure 14, C). Intriguingly, TH protein expression remained unperturbed between genotypes, but TH phosphorylation at Ser40 was significantly higher in HDAC5-KO ARH micropunches (Figure 14, D & E). Although, TH gene expression and phosphorylation have been described to be controlled by STAT5 and ERK1/2 in dmARH dopaminergic neurons (Lindgren et al., 2002; Yip et al., 2019), no changes in protein expression nor phosphorylation states were detected for STAT5 or ERK1/2 between genotypes. Recently, dmARH TH$^+$ neurons were reported to co-release dopamine and GABA, and TH$^+$ axons surrounding the PVH were shown to have this particular phenotype (Zhang and van den Pol, 2015, 2016). Surprisingly, both GABAergic enzymes *Gad1* and *Gad2* were up-regulated in the HDAC5-KO NeuN$^-$ nuclei whilst no changes were quantified in the NeuN$^+$ counterparts (Figure 14, B), further supporting the dopaminergic - GABAergic inhibitory neurotransmission. Finally, I found significantly elevated *Pomc* but unaltered *Agrp* expression in HDAC5-KO compared to WW+T NeuN$^+$ nuclei (Figure 14, C). Increased *Pomc* might be related to observed reduced food intake in the TSE system. In summary, I found an upregulation of *Th* and activation of TH protein along with increased expression of GABAergic enzymes in dmARH TH$^+$ NeuN$^-$ neurons of HDAC5-KO mice and an upregulation of *Pomc* in NeuN$^+$ neurons of HDAC5-KO mice.
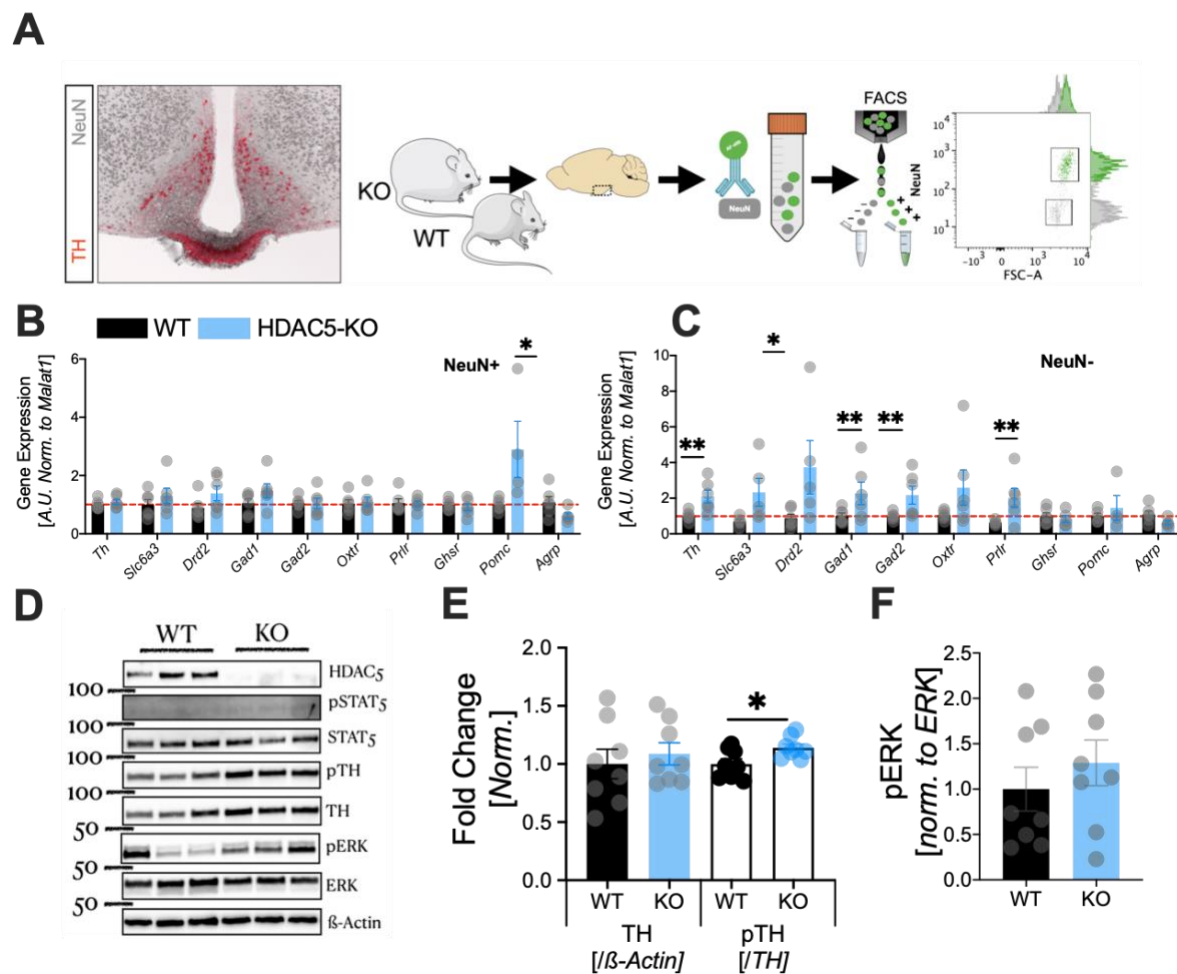
Figure 13. Gene and protein regulation of critical targets involved in the activation of ARH dopaminergic neurons.

A, workflow for the enrichment of ARH dopaminergic neurons using FACS; Gene expression of critical activation targets in ARH dopaminergic and melanocortin neurons in the B, NeuN⁺ sorted fractions and C, NeuN⁻ sorted fractions of the hypothalamus. D, western blot for classical targets in the activation of ARH dopaminergic neurons and densitometry for E, total TH (normalized to ß-actin) and pTH (normalized to total TH) and F, total ERK (normalized to ß-actin) and pERK (normalized to total ERK) in ARH micro punches from HDAC5-KO and WT mice (n=16, KO = 8 and WT = 8). Values represent means ± S.E.M. Statistical analysis were done by either two-tailed unpaired Students' t-test or two-way ANOVA with Bonferroni *post-hoc* test. * $p \leq 0.05$, ** $p \leq 0.01$, *** $p \leq 0.001$ and **** $p \leq 0.0001$.

STAT5b exclusively mediates prolactin signal transduction of dmARH dopaminergic neurons (Liu et al., 1995). STAT5 comprises as two highly homologous isomers, STAT5a and STAT5b that share

approximately 96% amino acid identity (Liu et al., 1995). Only, STAT5b undergoes nuclear translocation in response to prolactin both *in vivo* and *in vitro* (Ma et al., 2005; Yip et al., 2012). Transcriptionally active STAT5b requires acetylation and unphosphorylated STAT5b forms dimers in an acetylation-dependent manner after prolactin stimulation (Kosan et al., 2013). Upon ligand binding to PrlR, CREB-binding protein (CBP) was recruited to pT539 in PrlR cytoplasmic loop where it acetylated multiple lysine residues. Neutralization of those positive charges in lysine residues by the acetyl groups enabled two PrlR monomers to dimerize and phosphorylate one another (Ma et al., 2010). Downstream, PrlR signals through STAT5b which is also a substrate for recruited-CBP and becomes acetylated at 2 lysine residues (K694 and K701) in the SH2-dimerization domain and one lysine residue (K359) in the DNA binding domain. Pretreatment with the HDAC inhibitors TSA and NAM enhanced PRL-stimulated PrlR and STAT5b acetylation in the human breast cancer cell line T46D. Conversely, overexpression of SIRT1, SIRT2, HDAC3, and HDAC6 reversed CBP-mediated acetylation of PrlR and STAT5b.

Interaction among HDAC1 and HDAC3 with STAT5 have been reported for adequate development of pro-B cells (Xu et al., 2003, 5; Nanou et al., 2017). Thence I asseseed the possible interaction between STAT5b and HDAC5 in the hypothalamus by co-immunoprecipitacion. STAT5b positive interaction was detected from HDAC5 immunoprecipitates and vice-versa in WT hypothalamic samples (Figure 15, A & B). Such interaction was absent from immunoprecipitates in the HDAC5-KO hypothalamic samples. Subsequently, cellular fractioning into nuclear and cytosolic fractions demonstrated altered STAT5b subcellular distribution in the HDAC5-KO compared to WT hypothalamic samples. Nuclear STAT5b protein levels were significantly higher and a non-statistically significant tendency toward reduced cytoplasmic STAT5b was quantified in the HDAC5-KO extracts (Figure 15, C & D). My attempts to immunoprecipitate STAT5b from hypothalamic samples to assess total acetylated-lysine in those samples remained unsuccessful, no acetylation was detected in either genotype (data not shown). This criticial question requires additional work, and warrants additional studies, for instance by using alternative antibodies for acetylated STAT5b. Overall, my data suggest that HDAC5 interaction with STAT5b in the hypothalamus is necessary for STAT5b appropriate subcellular localization and possibly transcriptional activity.
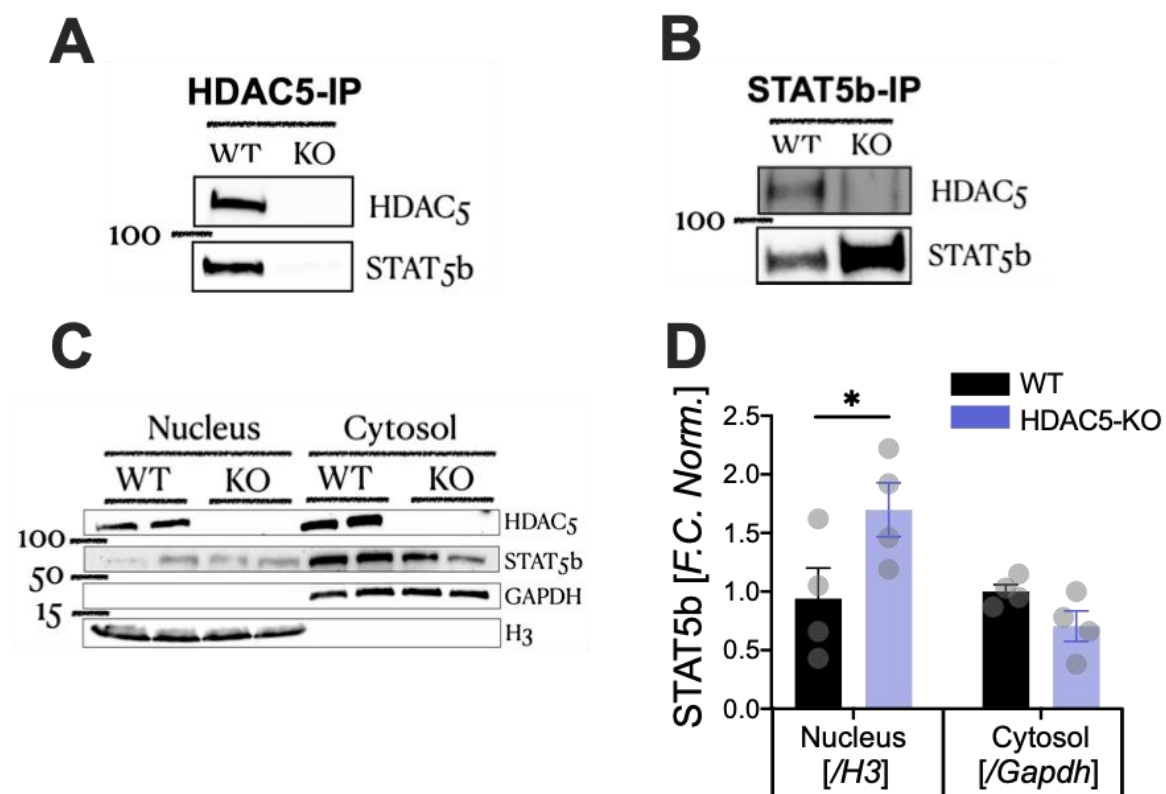
Figure 14. STAT5b-HDAC5 interaction and STAT5b subcellular localization.

Co-immunoprecipitations using A, anti-HDAC5 or B, anti-STAT5b in male WT and HDAC5-KO hypothalamic extracts. C, Western blot for nuclear and cytosolic fractions depicting the subcellular location of STAT5b and D, densitometry analysis for the house keeping proteins H3 in the nucleus and GAPDH in the cytosol of male WT and HDAC5-KO hypothalami. Values represent means ± S.E.M. Statistical analysis were done by two-way ANOVA with Bonferroni *post-hoc* tests. * $p \leq 0.05$, ** $p \leq 0.01$, *** $p \leq 0.001$ and **** $p \leq 0.0001$.

5.8. Unpertubed metabolic control in female HDAC5-KO mice

Several animal models have demonstrated sexual dimorphism in the risk towards the development of obesity and the role that sexual hormones play in it (Palmer and Clegg, 2015). In general, females gain less weight when fed high-fat diet compared to males. Estrogen protects against increased body adiposity and obesity by enhancing energy expenditure and reducing food intake (Brown et al., 2010;

Stubbins et al., 2012; Xu and López, 2018). For instance, HDAC5-KO females neither differ in body weight nor in body composition when compared to WT female mice over a period of 10 months (Figure 16. A & B). Similarly, postprandial blood glucose levels were unaltered between genotypes (Figure 16, C). Decreased BAT thermogenesis, a clear feature in HDAC5-KO male mice was inexistent in HDAC5-KO females in reference with WT counterparts (Figure 16, D & E). Of note, prolactin is a critical hormone for reproduction in females but not in males as portrayed in PrlR and prolactin null mice (Steger et al., 1998; Kelly et al., 2001; Binart et al., 2003; Le et al., 2012). Herein, I did not observe any alterations in fertility between genotypes. KO x KO breeding produced the same number of pups and sex-distribution per litter when contrasted to WT x WT breeding (Figure 16, F). Overall, my data does not suggest dmARH dopaminergic overactivation leading to inhibition of prolactin release from the pituitary in HDAC5-KO female mice.
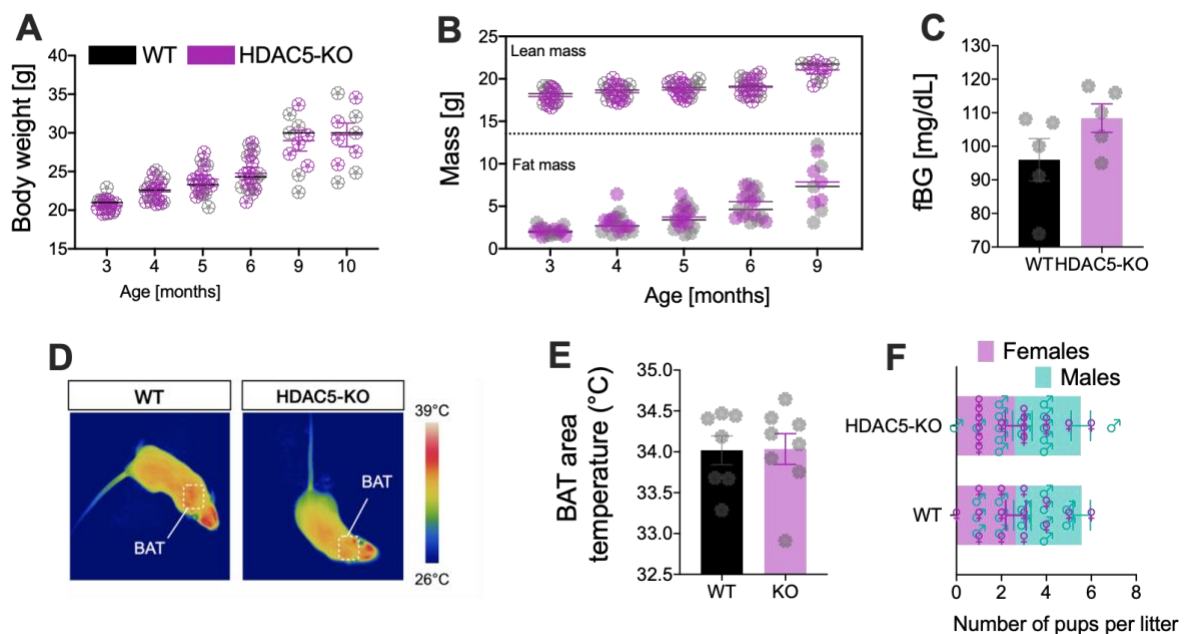
Figure 15. Unperturbed metabolic phenotype in HDAC5-KO female mice.

HDAC5-KO and WT female mice (*n*= 18, 9 KO & 9 WT) were evaluated for A. body weight and B. body composition over a period of 10 months. C, fasting blood glucose levels. D, infrared image depicting heat production and E respective quantification of BAT-temperature. F, Number of pups and sex distribution per litter over a period of six months.

6. Discussion

6.1. Sorting of cell subpopulations from brain tissue

Based on recent literature for fluorescent reporters, we successfully standardized a very low input FACS pipeline (INTACT-FACS) to analyze molecular mechanisms in specific cerebral subpopulations. For neuronal studies, using tagged- or labelled-nuclei was the most feasible approach due to the difficulty with isolation of intact neurons, which is only possible during embryonal development and early post-natal stages. In a relatively fast but very effective protocol we demonstrated the isolation of AgRP and oxytocin GFP-tagged nuclei with yields of approximately 2000 and 800 neurons per brain, respectively. The *Oxytocin-Cre: R26-CAG-LSL-Sun1-sfGFP-Myc* was further employed for single cell sequencing in a recent collaboration (data not shown). For astrocytes, from which single cell suspensions can be produced at any age, we demonstrated that the mTmG-MACS-FACS could be utilized to isolate specific astrocytic subpopulations for molecular and functional downstream studies. INTACT-FACS was the most versatile protocol that can be applied for the study of any specific population as long as a Cre-reporter line exists. Although we did not cross mTmG-mice with Aif1[tm1(EGFP/cre/ERT2)Wtsi]-mice for microglia validation, it should be feasible for single cell suspensions in this cell type to be achievable (Hammond et al., 2019).

6.2. Impaired lipolysis and thermogenesis drive mature-onset obesity in HDAC5-KO male mice

Obesity is a complex chronic disease characterized by an increase in body mass due to an enlargement of body fat depots, leading to the development of a cluster of health complications summarized as metabolic syndrome. The age of onset of obesity in humans is defined as either < 20 years (obesity in childhood and adolescence) or ≥ 20 years old (obesity in adulthood), as previously described (The et al., 2010; Ogden et al., 2013). In equivalence for human life phases and maturation rates, young mice are considered < 3 months and mature adult mice range from 3-6 months old (Hagan, 2017). Our results

unearthed for the first time to our knowledge, that HDAC5 deletion leads to mature-onset development of metabolic syndrome in male mice in a non-obesogenic environment *via* activation of dmARH dopaminergic neurons and reduction in energy expenditure. Previous studies based on the HDAC5-KO as a model probably failed to notice the phenotype due to using younger mice ranging 2-4 months (9-16 weeks) or by exposing them to HFD (Renthal et al., 2007; Taniguchi et al., 2012, 2017; Kabra et al., 2016a). Nonetheless, mature-onset obesity has been reported in other knockout murine models for interleukin-1 receptor I, interleukin-6, p62, and toll-like receptor 2 (Wallenius et al., 2002; García et al., 2006; Rodriguez et al., 2006; Shechter et al., 2013). The presented mature-onset phenotype in HDAC5-KO male mice was consistent with the WHO definition of the metabolic syndrome: obesity, hyperglycemia/insulin resistance and dyslipidemia (Figure 6). Thus, our data emphasize the importance of HDAC5 for metabolic homeostasis.

The assessment of energy homeostasis in WT and pre-obese HDAC5-KO by indirect calorimetry shed some light on the positive energy balance ultimately leading to obesity. HDAC5-KO were devoted to a slower energy metabolism with reductions in all measured parameters (energy expenditure, locomotor activity, food intake and RER) favoring the storage over the usage of energy. Our murine data are consistent with a 4-year follow-up study in southwestern American Indians that revealed an eight-times greater risk of gaining 10 kg in body weight for individuals with the lowest resting metabolic rate (RMR) compared to those with the highest RMR (Ravussin et al., 1988). Energy expenditure and food intake are coupled together in a dynamic balance to achieve homoeostasis and the most studied compensatory mechanism relies on the defence against energy store depletion by increasing food intake (Speakman et al., 2011). Compensatory decrements in food intake to limit unnecessary energy storage, although less frequently studied, have also been reported. Specifically, in mice acutely and chronically exposed to thermoneutrality (i.e. temperature range at which thermoregulatory energy expenditure is minimized, in mice typically between 27 and 33ºC) food intake was reduced in contrast with mice kept at ambient laboratory temperature (Williams et al., 2002; Yu et al., 2002; Stemmer et al., 2015; Cui et al., 2016). Interestingly, compensatory decrements in food intake were insufficient to neutralize the reductions in energy expenditure, leaving approximately a 4% bias to positive energy balance (Kaiyala et al., 2012). Sustained positive energy balance gradually promotes body weight gain. To the HDAC5-KO equation, we need to add the (tendency of) reduced physical activity during the dark

phase that possibly contributed to reduced energy expenditure. Finally, reduced food intake might have influenced the reduction in RER by lesser availability of glucose, forcing the system to move towards more utilization of fat (Even and Nadkarni, 2012).

Reduced energy expenditure correlated with reduced brown and white adipose tissue functionality in HDAC5-KO mice kept at standard laboratory housing conditions. Particularly, BAT is in charge of most of the thermoregulatory energy expenditure in rodents and BAT-inactivation in UCP1-KO mice was shown to predispose the animals to obesity upon HFD-exposure, thermoneutrality, and aging (Kontani et al., 2005; Feldmann et al., 2009). Such phenomena are supported in humans by the evidence of overweight and obese patients with lower BAT activity in contrast to age-matched healthy men and a significant, negative correlation between BAT activity and both BMI and fat-mass (van Marken Lichtenbelt et al., 2009). Similarly, BAT thermogenic activity in healthy men was higher in winter than in summer and BAT activity was again inversely correlated with BMI and total and visceral fat (Saito et al., 2009). BAT can use dietary nutrients in the fed state or rely on endogenous fuel during fasting. Hence, appropriate mobilization (reduction) of energy stores (fat mass) is required upon energetic demand. WAT-depletion of the Comparative Gene Identification-58 (CGI-58), a lipolytic activator essential for stimulated lipid-droplet lipolysis rendered mice cold-sensitive and hypothermic in a fasted state at room temperature whilst food supply reversed the effect. Conversely, CGI-58-deletion in BAT caused neither effect in fasted or fed mice (Shin et al., 2017). The importance of adequate lipolysis has been documented in humas, whose blunted *in vivo* catecholamine-induced lipolysis has been shown in obese subjects (Horowitz and Klein, 2000; Jocken and Blaak, 2008; Jocken et al., 2008).

Consistent with the literature, pre-obese *ad libitum* fed HDAC5-KO mice failed to maintain body temperature during 5h of cold exposure and exhibited a blunted lipolytic response to *ex vivo* adrenergic stimulation in eWAT explants when contrasted to WT. Our data are thus consistent with the concept that standard housing conditions of 22 to 24ºC can be considered as thermal stress in mice that requires BAT-induced thermogenesis to maintain body temperature and WAT-stimulated lipolysis as well as increased food consumption to supply fuel to thermogenic tissues. This compensatory adaptive process appears disturbed in our HDAC-5 KO model with its insufficient lipolysis and decreased food consumption. Moreover, our HDAC5-KO mice appear to suffer from impaired food partitioning as

revealed by explaining the statistically significant but biologically insignificant reduction in RER, which indicates an unfruitful attempt of the system to rely on lipids when lipolytic capacity is reduced. Both subtle but constant conditions are well-dealt with in WT mice, but promoted gradual gain weight as we observed by mature-onset obesity in HDAC5-KO mice. Additional analyses of gene and protein expression in obese HDAC5-KO mice confirmed the impairment of the eWAT(supply) →BAT(combustion)→EE (heat) chain by showing decreased gene expression and activation of HSL in eWAT and reduced UCP-1 levels in BAT at standard laboratory temperature. Furthermore, no changes were detected in adipogenic, lipogenic or beiging/browning markers in WAT between genotypes, discarding other possible mechanisms for fat accumulation.

6.3. Overactivation of dmARH dopaminergic neurons in HDAC5 KO mice is linked to neuronal inactivation in the PVH

Consistent with our finding of lower lipolytic and thermogenic capacity of WAT and BAT, we found reduced local SNS activity and central PVH inhibition in HDAC5-KO mice. Chronic SNS activity is largely associated with metabolic, renal, and cardiac dysfunction, but the effect is not equally distributed over all tissues due to the differential sympathetic outflow to end-organs. These region-specific changes in sympathetic nervous activity are referred to as sympathetic signatures (Morrison, 2001; Osborn John W. and Kuroki Marcos T., 2012). In obese HDAC5-KO mice, our chemical catecholamine analyses, gene expression and thermography studies pointed toward a local dysregulation of SNS outflow in BAT and eWAT, i.e. decreased noradrenaline release that translated into lower adrenergic-stimulated BAT-thermogenesis and eWAT-lipolysis. Such a phenotype in humans was found in the PIMA population in Arizona, US, and Mexico in which a high prevalence of obesity in young adults was predicted by low metabolic rate, low spontaneous physical activity, low fat-oxidation and low SNS activity (Ravussin and Tataranni, 1996; Tataranni et al., 1997; Galgani and Ravussin, 2008).

Low SNS activity in HDAC5-KO mice was accompanied by reduced neuronal activation in the medial posterior PVH. In mice, the selective ablation of BDNF in the medial and posterior PVH was shown to

abolish UCP1 expression and reduce norepinephrine levels in BAT causing severe obesity (An et al., 2015). Employing retrograde tracers and *Bdnf* mutant mice, the authors delineated that BDNF neurons in the dorsomedial parvicellular (PVHmpd) and posterior PVH project to sympathetic cholinergic preganglionic neurons in the intermediolateral column (IML) of the spinal cord which connect to sympathetic noradrenergic postganglionic neurons and ultimately activate BAT thermogenesis (Bamshad et al., 1999; An et al., 2015). Unfortunately, our data does not allow to fully reveal the identity of the neuronal population inhibited in the PVH and their innervation to BAT in HDAC5-KO mice. However, based on our data, we suggest that medio-posterior PVH BNDF neurons could be involved in the observed phenotype.

Central modulation of the sympathetic outflow into the BAT is largely mediated by dopamine. As historically evidenced, apomorphine and other dopaminergic agonists like quinpirole (LY171555) and 7-OH-DPAT (7-hy- droxy-2-(di-n-propylamino) tetralin) elicited hypothermic effects in rodents (Faunt and Crocker, 1987; Kurashima et al., 1995). Similarly, the sympathetic outflow during cold-inducted BAT-thermogenesis was inhibited when centrally acting dopaminergic D_2 selective agonists like quinpirole and 7-OH-DPAT were administered to rodents (Ootsuka et al., 2007). The central effect of dopamine in thermoregulation was attributed to the hypothalamus through early experiments using intrahypothalamic injections of selective agonists and antagonists (Cox and Lee, 1978, 1980). Recent reports showed intrahypothalamic inhibitory dopaminergic projections connecting the ARH to the PVH and possibly modulating thermogenesis (Zhang and van den Pol, 2016). Consistent with these reports, I quantified higher hypothalamic dopaminergic concentrations and larger numbers of TH[+] projections in conjunction with a lower number of cFOS^{+} neurons in the PVH in obese HDAC5-KO compared to WT. Notably, while I observed only few TH[+] cell bodies in the PVH and LH (data not shown), the number and activation of dmARH dopaminergic neurons was markedly increased in obese HDAC5-KO mice. My finding of prolactin gene repression in the pituitary and decreased circulating prolactin plasma levels physiologically corroborated the over-activation of dmARH dopaminergic neurons in HDAC5-KO compared to WT mice. Importantly, prolactin is described as the main signal activating dmARH dopaminergic neurons irrespectively of whether they project to the ME or to other hypothalamic nuclei, and endogenous prolactin signaling is required for correct development and differentiation of dmARH dopaminergic neurons in mature mice. My assessment of dmARH neurons at various stages of murine

development until adulthood was moreover consistent with earlier reports evidencing a peak within the first month of age and a subsequent decline in the number of dmARH dopaminergic neurons (Phelps et al., 2003). Collating these studies with ours revealed an important discrepancy: the decline in the number of dmARH dopaminergic neurons was greater in prolactin-deficient dwarf mice compared to WT controls. In our HDAC5-KO mice,which show similarly diminished prolactin levels, the decline in the number of dmARH dopaminergic neurons was smaller compared to their WT controls. This discrepancy indicates that dmARH dopaminergic neurons in our HDAC5-KO model are uncoupled from the influence of prolactin. My data further suggests that dmARH dopaminergic neurons remain hyperactivated in HDAC5-KO mice in a prolactin-independent manner.

Although my results do not provide full validation, HDAC5 might limit or terminate the dopaminergic activation in the ARH. In these neurons, firing can be induced by oxytocin, ghrelin, angiotensin II (AngII) and prolactin but only prolactin and AngII have been shown to stimulate TH gene expression and phosphorylation at Ser19, Ser31, and Ser40 (Myers and Steele, 1991; Arbogast and Voogt, 1995; Yu et al., 1996; Liu and Arbogast, 2008; Romanò et al., 2013; Zhang and van den Pol, 2016, 2016). TH phosphorylation is mediated by Erk1/2, PKA, PKC, and CaMPKII and its transcriptional regulation is supposed to be mediated by STAT5b although no clear evidence has probed STAT5b binding to the *Th* promoter (Ma et al., 2004; Brown et al., 2012; Yip et al., 2012, 2019). Prolactin treatment in human breast cancer T47D cells revealed a potential activation mechanism of STAT5b. Upon ligand binding, CBP is recruited to PRLR monomers promoting homodimerization. Cytoplasmic loop-dimerized PRLR then activates STAT5b, which is also acetylated by CBP and undergoes acetylation-dependent homodimerization. Protein kinase JAK2 docks within the PRLR cytoplasmic-loops and phosphorylates PRLR and loop-associated STAT5b, promoting dissociation of the later to form a transcriptionally active dimer (Ma et al., 2010). Furthermore, such acetylation-dependent homodimerization of PRLR and STAT5b was reverted by HDAC6, HDAC3, SIRT2 or SIRT2 overexpression. In accordance with these references, we demonstrated the interaction between HDAC5 and STAT5b in the hypothalamus and the subcellular phosphorylation-independent reallocation of STAT5b to the nuclear compartment in the absence of HDAC5. Future investigations are required to confirm hypothalamic STAT5b-hyperacetylation in HDAC5-KO mice but - supporting the potential transcriptional action of nuclear STAT5b - *Th* expression was increased in HDAC5-KO mice compared to WT controls. My finding of

elevated TH-phosphorylation at Ser40 without alterations in the expression or activation of Erk1/2 moreover suggested the involvement of other protein kinases such as PKA. Identifying these additional signaling factors involved in HDAC5-dependent dmARH dopamine neurons activation warrants in-depth future studies.

Dorsomedial ARH TH expression and activation has a higher layer of complexity in females compared to males. During late pregnancy and lactation, circulating prolactin levels increase to support lactation and promote maternal behavioral adaptations. dmARH dopaminergic neurons present remarkable plasticity under the presence of constantly elevated circulating prolactin or placental lactogen levels. The dopamine-mediated inhibitory tone is switched toward met-enkephalin-mediated stimulatory tone in lactotrophic cells in the pituitary via the reduction in pErk1/2, pTH and dopamine (Yip et al., 2019). Importantly, prolactin, or hypothalamic prolactin receptor, deficiency caused complete infertility in female mice (Christensen et al., 2013). Our results presented no differences in fertility, reproduction rate or the number of females and males per litter between genotypes. Even when sexually dimorphic protection to gain weight caused by estrogen in cycling females would alleviate the obese phenotype in HDAC5-KO female, such marked circulating prolactin deficiency would repercuss in fertility. Due to the plastic phenotype of dmARH dopaminergic neurons in females, HDAC5 might not play a similar role as it does in male mice. Deciphering the sexual dimorphism in the activation of dmARH dopaminergic neurons in HDAC5-KO mice escaped the present research project but warrants future studies.

7. Conclusions and outlook

In the first part of my thesis, I successfully established two FACS pipelines for the study of cell subpopulations from brain samples. Depending on the cell population, whether it was neuronal or astroglial, I validated a nucleus-specific or a whole-cell-specific sorting approach from frozen or fresh tissue, respectively. Using the nucleus sorting allowed me to over-come the difficulties of acquiring intact cell suspensions from adult mice. My work demonstrates the versatility of the pipelines and encourages future investigations to employ the pipelines for a better and more delineated comprehension of molecular mechanisms in specific subpopulations in relevant physiological and pathological conditions.

In the second part, I revealed that the presence of HDAC5 is essential for an appropriate regulation of energy homeostasis in mice exposed to a non-obesogenic environment. Male mice with a global deficiency for HDAC5 showed a reduced energy expenditure and insufficient compensatory reduction in energy intake that led to the excessive accumulation of energy in form of fat mass. This finding suggests that energy intake was decreased as a consequence of reduced energy expenditure. and supports previous hypotheses about behavioral compensatory mechanisms to limit the unrequired storage of energy (Speakman et al., 2011). Brown fat thermogenesis, and the noradrenergic stimulation of WAT lipolysis were impaired in the absence of HDAC5. Of note, my finding of decreased respiratory exchange ratios as measure for fuel utilization in male HDAC5 KO mice, compared to WT control, are consistent with an essential role of HDAC5 in controlling noradrenaline release from SNS terminals to ensure fuel supply from WAT-lipolysis when energy demand is high, for instance when thermogenesis by BAT is increased. Future studies should elaborate on this potential role of HDAC5 in orchestrating our fuel supply in response to changing environmental conditions, e.g. during an energetically demanding cold-exposure.

Future studies should moreover focus on the role of HDAC5 in the regulation of energy homeostasis In humans. To date, HDAC5 polymorphisms have not been associated with human pathologies. It would be interesting to assess whether a low metabolic rate, low spontaneous physical activity, or low SNS

activity in humans is linked with perturbations in HDAC5 expression or function in humans. Such studies could e.g. be assessed in the PIMA Indians, one of the most obese populations in the world with a particular adult-onset obesity and weight-gain predictive low metabolic rate, on whether HDAC5 expression/activity in these individuals is linked, or predictive, for the enhanced susceptibility to developing mature-onset obesity in such distinct genetic population.

Peripheral lower SNS activity carrying reduced thermogenic energy expenditure concurred with central neuronal activity inhibition in the PVH, but activation in the ARH. Albeit we did not provide causality, intrahypothalamic dysregulation appeared to be mediated by increased dopaminergic tone in HDAC5-KO mice. Consistent with this, we found higher hypothalamic dopamine levels, dopaminergic innervation in the PVH and dopaminergic neuronal activity in the dmARH that appeared first in young adult HDAC5-KO mice. Specific studies using DAT-Cre mice with AAV-mediated *Hdac5*-KD in the ARH and BDNF staining in the PVH would be necessary to provide evidence for our claims.

In the hypothalamus HDAC5 interacted with STAT5b regulating its subcellular localization and possibly its transcriptional regulation. We observed elevated nuclear STAT5b and *Th* expression in the hypothalamus in a prolactin-independent manner upon HDAC5-deletion. TH phosphorylation (Ser40) was augmented independently of Erk1/2. To gain more insight into the molecular mechanism, STAT5b-ChIP-qPCR for *Th* and measuring PKA/PKC activity in hypothalamic homogenates would be adequate approaches.

Overall, HDAC5 appears to orchestrate SNS activity in brown and white adipose tissue to control energy homeostasis. Deficiency for HDAC5 in male mice is thus causally linked the development of obesity, even under non-obesogenic conditions. Mechanistically, my data suggests that HDAC5 plays a leading role in the modulation of hypothalamic neuronal activity by governing the activity of dopaminergic neurons in the dorsomedial arcuate nucleus. However, due to the lack of appropriate genetic models, my data does not provide causality for the proposed model whereby HDAC5 is at the heart of a dmARH-PVN-SNS-WAT/BAT axis that controls thermogenesis and lipolysis. Future experiments are thus warranted to clarify this putative role of HDAC5 in governing dopaminergic activity in the ARH and SNS-driven metabolism in brown and white adipose tissue.

8. References

Acheson, K., Jéquier, E., and Wahren, J. (1983). Influence of beta-adrenergic blockade on glucose-induced thermogenesis in man. *J Clin Invest* 72, 981–986. doi:10.1172/JCI111070.

An, J. J., Liao, G.-Y., Kinney, C. E., Sahibzada, N., and Xu, B. (2015). Discrete BDNF Neurons in the Paraventricular Hypothalamus Control Feeding and Energy Expenditure. *Cell Metab* 22, 175–188. doi:10.1016/j.cmet.2015.05.008.

Anand, B. K., and Brobeck, J. R. (1951). Hypothalamic control of food intake in rats and cats. *Yale J Biol Med* 24, 123–140.

Anand, B. K., Dua, S., and Shoenberg, K. (1955). Hypothalamic control of food intake in cats and monkeys. *J Physiol* 127, 143–152. doi:10.1113/jphysiol.1955.sp005244.

Angelidis, I., Simon, L. M., Fernandez, I. E., Strunz, M., Mayr, C. H., Greiffo, F. R., et al. (2019). An atlas of the aging lung mapped by single cell transcriptomics and deep tissue proteomics. *Nat Commun* 10, 963. doi:10.1038/s41467-019-08831-9.

Arbogast, L. A., and Voogt, J. L. (1995). Hypoprolactinemia decreases tyrosine hydroxylase activity in the tuberoinfundibular dopaminergic neurons acutely by protein dephosphorylation and chronically by changes in gene expression. *Endocrine* 3, 801–806. doi:10.1007/BF02935684.

Astrup, A., Gøtzsche, P. C., van de Werken, K., Ranneries, C., Toubro, S., Raben, A., et al. (1999). Meta-analysis of resting metabolic rate in formerly obese subjects. *Am. J. Clin. Nutr.* 69, 1117–1122. doi:10.1093/ajcn/69.6.1117.

Bamshad, M., Song, C. K., and Bartness, T. J. (1999). CNS origins of the sympathetic nervous system outflow to brown adipose tissue. *American Journal of Physiology-Regulatory, Integrative and Comparative Physiology* 276, R1569–R1578. doi:10.1152/ajpregu.1999.276.6.R1569.

Bartness, T. J., Liu, Y., Shrestha, Y. B., and Ryu, V. (2014). Neural Innervation of White Adipose Tissue and the Control of Lipolysis. *Front Neuroendocrinol* 35, 473–493. doi:10.1016/j.yfrne.2014.04.001.

Baulande, S., Lasnier, F., Lucas, M., and Pairault, J. (2001). Adiponutrin, a transmembrane protein corresponding to a novel dietary- and obesity-linked mRNA specifically expressed in the adipose lineage. *J Biol Chem* 276, 33336–33344. doi:10.1074/jbc.M105193200.

Binart, N., Melaine, N., Pineau, C., Kercret, H., Touzalin, A. M., Imbert-Bolloré, P., et al. (2003). Male Reproductive Function Is Not Affected in Prolactin Receptor-Deficient Mice. *Endocrinology* 144, 3779–3782. doi:10.1210/en.2003-0409.

Blundell, J. E., Caudwell, P., Gibbons, C., Hopkins, M., Naslund, E., King, N., et al. (2012). Role of resting metabolic rate and energy expenditure in hunger and appetite control: a new formulation. *Dis Model Mech* 5, 608–613. doi:10.1242/dmm.009837.

Boyd, A. E., Mager, M., Angoff, G., and Lebovitz, H. E. (1974). Effect of acute administration of L-dopa on body temperature in man. *J Appl Physiol* 37, 675–678. doi:10.1152/jappl.1974.37.5.675.

Bray, G. A. (1991). Obesity, a disorder of nutrient partitioning: the MONA LISA hypothesis. *J Nutr* 121, 1146–1162. doi:10.1093/jn/121.8.1146.

Bray, G. A., Smith, S. R., de Jonge, L., Xie, H., Rood, J., Martin, C. K., et al. (2012). Effect of dietary protein content on weight gain, energy expenditure, and body composition during overeating: a randomized controlled trial. *JAMA* 307, 47–55. doi:10.1001/jama.2011.1918.

Brown, L. M., Gent, L., Davis, K., and Clegg, D. J. (2010). Metabolic impact of sex hormones on obesity. *Brain Res* 1350, 77–85. doi:10.1016/j.brainres.2010.04.056.

Brown, R. S. E., Piet, R., Herbison, A. E., and Grattan, D. R. (2012). Differential Actions of Prolactin on Electrical Activity and Intracellular Signal Transduction in Hypothalamic Neurons. *Endocrinology* 153, 2375–2384. doi:10.1210/en.2011-2005.

Burger, K. S., and Stice, E. (2011). Relation of dietary restraint scores to activation of reward-related brain regions in response to food intake, anticipated intake, and food pictures. *NeuroImage* 55, 233–239. doi:10.1016/j.neuroimage.2010.12.009.

Cahoy, J. D., Emery, B., Kaushal, A., Foo, L. C., Zamanian, J. L., Christopherson, K. S., et al. (2008). A transcriptome database for astrocytes, neurons, and oligodendrocytes: a new resource for understanding brain development and function. *J. Neurosci.* 28, 264–278. doi:10.1523/JNEUROSCI.4178-07.2008.

Campbell, J. N., Macosko, E. Z., Fenselau, H., Pers, T. H., Lyubetskaya, A., Tenen, D., et al. (2017). A molecular census of arcuate hypothalamus and median eminence cell types. *Nature Neuroscience* 20, 484–496. doi:10.1038/nn.4495.

Camps, S. G. J. A., Verhoef, S. P. M., and Westerterp, K. R. (2013). Weight loss, weight maintenance, and adaptive thermogenesis. *Am. J. Clin. Nutr.* 97, 990–994. doi:10.3945/ajcn.112.050310.

Cannon, B., and Nedergaard, J. (2004). Brown adipose tissue: function and physiological significance. *Physiol Rev* 84, 277–359. doi:10.1152/physrev.00015.2003.

Cao, J., Sun, L., Aramsangtienchai, P., Spiegelman, N. A., Zhang, X., Huang, W., et al. (2019). HDAC11 regulates type I interferon signaling through defatty-acylation of SHMT2. *PNAS* 116, 5487–5492. doi:10.1073/pnas.1815365116.

Carhuatanta, K. A. K., Demuro, G., Tschöp, M. H., Pfluger, P. T., Benoit, S. C., and Obici, S. (2011). Voluntary Exercise Improves High-Fat Diet-Induced Leptin Resistance Independent of Adiposity. *Endocrinology* 152, 2655–2664. doi:10.1210/en.2010-1340.

Catenacci, V. A., Odgen, L., Phelan, S., Thomas, J. G., Hill, J., Wing, R. R., et al. (2014). Dietary habits and weight maintenance success in high versus low exercisers in the National Weight Control Registry. *J Phys Act Health* 11, 1540–1548. doi:10.1123/jpah.2012-0250.

Caudwell, P., Finlayson, G., Gibbons, C., Hopkins, M., King, N., Näslund, E., et al. (2013). Resting metabolic rate is associated with hunger, self-determined meal size, and daily energy intake and may represent a marker for appetite. *Am. J. Clin. Nutr.* 97, 7–14. doi:10.3945/ajcn.111.029975.

Chen, R., Wu, X., Jiang, L., and Zhang, Y. (2017). Single-Cell RNA-Seq Reveals Hypothalamic Cell Diversity. *Cell Rep* 18, 3227–3241. doi:10.1016/j.celrep.2017.03.004.

Chhabra, K. H., Adams, J. M., Jones, G. L., Yamashita, M., Schlapschy, M., Skerra, A., et al. (2016). Reprogramming the body weight set point by a reciprocal interaction of hypothalamic leptin sensitivity and Pomc gene expression reverts extreme obesity. *Mol Metab* 5, 869–881. doi:10.1016/j.molmet.2016.07.012.

Cho, Y., Sloutsky, R., Naegle, K. M., and Cavalli, V. (2013). Injury-induced HDAC5 nuclear export is essential for axon regeneration. *Cell* 155, 894–908. doi:10.1016/j.cell.2013.10.004.

Christensen, H. R., Murawsky, M. K., Horseman, N. D., Willson, T. A., and Gregerson, K. A. (2013). Completely Humanizing Prolactin Rescues Infertility in Prolactin Knockout Mice and Leads to Human Prolactin Expression in Extrapituitary Mouse Tissues. *Endocrinology* 154, 4777–4789. doi:10.1210/en.2013-1476.

Contreras, R. E., Schriever, S. C., and Pfluger, P. T. (2019). Physiological and Epigenetic Features of Yoyo Dieting and Weight Control. *Front Genet* 10, 1015. doi:10.3389/fgene.2019.01015.

Cooper, K. E., Jones, D. L., Pittman, Q. J., and Veale, W. L. (1976). The effect of noradrenaline, injected into the hypothalamus, on thermoregulation in the cat. *J Physiol* 261, 211–222.

Corbett, S. W., Stern, J. S., and Keesey, R. E. (1986). Energy expenditure in rats with diet-induced obesity. *Am. J. Clin. Nutr.* 44, 173–180. doi:10.1093/ajcn/44.2.173.

Cornier, M.-A., Grunwald, G. K., Johnson, S. L., and Bessesen, D. H. (2004). Effects of short-term overfeeding on hunger, satiety, and energy intake in thin and reduced-obese individuals. *Appetite* 43, 253–259. doi:10.1016/j.appet.2004.06.003.

Corrigan, J. K., Ramachandran, D., He, Y., Palmer, C. J., Jurczak, M. J., Chen, R., et al. A big-data approach to understanding metabolic rate and response to obesity in laboratory mice. *eLife* 9. doi:10.7554/eLife.53560.

Cox, B., and Lee, T. F. (1978). Is acetylcholine involved in a dopamine receptor mediated hypothermia in mice and rats? *Br J Pharmacol* 62, 339–347.

Cox, B., and Lee, T. F. (1980). Further evidence for a physiological role for hypothalamic dopamine in thermoregulation in the rat. *The Journal of Physiology* 300, 7–17. doi:10.1113/jphysiol.1980.sp013147.

Crujeiras, A. B., Goyenechea, E., Abete, I., Lage, M., Carreira, M. C., Martínez, J. A., et al. (2010). Weight Regain after a Diet-Induced Loss Is Predicted by Higher Baseline Leptin and Lower Ghrelin Plasma Levels. *J Clin Endocrinol Metab* 95, 5037–5044. doi:10.1210/jc.2009-2566.

Cui, X., Nguyen, N. L. T., Zarebidaki, E., Cao, Q., Li, F., Zha, L., et al. (2016). Thermoneutrality decreases thermogenic program and promotes adiposity in high-fat diet-fed mice. *Physiological Reports* 4, e12799. doi:https://doi.org/10.14814/phy2.12799.

Dalton, M., Hollingworth, S., Blundell, J., and Finlayson, G. (2015). Weak Satiety Responsiveness Is a Reliable Trait Associated with Hedonic Risk Factors for Overeating among Women. *Nutrients* 7, 7421–7436. doi:10.3390/nu7095345.

Davis, C., Zai, C., Levitan, R. D., Kaplan, A. S., Carter, J. C., Reid-Westoby, C., et al. (2011). Opiates, overeating and obesity: a psychogenetic analysis. *International Journal of Obesity* 35, 1347–1354. doi:10.1038/ijo.2010.276.

de Castro, J. M., and Plunkett, S. (2002). A general model of intake regulation. *Neurosci Biobehav Rev* 26, 581–595.

Deal, R. B., and Henikoff, S. (2011). The INTACT method for cell type-specific gene expression and chromatin profiling in Arabidopsis thaliana. *Nat Protoc* 6, 56–68. doi:10.1038/nprot.2010.175.

Deng, G., Morselli, L. L., Wagner, V. A., Balapattabi, K., Sapouckey, S. A., Knudtson, K. L., et al. (2020). Single-Nucleus RNA Sequencing of the Hypothalamic Arcuate Nucleus of C57BL/6J Mice After Prolonged Diet-Induced Obesity. *Hypertension* 76, 589–597. doi:10.1161/HYPERTENSIONAHA.120.15137.

DeRosa, M. A., and Cryer, P. E. (2004). Hypoglycemia and the sympathoadrenal system: neurogenic symptoms are largely the result of sympathetic neural, rather than adrenomedullary, activation. *Am J Physiol Endocrinol Metab* 287, E32-41. doi:10.1152/ajpendo.00539.2003.

Doucet, E., St-Pierre, S., Alméras, N., Després, J. P., Bouchard, C., and Tremblay, A. (2001). Evidence for the existence of adaptive thermogenesis during weight loss. *Br. J. Nutr.* 85, 715–723.

Drapeau, V., King, N., Hetherington, M., Doucet, E., Blundell, J., and Tremblay, A. (2007). Appetite sensations and satiety quotient: predictors of energy intake and weight loss. *Appetite* 48, 159–166. doi:10.1016/j.appet.2006.08.002.

Duncan, R. E., Ahmadian, M., Jaworski, K., Sarkadi-Nagy, E., and Sul, H. S. (2007). Regulation of Lipolysis in Adipocytes. *Annu Rev Nutr* 27, 79–101. doi:10.1146/annurev.nutr.27.061406.093734.

Even, P. C., and Nadkarni, N. A. (2012). Indirect calorimetry in laboratory mice and rats: principles, practical considerations, interpretation and perspectives. *Am J Physiol Regul Integr Comp Physiol* 303, R459-476. doi:10.1152/ajpregu.00137.2012.

Farooqi, I. S., Jebb, S. A., Langmack, G., Lawrence, E., Cheetham, C. H., Prentice, A. M., et al. (1999). Effects of recombinant leptin therapy in a child with congenital leptin deficiency. *N. Engl. J. Med.* 341, 879–884. doi:10.1056/NEJM199909163411204.

Farooqi, I. S., and O'Rahilly, S. (2008). Mutations in ligands and receptors of the leptin-melanocortin pathway that lead to obesity. *Nat Clin Pract Endocrinol Metab* 4, 569–577. doi:10.1038/ncpendmet0966.

Faunt, J. E., and Crocker, A. D. (1987). The effects of selective dopamine receptor agonists and antagonists on body temperature in rats. *European Journal of Pharmacology* 133, 243–247. doi:10.1016/0014-2999(87)90019-7.

Feldberg, W., and Myers, R. D. (1963). A New Concept of Temperature Regulation by Amines in the Hypothalamus. *Nature* 200, 1325–1325. doi:10.1038/2001325a0.

Feldmann, H. M., Golozoubova, V., Cannon, B., and Nedergaard, J. (2009). UCP1 ablation induces obesity and abolishes diet-induced thermogenesis in mice exempt from thermal stress by living at thermoneutrality. *Cell Metab* 9, 203–209. doi:10.1016/j.cmet.2008.12.014.

Flurkey, K., Papaconstantinou, J., and Harrison, D. E. (2002). The Snell dwarf mutation Pit1(dw) can increase life span in mice. *Mech Ageing Dev* 123, 121–130. doi:10.1016/s0047-6374(01)00339-6.

Fothergill, E., Guo, J., Howard, L., Kerns, J. C., Knuth, N. D., Brychta, R., et al. (2016). Persistent metabolic adaptation 6 years after "The Biggest Loser" competition. *Obesity (Silver Spring)* 24, 1612–1619. doi:10.1002/oby.21538.

Friedman, J. (2016). The long road to leptin. doi:10.1172/JCI91578.

Froidevaux, F., Schutz, Y., Christin, L., and Jéquier, E. (1993). Energy expenditure in obese women before and during weight loss, after refeeding, and in the weight-relapse period. *Am. J. Clin. Nutr.* 57, 35–42. doi:10.1093/ajcn/57.1.35.

Galgani, J., and Ravussin, E. (2008). Energy metabolism, fuel selection and body weight regulation. *Int J Obes (Lond)* 32, S109–S119. doi:10.1038/ijo.2008.246.

Gallinari, P., Marco, S. D., Jones, P., Pallaoro, M., and Steinkühler, C. (2007). HDACs, histone deacetylation and gene transcription: from molecular biology to cancer therapeutics. *Cell Research* 17, 195–211. doi:10.1038/sj.cr.7310149.

García, M. C., Wernstedt, I., Berndtsson, A., Enge, M., Bell, M., Hultgren, O., et al. (2006). Mature-Onset Obesity in Interleukin-1 Receptor I Knockout Mice. *Diabetes* 55, 1205–1213. doi:10.2337/db05-1304.

García-Cáceres, C., Quarta, C., Varela, L., Gao, Y., Gruber, T., Legutko, B., et al. (2016). Astrocytic Insulin Signaling Couples Brain Glucose Uptake with Nutrient Availability. *Cell* 166, 867–880. doi:10.1016/j.cell.2016.07.028.

Gisolfi, C. V., Mora, F., and Wall, P. T. (1980). Dopamine and temperature regulation in the primate: Effects of apomorphine and pimozide. *Brain Research Bulletin* 5, 349–352. doi:10.1016/S0361-9230(80)80003-7.

Goldsmith, R., Joanisse, D. R., Gallagher, D., Pavlovich, K., Shamoon, E., Leibel, R. L., et al. (2010). Effects of experimental weight perturbation on skeletal muscle work efficiency, fuel utilization, and biochemistry in human subjects. *Am. J. Physiol. Regul. Integr. Comp. Physiol.* 298, R79-88. doi:10.1152/ajpregu.00053.2009.

González-García, I., Milbank, E., Martinez-Ordoñez, A., Diéguez, C., López, M., and Contreras, C. (2020). HYPOTHesizing about central comBAT against obesity. *J Physiol Biochem* 76, 193–211. doi:10.1007/s13105-019-00719-y.

Greco, T. M., Yu, F., Guise, A. J., and Cristea, I. M. (2011). Nuclear Import of Histone Deacetylase 5 by Requisite Nuclear Localization Signal Phosphorylation. *Molecular & Cellular Proteomics : MCP* 10. doi:10.1074/mcp.M110.004317.

Greenway, F. L. (2015). Physiological adaptations to weight loss and factors favouring weight regain. *Int J Obes (Lond)* 39, 1188–1196. doi:10.1038/ijo.2015.59.

Grozinger, C. M., and Schreiber, S. L. (2000). Regulation of histone deacetylase 4 and 5 and transcriptional activity by 14-3- 3-dependent cellular localization. *PNAS* 97, 7835–7840. doi:10.1073/pnas.140199597.

Haberland, M., Montgomery, R. L., and Olson, E. N. (2009). The many roles of histone deacetylases in development and physiology: implications for disease and therapy. *Nat Rev Genet* 10, 32–42. doi:10.1038/nrg2485.

Hagan, C. (2017). When are mice considered old? *The Jackson Laboratory.* Available at: https://www.jax.org/news-and-insights/jax-blog/2017/november/when-are-mice-considered-old [Accessed November 17, 2020].

Hai, Y., Shinsky, S. A., Porter, N. J., and Christianson, D. W. (2017). Histone deacetylase 10 structure and molecular function as a polyamine deacetylase. *Nature Communications* 8, 15368. doi:10.1038/ncomms15368.

Halaas, J. L., Boozer, C., Blair-West, J., Fidahusein, N., Denton, D. A., and Friedman, J. M. (1997). Physiological response to long-term peripheral and central leptin infusion in lean and obese mice. *Proc. Natl. Acad. Sci. U.S.A.* 94, 8878–8883.

Hames, K. C., Coen, P. M., King, W. C., Anthony, S. J., Stefanovic-Racic, M., Toledo, F. G. S., et al. (2016). Resting and exercise energy metabolism in weight-reduced adults with severe obesity. *Obesity (Silver Spring)* 24, 1290–1298. doi:10.1002/oby.21501.

Hammond, T. R., Dufort, C., Dissing-Olesen, L., Giera, S., Young, A., Wysoker, A., et al. (2019). Single-Cell RNA Sequencing of Microglia throughout the Mouse Lifespan and in the Injured Brain Reveals Complex Cell-State Changes. *Immunity* 50, 253-271.e6. doi:10.1016/j.immuni.2018.11.004.

Harrison, L., Schriever, S. C., Feuchtinger, A., Kyriakou, E., Baumann, P., Pfuhlmann, K., et al. (2018). Fluorescent blood–brain barrier tracing shows intact leptin transport in obese mice. *International Journal of Obesity*, 1. doi:10.1038/s41366-018-0221-z.

He, T., Huang, J., Chen, L., Han, G., Stanmore, D., Krebs-Haupenthal, J., et al. (2020). Cyclic AMP represses pathological MEF2 activation by myocyte-specific hypo-phosphorylation of HDAC5. *Journal of Molecular and Cellular Cardiology* 145, 88–98. doi:10.1016/j.yjmcc.2020.05.018.

He, W., Lam, T. K. T., Obici, S., and Rossetti, L. (2006). Molecular disruption of hypothalamic nutrient sensing induces obesity. *Nat. Neurosci.* 9, 227–233. doi:10.1038/nn1626.

Hill, J. O., Sparling, P. B., Shields, T. W., and Heller, P. A. (1987). Effects of exercise and food restriction on body composition and metabolic rate in obese women. *Am. J. Clin. Nutr.* 46, 622–630. doi:10.1093/ajcn/46.4.622.

Hill, J. O., Wyatt, H. R., and Peters, J. C. (2012). Energy Balance and Obesity. *Circulation* 126, 126–132. doi:10.1161/CIRCULATIONAHA.111.087213.

Hissa, R., and Rautenberg, W. (1974). The influence of centrally applied noradrenaline on shivering and body temperature in the pigeon. *The Journal of Physiology* 238, 427–435. doi:10.1113/jphysiol.1974.sp010534.

Holm, C. (2003). Molecular mechanisms regulating hormone-sensitive lipase and lipolysis. *Biochem Soc Trans* 31, 1120–1124. doi:10.1042/bst0311120.

Horowitz, J. F., and Klein, S. (2000). Whole body and abdominal lipolytic sensitivity to epinephrine is suppressed in upper body obese women. *Am J Physiol Endocrinol Metab* 278, E1144-1152. doi:10.1152/ajpendo.2000.278.6.E1144.

Hubbert, C., Guardiola, A., Shao, R., Kawaguchi, Y., Ito, A., Nixon, A., et al. (2002). HDAC6 is a microtubule-associated deacetylase. *Nature* 417, 455–458. doi:10.1038/417455a.

Jansson, J.-O., Palsdottir, V., Hägg, D. A., Schéle, E., Dickson, S. L., Anesten, F., et al. (2018). Body weight homeostat that regulates fat mass independently of leptin in rats and mice. *Proc. Natl. Acad. Sci. U.S.A.* 115, 427–432. doi:10.1073/pnas.1715687114.

Jiang, Y., Matevossian, A., Huang, H.-S., Straubhaar, J., and Akbarian, S. (2008). Isolation of neuronal chromatin from brain tissue. *BMC Neurosci* 9, 42. doi:10.1186/1471-2202-9-42.

Jimenez, M., Léger, B., Canola, K., Lehr, L., Arboit, P., Seydoux, J., et al. (2002). Beta(1)/beta(2)/beta(3)-adrenoceptor knockout mice are obese and cold-sensitive but have normal lipolytic responses to fasting. *FEBS Lett* 530, 37–40. doi:10.1016/s0014-5793(02)03387-2.

Jocken, J. W. E., and Blaak, E. E. (2008). Catecholamine-induced lipolysis in adipose tissue and skeletal muscle in obesity. *Physiology & Behavior* 94, 219–230. doi:10.1016/j.physbeh.2008.01.002.

Jocken, J. W. E., Goossens, G. H., van Hees, A. M. J., Frayn, K. N., van Baak, M., Stegen, J., et al. (2008). Effect of beta-adrenergic stimulation on whole-body and abdominal subcutaneous adipose tissue lipolysis in lean and obese men. *Diabetologia* 51, 320–327. doi:10.1007/s00125-007-0866-y.

Kabra, D. G., Pfuhlmann, K., García-Cáceres, C., Schriever, S. C., Casquero García, V., Kebede, A. F., et al. (2016a). Hypothalamic leptin action is mediated by histone deacetylase 5. *Nature Communications* 7, 10782. doi:10.1038/ncomms10782.

Kabra, D. G., Pfuhlmann, K., García-Cáceres, C., Schriever, S. C., Casquero García, V., Kebede, A. F., et al. (2016b). Hypothalamic leptin action is mediated by histone deacetylase 5. *Nat Commun* 7, 10782. doi:10.1038/ncomms10782.

Kaiyala, K. J., Morton, G. J., Thaler, J. P., Meek, T. H., Tylee, T., Ogimoto, K., et al. (2012). Acutely Decreased Thermoregulatory Energy Expenditure or Decreased Activity Energy Expenditure Both Acutely Reduce Food Intake in Mice. *PLOS ONE* 7, e41473. doi:10.1371/journal.pone.0041473.

Karatsoreos, I. N., Thaler, J. P., Borgland, S. L., Champagne, F. A., Hurd, Y. L., and Hill, M. N. (2013). Food for Thought: Hormonal, Experiential, and Neural Influences on Feeding and Obesity. *Journal of Neuroscience* 33, 17610–17616. doi:10.1523/JNEUROSCI.3452-13.2013.

Kelesidis, T., Kelesidis, I., Chou, S., and Mantzoros, C. S. (2010). Narrative Review: The Role of Leptin in Human Physiology: Emerging Clinical Applications. *Ann Intern Med* 152, 93–100. doi:10.1059/0003-4819-152-2-201001190-00008.

Kelley, K. W., Nakao-Inoue, H., Molofsky, A. V., and Oldham, M. C. (2018). Variation among intact tissue samples reveals the core transcriptional features of human CNS cell classes. *Nature Neuroscience* 21, 1171. doi:10.1038/s41593-018-0216-z.

Kelly, P. A., Binart, N., Lucas, B., Bouchard, B., and Goffin, V. (2001). Implications of multiple phenotypes observed in prolactin receptor knockout mice. *Front Neuroendocrinol* 22, 140–145. doi:10.1006/frne.2001.0212.

Kennedy, G. (1953). The role of depot fat in the hypothalamic control of food intake in the rat. *Proceedings of the Royal Society of London. Series B - Biological Sciences* 140, 578–592. doi:10.1098/rspb.1953.0009.

Kim, G. S., Jung, H.-E., Kim, J.-S., and Lee, Y. C. (2015). Mutagenesis Study Reveals the Rim of Catalytic Entry Site of HDAC4 and -5 as the Major Binding Surface of SMRT Corepressor. *PLoS One* 10, e0132680. doi:10.1371/journal.pone.0132680.

Kim, J. G., Suyama, S., Koch, M., Jin, S., Argente-Arizon, P., Argente, J., et al. (2014). Leptin signaling in astrocytes regulates hypothalamic neuronal circuits and feeding. *Nat. Neurosci.* 17, 908–910. doi:10.1038/nn.3725.

Kirchner, H., Hofmann, S. M., Fischer-Rosinsky, A., Hembree, J., Abplanalp, W., Ottaway, N., et al. (2012). Caloric Restriction Chronically Impairs Metabolic Programming in Mice. *Diabetes* 61, 2734–2742. doi:10.2337/db11-1621.

Kissileff, H. R., Thornton, J. C., Torres, M. I., Pavlovich, K., Mayer, L. S., Kalari, V., et al. (2012). Leptin reverses declines in satiation in weight-reduced obese humans. *Am. J. Clin. Nutr.* 95, 309–317. doi:10.3945/ajcn.111.012385.

Klymenko, O., Brecklinghaus, T., Dille, M., Springer, C., de Wendt, C., Altenhofen, D., et al. (2020). Histone deacetylase 5 regulates interleukin 6 secretion and insulin action in skeletal muscle. *Molecular Metabolism* 42, 101062. doi:10.1016/j.molmet.2020.101062.

Kontani, Y., Wang, Y., Kimura, K., Inokuma, K.-I., Saito, M., Suzuki-Miura, T., et al. (2005). UCP1 deficiency increases susceptibility to diet-induced obesity with age. *Aging Cell* 4, 147–155. doi:10.1111/j.1474-9726.2005.00157.x.

Kosan, C., Ginter, T., Heinzel, T., and Krämer, O. H. (2013). STAT5 acetylation: Mechanisms and consequences for immunological control and leukemogenesis. *JAKSTAT* 2, e26102. doi:10.4161/jkst.26102.

Kouzarides, T. (2000). Acetylation: a regulatory modification to rival phosphorylation? *EMBO J* 19, 1176–1179. doi:10.1093/emboj/19.6.1176.

Kovacs, J. J., Murphy, P. J. M., Gaillard, S., Zhao, X., Wu, J.-T., Nicchitta, C. V., et al. (2005). HDAC6 regulates Hsp90 acetylation and chaperone-dependent activation of glucocorticoid receptor. *Mol Cell* 18, 601–607. doi:10.1016/j.molcel.2005.04.021.

Kozyreva, T. V., Meyta, E. S., and Khramova, G. M. (2015). Effect of the sympathetic nervous system co-transmitters ATP and norepinephrine on thermoregulatory response to cooling. *Temperature* 2, 121–128. doi:10.1080/23328940.2014.1000705.

Krishnaswami, S. R., Grindberg, R. V., Novotny, M., Venepally, P., Lacar, B., Bhutani, K., et al. (2016a). Using single nuclei for RNA-seq to capture the transcriptome of postmortem neurons. *Nature Protocols* 11, 499–524. doi:10.1038/nprot.2016.015.

Krishnaswami, S. R., Grindberg, R. V., Novotny, M., Venepally, P., Lacar, B., Bhutani, K., et al. (2016b). Using single nuclei for RNA-seq to capture the transcriptome of postmortem neurons. *Nat Protoc* 11, 499–524. doi:10.1038/nprot.2016.015.

Kurashima, M., Yamada, K., Nagashima, M., Shirakawa, K., and Furukawa, T. (1995). Effects of putative dopamine D3 receptor agonists, 7-OH-DPAT, and quinpirole, on yawning, stereotypy, and body temperature in rats. *Pharmacology Biochemistry and Behavior* 52, 503–508. doi:10.1016/0091-3057(95)00103-4.

Lahm, A., Paolini, C., Pallaoro, M., Nardi, M. C., Jones, P., Neddermann, P., et al. (2007). Unraveling the hidden catalytic activity of vertebrate class IIa histone deacetylases. *Proc Natl Acad Sci U S A* 104, 17335–17340. doi:10.1073/pnas.0706487104.

Lam, B. Y. H., Cimino, I., Polex-Wolf, J., Nicole, S. K., Rimmington, D., Iyemere, V., et al. (2017). Heterogeneity of hypothalamic pro-opiomelanocortin-expressing neurons revealed by single-cell RNA sequencing. *Mol Metab* 6, 383–392. doi:10.1016/j.molmet.2017.02.007.

Lam, T. K. T., Pocai, A., Gutierrez-Juarez, R., Obici, S., Bryan, J., Aguilar-Bryan, L., et al. (2005). Hypothalamic sensing of circulating fatty acids is required for glucose homeostasis. *Nat. Med.* 11, 320–327. doi:10.1038/nm1201.

Le, J. A., Wilson, H. M., Shehu, A., Mao, J., Devi, Y. S., Halperin, J., et al. (2012). Generation of Mice Expressing Only the Long Form of the Prolactin Receptor Reveals That Both Isoforms of the Receptor Are Required for Normal Ovarian Function. *Biol Reprod* 86. doi:10.1095/biolreprod.111.095927.

Le Tissier, P., Campos, P., Lafont, C., Romanò, N., Hodson, D. J., and Mollard, P. (2017). An updated view of hypothalamic-vascular-pituitary unit function and plasticity. *Nat Rev Endocrinol* 13, 257–267. doi:10.1038/nrendo.2016.193.

Lechan, R. M., and Toni, R. (2000). "Functional Anatomy of the Hypothalamus and Pituitary," in *Endotext*, eds. K. R. Feingold, B. Anawalt, A. Boyce, G. Chrousos, W. W. de Herder, K. Dungan, et al. (South Dartmouth (MA): MDText.com, Inc.). Available at: http://www.ncbi.nlm.nih.gov/books/NBK279126/ [Accessed November 12, 2020].

Lee, T. F., Mora, F., and Myers, R. D. (1985). Dopamine and thermoregulation: An evaluation with special reference to dopaminergic pathways. *Neuroscience & Biobehavioral Reviews* 9, 589–598. doi:10.1016/0149-7634(85)90005-3.

Leibel, R. L., Rosenbaum, M., and Hirsch, J. (1995). Changes in energy expenditure resulting from altered body weight. *N. Engl. J. Med.* 332, 621–628. doi:10.1056/NEJM199503093321001.

Levine, J. A., Eberhardt, N. L., and Jensen, M. D. (1999). Role of nonexercise activity thermogenesis in resistance to fat gain in humans. *Science* 283, 212–214. doi:10.1126/science.283.5399.212.

Li, G., Zhang, W., Baker, M. S., Laritsky, E., Mattan-Hung, N., Yu, D., et al. (2014). Major epigenetic development distinguishing neuronal and non-neuronal cells occurs postnatally in the murine hypothalamus. *Hum. Mol. Genet.* 23, 1579–1590. doi:10.1093/hmg/ddt548.

Li, Z.-M., Albrecht, M., Fromme, H., Schramm, K.-W., and De Angelis, M. (2020). Persistent Organic Pollutants in Human Breast Milk and Associations with Maternal Thyroid Hormone Homeostasis. *Environ. Sci. Technol.* 54, 1111–1119. doi:10.1021/acs.est.9b06054.

Lindgren, N., Goiny, M., Herrera-Marschitz, M., Haycock, J. W., Hökfelt, T., and Fisone, G. (2002). Activation of extracellular signal-regulated kinases 1 and 2 by depolarization stimulates tyrosine hydroxylase phosphorylation and dopamine synthesis in rat brain. *Eur J Neurosci* 15, 769–773. doi:10.1046/j.1460-9568.2002.01901.x.

Liu, B., and Arbogast, L. A. (2008). Phosphorylation State of Tyrosine Hydroxylase in the Stalk-Median Eminence Is Decreased by Progesterone in Cycling Female Rats. *Endocrinology* 149, 1462–1469. doi:10.1210/en.2007-1345.

Liu, X., Robinson, G. W., Gouilleux, F., Groner, B., and Hennighausen, L. (1995). Cloning and expression of Stat5 and an additional homologue (Stat5b) involved in prolactin signal transduction in mouse mammary tissue. *Proc Natl Acad Sci U S A* 92, 8831–8835. doi:10.1073/pnas.92.19.8831.

Longhi, S., and Radetti, G. (2013). Thyroid Function and Obesity. *J Clin Res Pediatr Endocrinol* 5, 40–44. doi:10.4274/Jcrpe.856.

Ma, F. Y., Grattan, D. R., Bobrovskaya, L., Dunkley, P. R., and Bunn, S. J. (2004). Angiotensin II regulates tyrosine hydroxylase activity and mRNA expression in rat mediobasal hypothalamic cultures: the role of specific protein kinases. *Journal of Neurochemistry* 90, 431–441. doi:https://doi.org/10.1111/j.1471-4159.2004.02492.x.

Ma, F. Y., Grattan, D. R., Goffin, V., and Bunn, S. J. (2005). Prolactin-regulated tyrosine hydroxylase activity and messenger ribonucleic acid expression in mediobasal hypothalamic cultures: the differential role of specific protein kinases. *Endocrinology* 146, 93–102. doi:10.1210/en.2004-0800.

Ma, L., Gao, J., Guan, Y., Shi, X., Zhang, H., Ayrapetov, M. K., et al. (2010). Acetylation modulates prolactin receptor dimerization. *PNAS* 107, 19314–19319. doi:10.1073/pnas.1010253107.

Maclean, P. S., Bergouignan, A., Cornier, M.-A., and Jackman, M. R. (2011). Biology's response to dieting: the impetus for weight regain. *Am. J. Physiol. Regul. Integr. Comp. Physiol.* 301, R581-600. doi:10.1152/ajpregu.00755.2010.

MacLean, P. S., Higgins, J. A., Johnson, G. C., Fleming-Elder, B. K., Peters, J. C., and Hill, J. O. (2004). Metabolic adjustments with the development, treatment, and recurrence of obesity in obesity-prone rats. *Am. J. Physiol. Regul. Integr. Comp. Physiol.* 287, R288-297. doi:10.1152/ajpregu.00010.2004.

Maffei, M., Halaas, J., Ravussin, E., Pratley, R. E., Lee, G. H., Zhang, Y., et al. (1995). Leptin levels in human and rodent: measurement of plasma leptin and ob RNA in obese and weight-reduced subjects. *Nat. Med.* 1, 1155–1161.

Martin, D., Xu, J., Porretta, C., and Nichols, C. D. (2017). Neurocytometry: Flow Cytometric Sorting of Specific Neuronal Populations from Human and Rodent Brain. *ACS Chem. Neurosci.* 8, 356–367. doi:10.1021/acschemneuro.6b00374.

Martins, A. C. P., Souza, K. L. A., Shio, M. T., Mathias, P. C. F., Lelkes, P. I., and Garcia, R. M. G. (2004). Adrenal medullary function and expression of catecholamine-synthesizing enzymes in mice with hypothalamic obesity. *Life Sci* 74, 3211–3222. doi:10.1016/j.lfs.2003.10.034.

McKinsey, T. A., Zhang, C. L., and Olson, E. N. (2000). Activation of the myocyte enhancer factor-2 transcription factor by calcium/calmodulin-dependent protein kinase-stimulated binding of 14-3-3 to histone deacetylase 5. *Proc. Natl. Acad. Sci. U.S.A.* 97, 14400–14405. doi:10.1073/pnas.260501497.

Melby, C. L., Paris, H. L., Foright, R. M., and Peth, J. (2017). Attenuating the Biologic Drive for Weight Regain Following Weight Loss: Must What Goes Down Always Go Back Up? *Nutrients* 9. doi:10.3390/nu9050468.

Melby, C. L., Schmidt, W. D., and Corrigan, D. (1990). Resting metabolic rate in weight-cycling collegiate wrestlers compared with physically active, noncycling control subjects. *Am. J. Clin. Nutr.* 52, 409–414. doi:10.1093/ajcn/52.3.409.

Meng, Z.-X., Gong, J., Chen, Z., Sun, J., Xiao, Y., Wang, L., et al. (2017). Glucose Sensing by Skeletal Myocytes Couples Nutrient Signaling to Systemic Homeostasis. *Mol Cell* 66, 332-344.e4. doi:10.1016/j.molcel.2017.04.007.

Michalaki, M. A., Vagenakis, A. G., Leonardou, A. S., Argentou, M. N., Habeos, I. G., Makri, M. G., et al. (2006). Thyroid Function in Humans with Morbid Obesity. *Thyroid* 16, 73–78. doi:10.1089/thy.2006.16.73.

Mirch, M. C., McDuffie, J. R., Yanovski, S. Z., Schollnberger, M., Tanofsky-Kraff, M., Theim, K. R., et al. (2006). Effects of binge eating on satiation, satiety, and energy intake of overweight children. *Am J Clin Nutr* 84, 732–738.

Mo, A., Mukamel, E. A., Davis, F. P., Luo, C., Henry, G. L., Picard, S., et al. (2015). Epigenomic Signatures of Neuronal Diversity in the Mammalian Brain. *Neuron* 86, 1369–1384. doi:10.1016/j.neuron.2015.05.018.

Moffitt, J. R., Bambah-Mukku, D., Eichhorn, S. W., Vaughn, E., Shekhar, K., Perez, J. D., et al. (2018). Molecular, spatial, and functional single-cell profiling of the hypothalamic preoptic region. *Science* 362. doi:10.1126/science.aau5324.

Morrison, S. F. (2001). Differential control of sympathetic outflow. *American Journal of Physiology-Regulatory, Integrative and Comparative Physiology* 281, R683–R698. doi:10.1152/ajpregu.2001.281.3.R683.

Muzumdar, M. D., Tasic, B., Miyamichi, K., Li, L., and Luo, L. (2007). A global double-fluorescent Cre reporter mouse. *Genesis* 45, 593–605. doi:10.1002/dvg.20335.

Myers, L. S., and Steele, M. K. (1991). The Brain Renin-Angiotensin System and Prolactin Secretion in the Male Rat. *Endocrinology* 129, 1744–1748. doi:10.1210/endo-129-4-1744.

Myers, R. D., and Yaksh, T. L. (1969). Control of body temperature in the unanaesthetized monkey by cholinergic and aminergic systems in the hypothalamus. *J Physiol* 202, 483–500. doi:10.1113/jphysiol.1969.sp008822.

Nagler, J., Schriever, S. C., De Angelis, M., Pfluger, P. T., and Schramm, K.-W. (2018). Comprehensive analysis of nine monoamines and metabolites in small amounts of peripheral murine (C57Bl/6 J) tissues. *Biomed. Chromatogr.* 32. doi:10.1002/bmc.4151.

Nanou, A., Toumpeki, C., Lavigne, M. D., Lazou, V., Demmers, J., Paparountas, T., et al. (2017). The dual role of LSD1 and HDAC3 in STAT5-dependent transcription is determined by protein interactions, binding affinities, motifs and genomic positions. *Nucleic Acids Res* 45, 142–154. doi:10.1093/nar/gkw832.

Näslund, E., Andersson, I., Degerblad, M., Kogner, P., Kral, J. G., Rössner, S., et al. (2000). Associations of leptin, insulin resistance and thyroid function with long-term weight loss in

dieting obese men. *Journal of Internal Medicine* 248, 299–308. doi:10.1046/j.1365-2796.2000.00737.x.

O, U., Dr, J., A, T., and C, B. (2003). Na+-K+-ATPase alpha 2-gene and skeletal muscle characteristics in response to long-term overfeeding. *Journal of applied physiology (Bethesda, Md. : 1985)* 94. doi:10.1152/japplphysiol.00942.2002.

Ogden, C. L., Carroll, M. D., Kit, B. K., and Flegal, K. M. (2013). Prevalence of obesity among adults: United States, 2011-2012. *NCHS Data Brief*, 1–8.

Ootsuka, Y., Heidbreder, C. A., Hagan, J. J., and Blessing, W. W. (2007). Dopamine D2 receptor stimulation inhibits cold-initiated thermogenesis in brown adipose tissue in conscious rats. *Neuroscience* 147, 127–135. doi:10.1016/j.neuroscience.2007.04.015.

Osborn John W., and Kuroki Marcos T. (2012). Sympathetic Signatures of Cardiovascular Disease. *Hypertension* 59, 545–547. doi:10.1161/HYPERTENSIONAHA.111.182899.

Ottaway, N., Mahbod, P., Rivero, B., Norman, L. A., Gertler, A., D'Alessio, D., et al. (2015). Diet-induced obese mice retain endogenous leptin action. *Cell Metab* 21, 877–882. doi:10.1016/j.cmet.2015.04.015.

Paden, C. M., Berglund, D. L., Hapner, S. J., and Welsh, C. J. (1986). A flow cytometric method for intracellular labeling and purification of rare neuronal populations: isolation of fixed neurophysin neurons. *Brain Res.* 376, 310–319.

Paeger, L., Karakasilioti, I., Altmüller, J., Frommolt, P., Brüning, J., and Kloppenburg, P. (2017). Antagonistic modulation of NPY/AgRP and POMC neurons in the arcuate nucleus by noradrenalin. *eLife* 6, e25770. doi:10.7554/eLife.25770.

Palmer, B. F., and Clegg, D. J. (2015). The sexual dimorphism of obesity. *Mol Cell Endocrinol* 402, 113–119. doi:10.1016/j.mce.2014.11.029.

Pan, W. W., and Myers Jr, M. G. (2018). Leptin and the maintenance of elevated body weight. *Nature Reviews Neuroscience* 19, 95–105. doi:10.1038/nrn.2017.168.

Pasquet, P., and Apfelbaum, M. (1994). Recovery of initial body weight and composition after long-term massive overfeeding in men. *Am J Clin Nutr* 60, 861–863. doi:10.1093/ajcn/60.6.861.

Pédelacq, J.-D., Cabantous, S., Tran, T., Terwilliger, T. C., and Waldo, G. S. (2006). Engineering and characterization of a superfolder green fluorescent protein. *Nat Biotechnol* 24, 79–88. doi:10.1038/nbt1172.

Phelps, C. J., Carlson, S. W., Vaccarella, M. Y., and Felten, S. Y. (1993). Developmental assessment of hypothalamic tuberoinfundibular dopamine in prolactin-deficient dwarf mice. *Endocrinology* 132, 2715–2722. doi:10.1210/en.132.6.2715.

Phelps, C. J., Romero, M. I., and Hurley, D. L. (2003). Prolactin replacement must be continuous and initiated prior to 21 d of age to maintain hypothalamic dopaminergic neurons in hypopituitary mice. *Endocr* 20, 139–148. doi:10.1385/ENDO:20:1-2:139.

Phelps, C. J., Vaccarella, M. Y., Romero, M. I., and Hurley, D. L. (1994). Postnatal reduction in number of hypothalamic tuberoinfundibular dopaminergic neurons in prolactin-deficient dwarf mice. *Neuroendocrinology* 59, 189–196. doi:10.1159/000126658.

Pita-Thomas, W., Mahar, M., Joshi, A., Gan, D., and Cavalli, V. (2019). HDAC5 promotes optic nerve regeneration by activating the mTOR pathway. *Exp Neurol* 317, 271–283. doi:10.1016/j.expneurol.2019.03.011.

Plass, M., Solana, J., Wolf, F. A., Ayoub, S., Misios, A., Glažar, P., et al. (2018). Cell type atlas and lineage tree of a whole complex animal by single-cell transcriptomics. *Science* 360. doi:10.1126/science.aaq1723.

Preite, N. Z., do Nascimento, B. P. P., Muller, C. R., Américo, A. L. V., Higa, T. S., Evangelista, F. S., et al. (2016). Disruption of beta3 adrenergic receptor increases susceptibility to DIO in mouse. *J Endocrinol* 231, 259–269. doi:10.1530/JOE-16-0199.

Pyörnilä, A. (1980). Apomorphine and oxotremorine hypothermia in the pigeon: dopaminergic-cholinergic interaction and the effect of paleostriatal lesions. *Med Biol* 58, 87–93.

Ravussin, E., Lillioja, S., Knowler, W. C., Christin, L., Freymond, D., Abbott, W. G., et al. (1988). Reduced rate of energy expenditure as a risk factor for body-weight gain. *N Engl J Med* 318, 467–472. doi:10.1056/NEJM198802253180802.

Ravussin, E., and Tataranni, P. A. (1996). The role of altered sympathetic nervous system activity in the pathogenesis of obesity. *Proc Nutr Soc* 55, 793–802. doi:10.1079/pns19960079.

Ravussin, Y., LeDuc, C. A., Watanabe, K., Mueller, B. R., Skowronski, A., Rosenbaum, M., et al. (2014). Effects of chronic leptin infusion on subsequent body weight and composition in mice: Can body weight set point be reset? *Mol Metab* 3, 432–440. doi:10.1016/j.molmet.2014.02.003.

Reimann, M., Qin, N., Gruber, M., Bornstein, S. R., Kirschbaum, C., Ziemssen, T., et al. (2017). Adrenal medullary dysfunction as a feature of obesity. *Int J Obes (Lond)* 41, 714–721. doi:10.1038/ijo.2017.36.

Renthal, W., Maze, I., Krishnan, V., Covington, H. E., Xiao, G., Kumar, A., et al. (2007). Histone deacetylase 5 epigenetically controls behavioral adaptations to chronic emotional stimuli. *Neuron* 56, 517–529. doi:10.1016/j.neuron.2007.09.032.

Rodriguez, A., Durán, A., Selloum, M., Champy, M.-F., Diez-Guerra, F. J., Flores, J. M., et al. (2006). Mature-onset obesity and insulin resistance in mice deficient in the signaling adapter p62. *Cell Metab* 3, 211–222. doi:10.1016/j.cmet.2006.01.011.

Romanò, N., Yip, S. H., Hodson, D. J., Guillou, A., Parnaudeau, S., Kirk, S., et al. (2013). Plasticity of Hypothalamic Dopamine Neurons during Lactation Results in Dissociation of Electrical Activity and Release. *J. Neurosci.* 33, 4424–4433. doi:10.1523/JNEUROSCI.4415-12.2013.

Romanov, R. A., Zeisel, A., Bakker, J., Girach, F., Hellysaz, A., Tomer, R., et al. (2017). Molecular interrogation of hypothalamic organization reveals distinct dopamine neuronal subtypes. *Nature Neuroscience* 20, 176–188. doi:10.1038/nn.4462.

Rosenbaum, M., Goldsmith, R., Bloomfield, D., Magnano, A., Weimer, L., Heymsfield, S., et al. (2005). Low-dose leptin reverses skeletal muscle, autonomic, and neuroendocrine adaptations to maintenance of reduced weight. *J. Clin. Invest.* 115, 3579–3586. doi:10.1172/JCI25977.

Rosenbaum, M., Hirsch, J., Gallagher, D. A., and Leibel, R. L. (2008). Long-term persistence of adaptive thermogenesis in subjects who have maintained a reduced body weight. *Am. J. Clin. Nutr.* 88, 906–912. doi:10.1093/ajcn/88.4.906.

Rosenbaum, M., Kissileff, H. R., Mayer, L. E. S., Hirsch, J., and Leibel, R. L. (2010). Energy intake in weight-reduced humans. *Brain Research* 1350, 95–102. doi:10.1016/j.brainres.2010.05.062.

Rotondi, M., Leporati, P., La Manna, A., Pirali, B., Mondello, T., Fonte, R., et al. (2009). Raised serum TSH levels in patients with morbid obesity: is it enough to diagnose subclinical hypothyroidism? *Eur J Endocrinol* 160, 403–408. doi:10.1530/EJE-08-0734.

Saito, M., Okamatsu-Ogura, Y., Matsushita, M., Watanabe, K., Yoneshiro, T., Nio-Kobayashi, J., et al. (2009). High Incidence of Metabolically Active Brown Adipose Tissue in Healthy Adult Humans: Effects of Cold Exposure and Adiposity. *Diabetes* 58, 1526–1531. doi:10.2337/db09-0530.

Saxena, P. N., Chawla, N., Johri, M. B. L., and Iqbal, S. (1977). Nature of receptors involved in apomorphine responses in pigeons. *Psychopharmacology* 53, 89–95. doi:10.1007/BF00426699.

Schelkunov, E. L., Andreeva, O. G., Korovin, K. F., and Ostroumova, M. N. (1981). The functional role of the noradrenergic neurons in the thermoregulatory circuits in mice. *J Neural Transm* 50, 113–137. doi:10.1007/BF01249134.

Schwartz, M. W., Peskind, E., Raskind, M., Boyko, E. J., and Porte, D. (1996). Cerebrospinal fluid leptin levels: Relationship to plasma levels and to adiposity in humans. *Nature Medicine* 2, 589. doi:10.1038/nm0596-589.

Seto, E., and Yoshida, M. (2014). Erasers of Histone Acetylation: The Histone Deacetylase Enzymes. *Cold Spring Harb Perspect Biol* 6. doi:10.1101/cshperspect.a018713.

Shechter, R., London, A., Kuperman, Y., Ronen, A., Rolls, A., Chen, A., et al. (2013). Hypothalamic neuronal toll-like receptor 2 protects against age-induced obesity. *Scientific Reports* 3, 1254. doi:10.1038/srep01254.

Shin, H., Ma, Y., Chanturiya, T., Cao, Q., Wang, Y., Kadegowda, A. K. G., et al. (2017). Lipolysis in Brown Adipocytes Is Not Essential for Cold-Induced Thermogenesis in Mice. *Cell Metab* 26, 764-777.e5. doi:10.1016/j.cmet.2017.09.002.

Soni, K. G., Lehner, R., Metalnikov, P., O'Donnell, P., Semache, M., Gao, W., et al. (2004). Carboxylesterase 3 (EC 3.1.1.1) is a major adipocyte lipase. *J Biol Chem* 279, 40683–40689. doi:10.1074/jbc.M400541200.

Speakman, J. R. (2007). A nonadaptive scenario explaining the genetic predisposition to obesity: the "predation release" hypothesis. *Cell Metab.* 6, 5–12. doi:10.1016/j.cmet.2007.06.004.

Speakman, J. R. (2018). Why lipostatic set point systems are unlikely to evolve. *Molecular Metabolism* 7, 147–154. doi:10.1016/j.molmet.2017.10.007.

Speakman, J. R., Levitsky, D. A., Allison, D. B., Bray, M. S., de Castro, J. M., Clegg, D. J., et al. (2011). Set points, settling points and some alternative models: theoretical options to understand how genes and environments combine to regulate body adiposity. *Disease Models & Mechanisms* 4, 733–745. doi:10.1242/dmm.008698.

Steger, R. W., Chandrashekar, V., Zhao, W., Bartke, A., and Horseman, N. D. (1998). Neuroendocrine and Reproductive Functions in Male Mice with Targeted Disruption of the Prolactin Gene. *Endocrinology* 139, 3691–3695. doi:10.1210/endo.139.9.6209.

Stemmer, K., Kotzbeck, P., Zani, F., Bauer, M., Neff, C., Müller, T. D., et al. (2015). Thermoneutral housing is a critical factor for immune function and diet-induced obesity in C57BL/6 nude mice. *Int J Obes (Lond)* 39, 791–797. doi:10.1038/ijo.2014.187.

Stice, E., Yokum, S., Blum, K., and Bohon, C. (2010). Weight Gain Is Associated with Reduced Striatal Response to Palatable Food. *J. Neurosci.* 30, 13105–13109. doi:10.1523/JNEUROSCI.2105-10.2010.

Strålfors, P., Björgell, P., and Belfrage, P. (1984). Hormonal regulation of hormone-sensitive lipase in intact adipocytes: identification of phosphorylated sites and effects on the phosphorylation by lipolytic hormones and insulin. *PNAS* 81, 3317–3321. doi:10.1073/pnas.81.11.3317.

Stubbins, R. E., Holcomb, V. B., Hong, J., and Núñez, N. P. (2012). Estrogen modulates abdominal adiposity and protects female mice from obesity and impaired glucose tolerance. *Eur J Nutr* 51, 861–870. doi:10.1007/s00394-011-0266-4.

Sumithran, P., Prendergast, L. A., Delbridge, E., Purcell, K., Shulkes, A., Kriketos, A., et al. (2011). Long-term persistence of hormonal adaptations to weight loss. *N. Engl. J. Med.* 365, 1597–1604. doi:10.1056/NEJMoa1105816.

Taniguchi, M., Carreira, M. B., Cooper, Y. A., Bobadilla, A.-C., Heinsbroek, J. A., Koike, N., et al. (2017). HDAC5 and Its Target Gene, Npas4, Function in the Nucleus Accumbens to Regulate Cocaine-Conditioned Behaviors. *Neuron* 96, 130-144.e6. doi:10.1016/j.neuron.2017.09.015.

Taniguchi, M., Carreira, M. B., Smith, L. N., Zirlin, B. C., Neve, R. L., and Cowan, C. W. (2012). Histone deacetylase 5 limits cocaine reward through cAMP-induced nuclear import. *Neuron* 73, 108–120. doi:10.1016/j.neuron.2011.10.032.

Tataranni, P. A., Young, J. B., Bogardus, C., and Ravussin, E. (1997). A low sympathoadrenal activity is associated with body weight gain and development of central adiposity in Pima Indian men. *Obes Res* 5, 341–347. doi:10.1002/j.1550-8528.1997.tb00562.x.

The, N. S., Suchindran, C., North, K. E., Popkin, B. M., and Gordon-Larsen, P. (2010). Association of adolescent obesity with risk of severe obesity in adulthood. *JAMA* 304, 2042–2047. doi:10.1001/jama.2010.1635.

Thorp, A. A., and Schlaich, M. P. (2015). Relevance of Sympathetic Nervous System Activation in Obesity and Metabolic Syndrome. *Journal of Diabetes Research* 2015, e341583. doi:https://doi.org/10.1155/2015/341583.

Tian, H., Liu, S., Ren, J., Lee, J. K. W., Wang, R., and Chen, P. (2020). Role of Histone Deacetylases in Skeletal Muscle Physiology and Systemic Energy Homeostasis: Implications for Metabolic Diseases and Therapy. *Front. Physiol.* 11. doi:10.3389/fphys.2020.00949.

Tong, Q., Ye, C.-P., Jones, J. E., Elmquist, J. K., and Lowell, B. B. (2008). Synaptic release of GABA by AgRP neurons is required for normal regulation of energy balance. *Nat Neurosci* 11, 998–1000. doi:10.1038/nn.2167.

Tremblay, A., Després, J. P., Thériault, G., Fournier, G., and Bouchard, C. (1992). Overfeeding and energy expenditure in humans. *Am J Clin Nutr* 56, 857–862. doi:10.1093/ajcn/56.5.857.

Tritschler, S., Theis, F. J., Lickert, H., and Böttcher, A. (2017). Systematic single-cell analysis provides new insights into heterogeneity and plasticity of the pancreas. *Mol Metab* 6, 974–990. doi:10.1016/j.molmet.2017.06.021.

Trujillo, J. M., Nuffer, W., and Ellis, S. L. (2015). GLP-1 receptor agonists: a review of head-to-head clinical studies. *Ther Adv Endocrinol Metab* 6, 19–28. doi:10.1177/2042018814559725.

Tschöp, M. H., Speakman, J. R., Arch, J. R. S., Auwerx, J., Brüning, J. C., Chan, L., et al. (2012). A guide to analysis of mouse energy metabolism. *Nature Methods* 9, 57–63. doi:10.1038/nmeth.1806.

Turner, R. C., Holman, R. R., Matthews, D., Hockaday, T. D. R., and Peto, J. (1979). Insulin deficiency and insulin resistance interaction in diabetes: Estimation of their relative contribution by feedback analysis from basal plasma insulin and glucose concentrations. *Metabolism - Clinical and Experimental* 28, 1086–1096. doi:10.1016/0026-0495(79)90146-X.

Ukkola, O., and Bouchard, C. (2004). Role of candidate genes in the responses to long-term overfeeding: review of findings. *Obes Rev* 5, 3–12. doi:10.1111/j.1467-789x.2004.00118.x.

van Marken Lichtenbelt, W. D., Vanhommerig, J. W., Smulders, N. M., Drossaerts, J. M. A. F. L., Kemerink, G. J., Bouvy, N. D., et al. (2009). Cold-Activated Brown Adipose Tissue in Healthy Men. *New England Journal of Medicine* 360, 1500–1508. doi:10.1056/NEJMoa0808718.

Vega, R. B., Harrison, B. C., Meadows, E., Roberts, C. R., Papst, P. J., Olson, E. N., et al. (2004). Protein Kinases C and D Mediate Agonist-Dependent Cardiac Hypertrophy through Nuclear Export of Histone Deacetylase 5. *Molecular and Cellular Biology* 24, 8374–8385. doi:10.1128/MCB.24.19.8374-8385.2004.

Villagra, A., Cheng, F., Wang, H.-W., Suarez, I., Glozak, M., Maurin, M., et al. (2009). The histone deacetylase HDAC11 regulates the expression of interleukin 10 and immune tolerance. *Nat Immunol* 10, 92–100. doi:10.1038/ni.1673.

Villena, J. A., Roy, S., Sarkadi-Nagy, E., Kim, K.-H., and Sul, H. S. (2004). Desnutrin, an adipocyte gene encoding a novel patatin domain-containing protein, is induced by fasting and glucocorticoids: ectopic expression of desnutrin increases triglyceride hydrolysis. *J Biol Chem* 279, 47066–47075. doi:10.1074/jbc.M403855200.

Vodnik, M., Štrukelj, B., and Lunder, M. (2016). Ghrelin Receptor Ligands Reaching Clinical Trials: From Peptides to Peptidomimetics; from Agonists to Antagonists. *Horm. Metab. Res.* 48, 1–15. doi:10.1055/s-0035-1564149.

Wallenius, V., Wallenius, K., Ahrén, B., Rudling, M., Carlsten, H., Dickson, S. L., et al. (2002). Interleukin-6-deficient mice develop mature-onset obesity. *Nat Med* 8, 75–79. doi:10.1038/nm0102-75.

Waterson, M. J., and Horvath, T. L. (2015). Neuronal Regulation of Energy Homeostasis: Beyond the Hypothalamus and Feeding. *Cell Metab.* 22, 962–970. doi:10.1016/j.cmet.2015.09.026.

Williams, T. D., Chambers, J. B., Henderson, R. P., Rashotte, M. E., and Overton, J. M. (2002). Cardiovascular responses to caloric restriction and thermoneutrality in C57BL/6J mice. *American Journal of Physiology-Regulatory, Integrative and Comparative Physiology* 282, R1459–R1467. doi:10.1152/ajpregu.00612.2001.

Wollmuth, L. P., Crawshaw, L. I., and Panayiotides-Djaferis, H. (1989). The effects of dopamine on temperature regulation in goldfish. *J Comp Physiol B* 159, 83–89. doi:10.1007/BF00692686.

World Health Organization (2018). *World Health Organization*. Available at: http://www.who.int/news-room/fact-sheets/detail/obesity-and-overweight [Accessed November 4, 2018].

Xu, M., Nie, L., Kim, S.-H., and Sun, X.-H. (2003). STAT5-induced Id-1 transcription involves recruitment of HDAC1 and deacetylation of C/EBPβ. *EMBO J* 22, 893–904. doi:10.1093/emboj/cdg094.

Xu, R., Huang, F., Zhang, S., Lv, Y., and Liu, Q. (2019). Thyroid function, body mass index, and metabolic risk markers in euthyroid adults: a cohort study. *BMC Endocrine Disorders* 19, 58. doi:10.1186/s12902-019-0383-2.

Xu, X., Stoyanova, E. I., Lemiesz, A. E., Xing, J., Mash, D. C., and Heintz, N. (2018). Species and cell-type properties of classically defined human and rodent neurons and glia. *eLife* 7, e37551. doi:10.7554/eLife.37551.

Xu, Y., and López, M. (2018). Central regulation of energy metabolism by estrogens. *Mol Metab* 15, 104–115. doi:10.1016/j.molmet.2018.05.012.

Yip, S. H., Eguchi, R., Grattan, D. R., and Bunn, S. J. (2012). Prolactin signalling in the mouse hypothalamus is primarily mediated by signal transducer and activator of transcription factor 5b but not 5a. *J Neuroendocrinol* 24, 1484–1491. doi:10.1111/j.1365-2826.2012.02357.x.

Yip, S. H., Romanò, N., Gustafson, P., Hodson, D. J., Williams, E. J., Kokay, I. C., et al. (2019). Elevated Prolactin during Pregnancy Drives a Phenotypic Switch in Mouse Hypothalamic Dopaminergic Neurons. *Cell Rep* 26, 1787-1799.e5. doi:10.1016/j.celrep.2019.01.067.

Yu, K., Lu, D., Rowland, N. E., and Raizada, M. K. (1996). Angiotensin II regulation of tyrosine hydroxylase gene expression in the neuronal cultures of normotensive and spontaneously hypertensive rats. *Endocrinology* 137, 3566–3576. doi:10.1210/endo.137.8.8754788.

Yu, X. X., Lewin, D. A., Forrest, W., and Adams, S. H. (2002). Cold elicits the simultaneous induction of fatty acid synthesis and β-oxidation in murine brown adipose tissue: prediction from differential gene expression and confirmation in vivo. *The FASEB Journal* 16, 155–168. doi:https://doi.org/10.1096/fj.01-0568com.

Zeisel, A., Muñoz-Manchado, A. B., Codeluppi, S., Lönnerberg, P., La Manno, G., Juréus, A., et al. (2015). Brain structure. Cell types in the mouse cortex and hippocampus revealed by single-cell RNA-seq. *Science* 347, 1138–1142. doi:10.1126/science.aaa1934.

Zhang, X., and van den Pol, A. N. (2015). Dopamine/Tyrosine Hydroxylase Neurons of the Hypothalamic Arcuate Nucleus Release GABA, Communicate with Dopaminergic and Other Arcuate Neurons, and Respond to Dynorphin, Met-Enkephalin, and Oxytocin. *J Neurosci* 35, 14966–14982. doi:10.1523/JNEUROSCI.0293-15.2015.

Zhang, X., and van den Pol, A. N. (2016). Hypothalamic arcuate nucleus tyrosine hydroxylase neurons play orexigenic role in energy homeostasis. *Nat Neurosci* 19, 1341–1347. doi:10.1038/nn.4372.

Zhang, Y., Proenca, R., Maffei, M., Barone, M., Leopold, L., and Friedman, J. M. (1994). Positional cloning of the mouse obese gene and its human homologue. *Nature* 372, 425. doi:10.1038/372425a0.